ISSN 2413-5577

№ 3 Июль – Сентябрь 2023

Экологическая безопасность прибрежной и шельфовой зон моря

Ecological Safety of Coastal and Shelf Zones of Sea

No. 3 July – September 2023

ecological-safety.ru

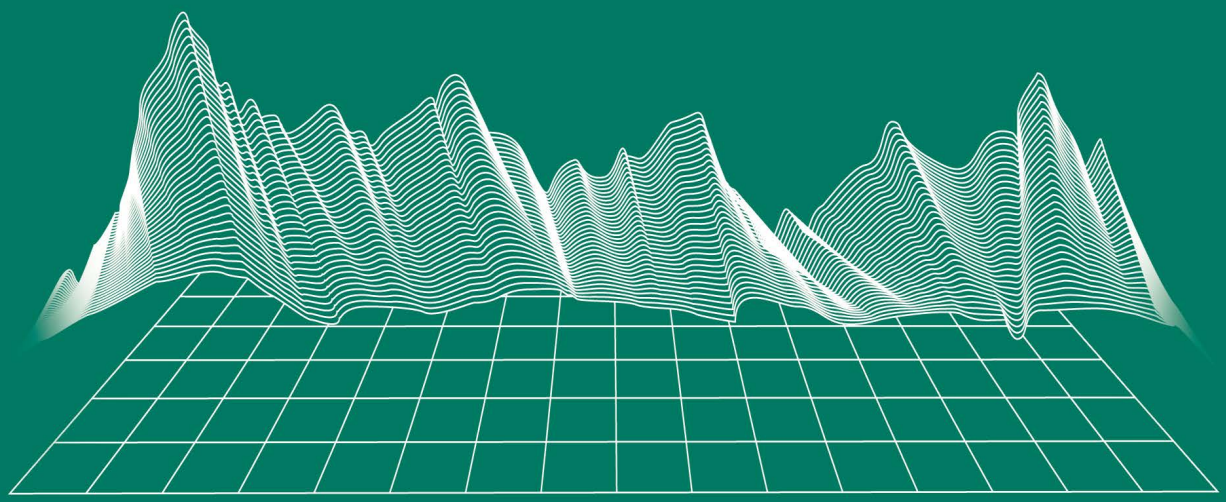

ISSN 2413-5577
No. 3, 2023
July – September
Publication frequency:
Quarterly
16+

ECOLOGICAL SAFETY OF COASTAL AND SHELF ZONES OF SEA

Scientific and theoretical peer reviewed journal

FOUNDER AND PUBLISHER:
Federal State Budget Scientific Institution
Federal Research Centre
"Marine Hydrophysical Institute of RAS"

The Journal publishes original research results, review articles (at the editorial board's request) and brief reports.

The Journal aims at publication of results of original scientific research concerning the state and interaction of geospheres (atmosphere, lithosphere, hydrosphere, and biosphere) within coastal and shelf areas of seas and oceans, methods and means of study thereof, ecological state of these areas under anthropogenic load as well as environmental protection issues.

The Journal's editorial board sees its mission as scientific, educational and regulatory work to preserve the ecological balance and restore the resource potential of coastal and shelf areas believing that despite the geographical limitations of the areas under study, the processes taking place within them have a significant impact on the waters of the seas and oceans and economic activity.

The Journal publishes original research materials, results of research performed by national and foreign scientific institutions in the coastal and shelf zones of seas and oceans, review articles (at the editorial board's request) and brief reports on the following major topics:
- Scientific basis for complex use of shelf natural resources
- Marine environment state and variability
- Coastal area state and variability; coast protection structures
- Monitoring and estimates of possible effects of anthropogenic activities
- Development and implementation of new marine environment control and monitoring technologies

The outcome of the research is information on the status, variability and possible effects of anthropogenic activities in the coastal and shelf marine areas, as well as the means to perform calculations and to provide information for making decisions on the implementation of activities in the coastal zone.

e-mail: ecology-safety@mhi-ras.ru

website: http://ecological-safety.ru

Founder, Publisher and Editorial Office address:
2, Kapitanskaya St.,
Sevastopol, 299011, Russia

Phone, fax: + 7 (8692) 54-57-16

EDITORIAL BOARD

РЕДАКЦИОННАЯ КОЛЛЕГИЯ

CONTENTS

№ 3. 2023 July – September, 2023

СОДЕРЖАНИЕ

№ 3. 2023 Июль – Сентябрь, 2023

Original article

Assessment of the Black Sea Steric Level Variability: New Approaches and Prospects for the Use of Satellite Information

V. P. Novitskaya *, E. M. Lemeshko, V. N. Belokopytov

Marine Hydrophysical Institute of RAS, Sevastopol, Russia

* *e-mail: victory.novitskaya@mhi-ras.ru*

Abstract

Based on satellite altimetry and gravimetric data, the time series of steric level oscillations averaged over the Black Sea for 2002–2016 is reconstructed. The steric sea level oscillations were calculated as the difference between the total sea level measured by altimeters and the manometric (barystatic) component determined from gravimetric measurements GRACE. A good agreement was obtained between the steric component of the sea level and the estimates obtained from archival hydrological data and Argo floats. The maxima of the range of the seasonal variation of the steric component of the level are noted in the areas with maximum seasonal vertical displacements of the main pycnocline. Estimates of the steric level seasonal cycle were obtained, the range of oscillations was up to 12 cm. The minimum is reached in the winter period (March), and the maximum – in the summer period (August). It is noted that the seasonal cycle of the manometric component of the sea level is in good agreement with the seasonal cycle of the freshwater balance of the Black Sea constructed according to climatic hydrometeorological data. The estimate of the linear trend of the reconstructed steric oscillations is –0.6 ± 0.2 cm/year. This indicates that, despite the positive trend in water temperature in the main pycnocline and desalination of the surface layer, the contribution of the modern increase in salinity in all layers of the sea to the changes in water density in the Black Sea generally predominates.

Keywords: Black Sea, steric level, manometric level, water balance, altimetry, gravimetry, GRACE, climate

Acknowledgments: The work was performed under state assignment of MHI RAS on topics no. FNNN-2021-0005, FNNN-2021-0002. The authors gratefully acknowledge the GSFC for providing the GRACE RL06 mascon data and Copernicus Marine Environment Monitoring Service for altimetry data.

For citation: Novitskaya, V.P., Lemeshko, E.M. and Belokopytov, V.N., 2023. Assessment of the Black Sea Steric Level Variability: New Approaches and Prospects for the Use of Satellite Information. *Ecological Safety of Coastal and Shelf Zones of Sea*, (3), pp. 6–21.

Оценка изменчивости стерического уровня Черного моря: новые подходы и перспективы использования спутниковой информации

В. П. Новицкая *, Е. М. Лемешко, В. Н. Белокопытов

Морской гидрофизический институт РАН, Севастополь, Россия
** e-mail: victory.novitskaya@mhi-ras.ru*

Аннотация

На основе спутниковых альтиметрических и гравиметрических данных реконструирован временной ряд стерических колебаний уровня, осредненных по акватории Черного моря за 2002–2016 гг. Стерические колебания уровня моря рассчитывались как разница между общим уровнем, измеряемым альтиметрами, и манометрической (баристатической) составляющей, определяемой по гравиметрическим измерениям *GRACE*. Получено хорошее соответствие реконструированной стерической компоненты уровня моря оценкам, полученным по архивным гидрологическим данным и данным буев Арго. Максимумы размаха сезонного хода стерической составляющей уровня отмечаются в районах с максимальными сезонными вертикальными смещениями основного пикноклина. Получены оценки сезонного цикла стерического уровня с размахом колебаний до 12 см, минимум отмечается в зимний период (март), максимум – в летний период (август). Кроме того, выявлено хорошее соответствие сезонного хода манометрической компоненты уровня и пресноводного баланса Черного моря, рассчитанного по климатическим гидрометеорологическим данным. Оценка коэффициента линейного тренда реконструированных стерических колебаний составила –0.6±0.2 см/год. Это свидетельствует о том, что, несмотря на положительный тренд температуры воды в основном пикноклине и распреснение поверхностного слоя, вклад современного роста солености во всех слоях моря в изменения плотности воды в Черном море в целом преобладает.

Ключевые слова: Черное море, стерический уровень, манометрический уровень, водный баланс, альтиметрия, гравиметрия, *GRACE*, климат

Благодарности: работа выполнена в рамках государственного задания по темам FNNN-2021-0005, FNNN-2021-0002. Авторы благодарят *GSFC* за предоставление данных *GRACE RL*06 и Службу мониторинга морской среды *Copernicus* за данные альтиметрии.

Для цитирования: *Новицкая В. П., Лемешко Е. М., Белокопытов В. Н.* Оценка изменчивости стерического уровня Черного моря: новые подходы и перспективы использования спутниковой информации // Экологическая безопасность прибрежной и шельфовой зон моря. 2023. № 3. С. 6–21. EDN YVYIIC.

Introduction

The modern advanced stage of remote sensing development allows to realize continuous sea level monitoring, which permits to restore its steric component, which characterizes integral changes in the heat and salts content through the entire water column.

The steric oscillations of sea level H_{ster} are caused by changes in the density of sea water if the mass of a water column does not change. The manometric changes in a sea level H_{man} are caused by changes in the mass of a water column under

the assumption that the sea water density remains unchanged [1, 2]. The steric and manometric components add up to give the resulting sea level [3]:

$$H = H_{\text{ster}} + H_{\text{man}}. \quad (1)$$

The resulting sea level is determined using tide-gauge or altimetry measurements. Satellite gravimetric measurements obtained as part of the Gravity Recovery and Climate Experiment (GRACE) project are used for the manometric component. The steric component can be estimated directly from CTD data or from satellite data using relation (1).

In seas that have limited connection with the World Ocean, such as the Black Sea, regional features of climate variability and their links to global changes are most pronounced. The lowest values of long-term oscillations in the steric level of the Black Sea (up to –6 cm), estimated from archival hydrological CTD data, are observed in the central part of the basin. Near the coast, the steric component of the level increases, the maximum occurs in the southeast of the sea (6–7 cm). The largest seasonal range of steric level oscillations is typical for the central (up to 20 cm) and southeastern (up to 16 cm) regions; the smallest range values are observed in the center of the eastern part of the Black Sea [4]. The contribution of the temperature component to steric oscillations of sea level is predominant, reaching the maximum in coastal areas (up to 90 %) [4].

The spatiotemporal steric oscillations variability in the Black Sea is directly related to their specific thermohaline structure, characterized by low surface salinity and sharp haline stratification. In the 0–50 m surface layer of the sea, water temperature brings in a more significant contribution to changes in density. With increasing depth, the spatial contribution of salinity to water density in the 50–300 m layer is comparable to the contribution of spatial temperature variability.

A distinctive feature of the hydrological structure of the Black Sea, which affects the vertical stratification of waters, is the presence of a cold intermediate layer (CIL), located at depths of 50–100 m. In the layer between the core and the lower boundary of the CIL, compensation occurs for the thermosteric and halosteric components of the sea water density. The maximum correlation of these characteristics is located at a depth of 250 m [5]. According to the Argo floats CTD data, salinity anomalies in the CIL were quite irregular in the period before 2010. Considerable temperature variations were also observed in the CIL. After 2010, there was a weak renewal of the CIL waters and an almost complete disappearance of the layer after 2014 [5].

There are various estimates of changes in the thermohaline characteristics of the Black Sea on the scale of interannual and interdecadal variability. Thus, according to the retrospective analysis [6], a long-term negative trend in water temperature was revealed in the 0–100 m layer, and a positive trend was revealed in the layer deeper than 200 m. In 1951–1995, salinity decreased in the upper layer

of 0–50 m and increased in deeper layers, which enhanced the density stratification of waters.

According to [7], the decadal variability of temperature and salinity in the upper 0–50 m layer of the sea has a quasi-periodic nature, while in the winter and summer seasons temperature fluctuations differ in amplitude and phase characteristics. In addition, in paper [6], a negative linear trend of salinity in the 0–50 m layer is defined, which is consistent with the positive trend of the freshwater balance in the Black Sea. In recent decades, it was an increase in salinity and temperature in the layer of 75–300 m at the average rate of 0.05 PSU/10 years and 0.02 °C/10 years. The change in the sign of trends in interdecadal salinity variability occurs in the upper part of the pycnocline between the depths of 50 and 75 m. Since 2010, an increase in salinity has also been observed in the surface layer, which is explained by a decrease of the Azov-Black Sea basin freshwater balance.

In [8], three characteristic periods were defined based on the results of numerical modeling: 1960–1970, 1970–1995 and 1995–2015, characterized by different circulation states: weakening (1st period) and increasing intensity of cyclonic circulation (2nd and 3rd periods). An increase in temperature and salinity is observed in the permanent pycnocline layer, which is consistent with the results of [6, 7].

The aim of the work is to estimate the seasonal and interannual variability of the thermohaline structure of the Black Sea using the steric component of the sea level as an indicator. The novelty is in the use of the steric level for these purposes, which was reconstructed from satellite altimetric and gravimetric data on the Black Sea level, and in validation of the obtained assessments based on independent calculations from hydrological data.

Observational data

The following data were used in the work:

– oceanographic data archive of Marine Hydrophysical Institute (available at: http://bod-mhi.ru/ru/index.shtml) for a long period of 1923–2015 [9];

– Argo profiling floats data array for 2006–2015 provided by Copernicus Marine Environment Monitoring Service (CMEMS) (https://doi.org/10.48670/moi-00033);

– mean monthly values of gravimetric measurements of GRACE Release 06, GSFC v1.0, 1° × 1° grid (https://earth.gsfc.nasa.gov/geo/data/grace-mascons) for 2002–2016;

– mean monthly values of sea level anomalies from CMEMS altimetry data, grid 0.125° × 0.125°, product identifier SEALEVEL_BS_PHY_L4_REP_OBSERVATIONS_008_04

Research methods

In calculating the steric sea level values from sea water density profiles, a reanalysis of thermohaline fields of the Black Sea was used [9]. The thermosteric H_T and the halosteric H_S components of the steric sea level H_{ster} were calculated as follows:

$$H_{ster} = H_T + H_S,$$
$$H_T = -\int_{z_1}^{z_2} \alpha(z) T'(z) dz, \qquad H_S = \int_{z_1}^{z_2} \beta(z) S'(z) dz, \tag{2}$$
$$T'(z) = T(z) - \overline{T}, \qquad S'(z) = S(z) - \overline{S},$$
$$\alpha(z) = \frac{1}{\rho_0} \frac{\partial \rho(z)}{\partial T}, \qquad \beta(z) = \frac{1}{\rho_0} \frac{\partial \rho(z)}{\partial S},$$

where H_{ster} is the steric level; H_T is the thermosteric level component; H_S is the halosteric level component; and $\overline{T}$, $\overline{S}$ are taken as climatic mean values of temperature and salinity of the Black Sea water. The thermal expansion coefficient α and the salinity compression coefficient β were calculated based on the Gibbs Seawater Oceanographic Toolbox TEOS-10 software package (http://www.teos-10.org/) using a polynomial expression as a function of absolute salinity, conservative temperature and pressure [10]. Since α and β do not change sign over a wide range of temperatures, salinity and pressure, with increasing temperature due to thermal expansion H_T increases, and with increasing salinity the halosteric component of the steric level H_S decreases due to salinity compression.

Results

Using the archive of long-term hydrological data (http://bod-mhi.ru/ru/index.shtml) for 1923–2015 [9] and formula (2) the steric level and its thermosteric and halosteric components were calculated.

A map of the mean annual values of the steric level of the Black Sea is presented in Fig. 1, *a*. The steric level is maximal at the periphery of the sea, where less saline and generally warmer waters predominate. The difference in steric level between the periphery and the central part of the sea is about 15 cm. The spatial distribution does not change qualitatively throughout the year, the level difference decreases from winter to summer.

For the deep-water part of the sea, the difference in steric level values between the maximum in August and the minimum in March can serve as a simple assessment of its seasonal variability. When approaching the continental slope, this difference decreases and even changes the sign (Fig. 1, *b*). This is due not so much to a decrease in the seasonal cycle amplitude, but to changes in its phase, which is explained by the peculiarities of oceanographic processes in the coastal zone.

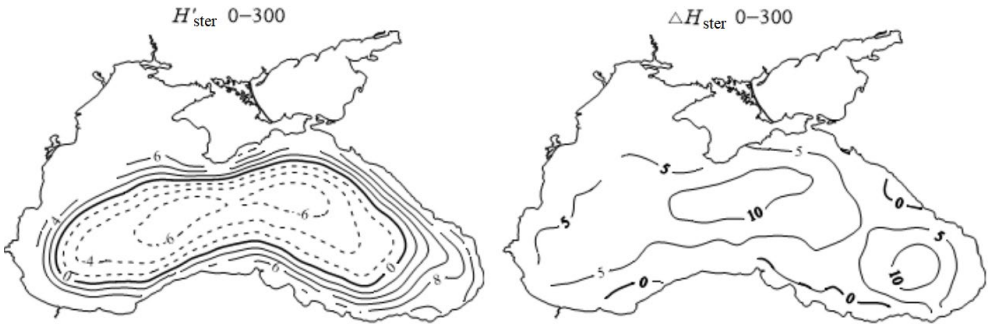

Fig. 1. Mean annual values (cm) of the steric level of the Black Sea H'_{ster} (deviations from the basin mean) in the 0–300 m layer (*a*); difference values of the steric level in August and March, ΔH_{ster} (cm) in the 0–300 m layer (*b*)

Seasonal oscillations of the thermosteric and halosteric level components, which directly reflect changes in the total heat and salt contents of the layer, are almost synchronous in the deep-water part of the sea (Fig. 2). This ensures a stable seasonal cycle of the steric level over most of the sea area, corresponding to the mean seasonal cycle of *T*,*S* ratios in the upper layer of 0–50 m (Fig. 3, *a*). The steric level anomaly is positive from July to October, and it reaches a maximum of 7 cm in August. Moreover, the contribution of the thermosteric component to seasonal variability during this period exceeds the contribution of the halosteric component. In January, H_{ster} is also positive, but with a predominant contribution from the halosteric component (Fig. 2). The steric level becomes negative from February to June, reaching a minimum (–4.5 cm) in March; the contribution of the halosteric component predominates from February to May (Fig. 2).

A comparison of the mean annual values of steric sea level (deviations from the mean for the basin) in the layer of 0–50 m (Fig. 3, *a*) and in the layer of 50–300 m (Fig. 3, *b*) shows that the spatial structure of the distribution of mean long-term values in these layers has a qualitative correspondence, despite positive and negative decadal trends in temperature and salinity in the upper layer [6–8].

In the coastal zone, the relationship between the phases of the seasonal cycle of H_T and H_S can have significant regional differences, which depends on two main factors. The first of them is the spatiotemporal heterogeneity of river runoff and atmospheric precipitation, which affects the seasonal cycle of the steric level in the upper layer of the sea (Fig. 3, *c*). The Dnieper, Southern Bug, Dniester, and Danube rivers flow into the western part of the sea, generally providing more than 80 % of the river runoff into the Black Sea. The influx of the Azov Sea waters with low salinity through the Kerch Strait is also a factor in the desalination of surface waters in the central and western parts of the sea.

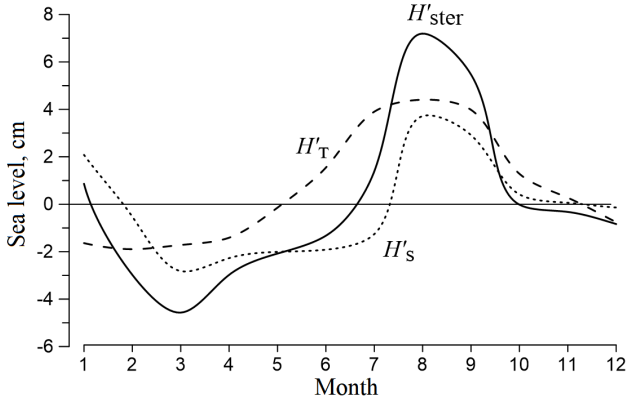

Fig. 2. Seasonal cycle of the mean monthly anomalies (cm) of the steric sea level H'_{ster}, thermosteric H'_T and halosteric H'_s components in the central part of the Black Sea (deviations from the mean values for the year)

Taken together, this manifests itself in an increase in the steric level by more than 5 cm in the western part of the sea (Fig. 3, *c*). The second factor is the general circulation of the sea, which affects the thermohaline structure of waters in the layer of the main pycnocline through vertical movements. The maximum difference in steric level values, reaching 6 cm, occurs at the centers of cyclonic gyres and the Batumi anticyclone (Fig. 3, *d*).

The results of calculations of the steric level oscillations make it possible to indirectly estimate the basin water balance as the difference between the resulting and steric levels. Fig. 4 presents such an assessment based on the steric level data in the central part of the sea and sea level measurements at coastal hydrometeorological stations (mean values from Sevastopol to Batumi). The assessment of the sea level component due to water inflow/outflow H_{wb} corresponds qualitatively to the conventional estimates of the Black Sea water balance [11]: the maximum occurs in May–June, the minimum occurs in September–October. It should be noted that comparison of the sea level measured in the coastal zone with the steric level in the deep sea is not entirely correct. As mentioned above, steric oscillations on the periphery of the sea have their own regional characteristics, so it seems more promising to use mean altimetry data over the entire basin as the resulting sea level [12].

Traditionally, sea level measurements are carried out at coastal tide-gauges (water level stations), unevenly distributed along the Black Sea coast.

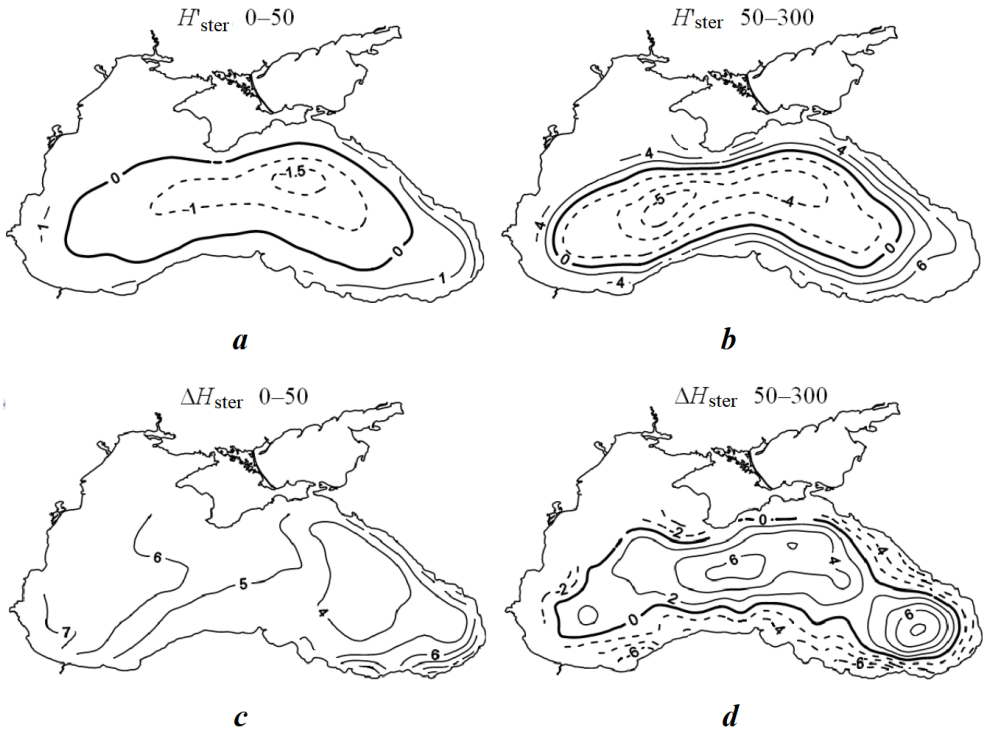

Fig. 3. Mean annual values (cm) of the steric sea level (deviations from the basin mean) in the 0–50 m layer (*a*) and in the 50–300 m layer (*b*); the seasonal cycle (cm) of steric sea level as the difference in values in August and March for the 0–50 m layer (*c*) and the 50–300 m layer (*d*)

Satellite altimeter data are currently used to study sea level variability throughout the basin. According to altimetry data, an increase in the Black Sea level was observed from January 1993 to May 2017 at a mean rate of 2.5 ± 0.5 mm/year [12] against the background of fairly strong interannual variability. In addition, with the launch of a satellite within the framework of the GRACE project in 2002, it became possible to evaluate the contribution of the sea level manometric component H_{man} [12]. The GRACE data are in fairly good agreement with data on the ocean variability and can be used to assess the freshwater balance of the Black Sea and reconstruct the steric level of the Black Sea based on relation (1). To calculate steric oscillations of the Black Sea level based on relation (1) and estimates of their seasonal and interannual variability, satellite altimetry data H and GRACE RL06 H_{man} data for 2002–2016 were used [3, 13]. As a result, the seasonal cycle of the steric sea level H_{ster}, reconstructed from satellite data, was calculated, which corresponds quite well to the seasonal cycle of the Black Sea steric level H'_{ster}, calculated from archival hydrological CTD data (Fig. 5).

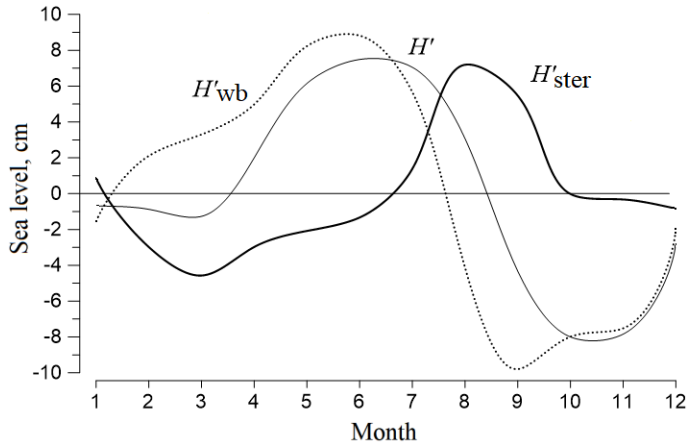

F i g . 4 . Seasonal cycle of the mean monthly values of the steric sea level H'_{ster}, and the sea level according to the tide-gauge measurements at coastal stations H' and sea level component due to the water balance H'_{wb} as difference between H' and H'_{ster}

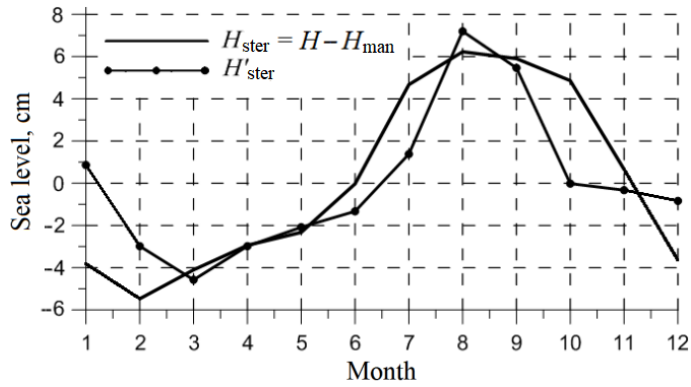

F i g . 5 . Seasonal cycle of the mean monthly values of the steric sea level H'_{ster} according to hydrological observations and the steric sea level according to the altimetry data H and GRACE H_{man} as estimates of the $H_{ster} = H – H_{man}$

The plot of the reconstructed steric level has a smoother shape in the period from June to November, the maximum in August coincides in time with the maximum of the steric level H'_{ster} according to hydrological observations, and the minimum in the seasonal cycle occurs a month earlier than H'_{ster} – in February (Fig. 5). The seasonal cycle of the manometric level according to GRACE data, averaged over the entire sea area, gives more adequate estimates of the water balance component of the sea level in comparison with the preliminary assessment of H_{wb} based on coastal data (see Fig. 4 and 6). The H_{wb} graph has a maximum in June, a month later than H_{man}, and a minimum in September, which coincides with H_{man}; the values of their amplitudes are close (see Fig. 4 and 6). The maxima of the seasonal cycle of both plots in Fig. 6 coincide in April – May, and the minima for the freshwater balance according to the climate data falls on August [11], and for the manometric level H_{man} – on September (a month later) (Fig. 6). This is apparently due to the fact that the seasonal cycle of H_{man} according to GRACE data was averaged for 2002–2016 and actually belongs to a different climatic period. In addition, differences in the phase and amplitude of the seasonal cycle of H_{man} and the freshwater balance are due to the fact that variations in the water balance of the sea are influenced not only by its freshwater balance (rivers, precipitation, evaporation), but also by water exchange through the straits (Fig. 6).

The sea level according to the altimetry data H and the manometric component of sea level H_{man} according to GRACE RL06 GFSC data, averaged over the Black Sea, are characterized by significant interannual variability (Fig. 7). The maxima and minima of level oscillations and its manometric component coincide in phase, and the difference in their amplitudes gives the steric component of the sea level (Fig. 7, 8).

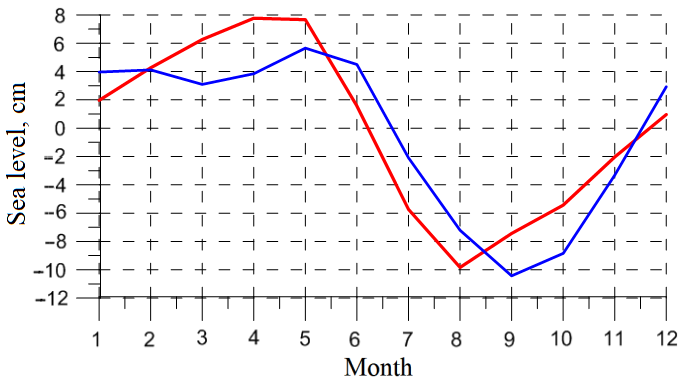

Fig. 6. Seasonal cycle of monthly average values of the Black Sea freshwater balance according to climate data [11] (red line) and manometric level H_{man} (GRACE RL06 GSFC 2003–2016) (blue line)

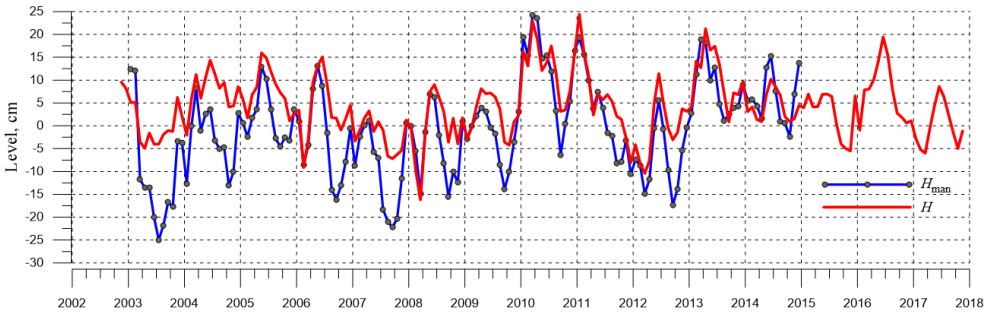

Fig. 7. Mean level of the Black Sea according to altimetry data H and manometric component of sea level H_{man} from GRACE RL06 GFSC data

There are several periods with different modes of mean sea level variability: 2004–2006 and 2012–2013 with a pronounced seasonal cycle with an amplitude of up to 15 cm; 2007–2009 – with the absence of a summer maximum level in 2007 and small amplitudes of up to 10 cm; 2010–2011 – with maximum amplitudes up to 25 cm; 2012–2013 and 2014–2015 – with the minimum amplitudes for the entire period of 2003–2018 (less than 10 cm) (Fig. 7). The coincidence of the sea level maxima and the manometric component in amplitude and phase in 2010 and 2011 indicates that in these years the main contribution to the sea level was provided by the water balance component (Fig. 7). The authors of [14] D. L. Volkov and F. V. Landerer also came to the conclusion that the maximum sea level and manometric component in 2010 and 2011 were caused by the maximum moisture content in the Black Sea drainage basin, which led to an increase in the total river flow.

Based on relation (1) using basin sea level averaged according to the altimetry data H and the manometric component of sea level H_{man} according to GRACE RL06 GFSC data, the mean reconstructed steric level H_{ster} for the Black Sea was obtained (Fig. 8). The steric component is also characterized by significant interannual variability with different modes of oscillation: 2005–2009 and 2012 – quasi-regular oscillations of the steric level with an amplitude of up to 15 cm; 2010–2011 and 2013–2015 – violation of quasi-regularity of oscillations and a decrease in amplitude to 5 cm (Fig. 8). In addition, the trend of the reconstructed steric level is negative (–0.59 ± 0.21 cm/year). The estimates of interannual oscillations in the H_{ster} level reconstructed from the satellite data are confirmed by calculations of the mean steric level based on CTD data from Argo profiler floats No. 4900542, 6900805, 2901200 (Fig. 8). The trajectory of the Argo float No. 4900542 passed through the deep-water part of the sea, then the float was in the Batumi anticyclone for a long time. Floats No. 6900805 and 2901200 made

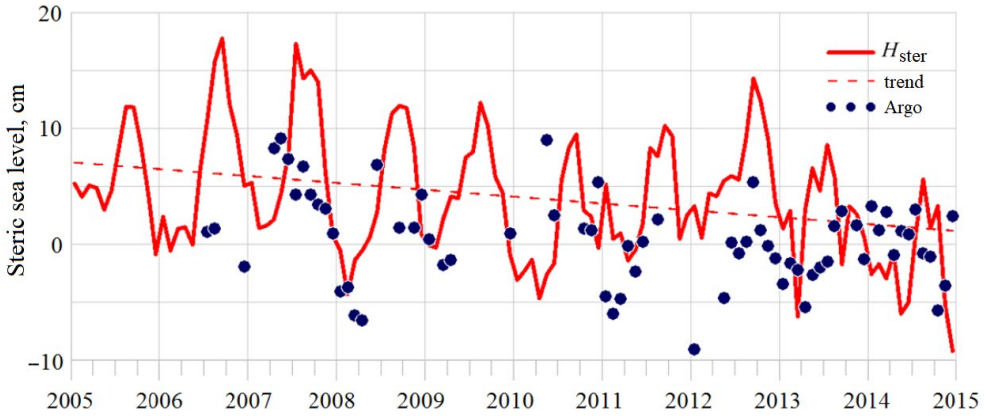

Fig. 8. Reconstruction of the sea mean steric level $H_{ster} = H - H_{man}$ and mean steric level according to Argo floats No. 4900542, 6900805, and 2901200

several revolutions in the deep-water part of the sea approximately along the Rim Current. Despite the incomplete coverage of the Black Sea with data from these floats, the steric level calculated from their CTD profiles can be considered as an independent instrumental assessment confirming the general trend of interannual changes in the H_{ster} level reconstructed from satellite data. The range of steric oscillations according to Argo floats is approximately twice smaller than that of H_{ster}, and, accordingly, the negative trend is also smaller: −0.22 ± 0.05 cm/year (Fig. 8).

Discussion

The importance of studying sea level variability, including its steric and manometric components, is due to the direct connection of the sea level with the basin water balance and the sea thermohaline structure. The use of satellite altimetry and gravimetric data revealed that the contribution of these both components to the interannual variability of the Black Sea level is approximately the same. The inland Black Sea is a suitable case study for conducting methodological work on the joint use of altimetry and gravimetric data as an alternative to conventional assessments of steric oscillations and basin water balance. However, the variability of the manometric level component is additionally affected by the Black Sea drainage basin soil moisture. To eliminate these errors, our work used GRACE RL06 GSFC data obtained based on the calculation method using mascons [15]. Another approach to correcting the influence of the signal from the variability of soil moisture is to use the hydrological reanalysis models [16] and take into account the soil moisture signal of the Black Sea drainage basin according to GRACE data for land [14, 16].

Our estimates of interannual variability and negative trend in the steric level of the Black Sea reflect the integral effect of thermohaline changes throughout the entire water column. In the seasonal cycle for the upper 300-meter layer, the contribution of the thermosteric component of the steric level in the summer period is 1–2 cm higher than the contribution of the halosteric component, and vice versa in the winter period (see Fig. 2). In recent decades, according to numerical modeling and field observations, a negative linear trend in salinity (–0.02 PSU/year) in the 0–50 m layer has been identified, which is due to a positive trend in the fresh water balance of the Black Sea. There are not statistically significant trends in the Black Sea surface temperature in recent years [8]. With increasing depth between the CIL core and its lower boundary, thermosteric and halosteric effects compensate each other [5]. In the 75–300 m layer, positive trends in salinity and temperature have been observed in recent decades at an average rate of 0.05 PSU/10 years and 0.02 °C/10 years [7]. Instrumental measurements revealed that for the northeastern part of the Black Sea, climate changes led to a noticeable increase in salinity in the upper 200-meter layer, as well as an increase in temperature in the layers located below the temperature minimum layer (CIL) [17]. Thus, in the layer below 50–75 m, a simultaneous increase in salinity and temperature leads to multidirectional trends in the steric component of sea level oscillations.

Nevertheless, the trends in the steric level reconstructed from satellite data, reflecting changes in the entire sea water column from the surface to the bottom, and the trends from Argo floats CTD profiles in the 0–500 m layer have negative values (Fig. 8). This means that, integrally over depth in the layer below 50 m, an increase in salinity leads to a decrease in the steric level throughout the sea, exceeding the positive contribution of the thermosteric component from an increase in temperature. The inflow of more saline and warm waters into the deep layers of the Black Sea occurs through the system of Turkish straits. However, determining the water fluxes through the Bosphorus using traditional methods is attended with great difficulties. In the future, it will be possible to estimate water exchange through the straits using the sea level according to the altimetry data and the manometric level component according to GRACE data [16].

Conclusions

Based on satellite altimetry and gravimetric data, the time-series of steric oscillations in the Black Sea level for 2002–2016 was reconstructed. Its comparison with the steric level estimates calculated from archival hydrological data confirmed good agreement between them. The estimates of the seasonal cycle of the steric level were obtained: the range of oscillations reaches 12 cm, the minimum occurs in the winter period (March), the maximum occurs in the summer period (August). The seasonal cycle of the steric level reconstructed from satellite data has a smoother shape compared to the calculations of the steric level H'_{ster} from archival hydrological data. The reconstructed steric level attains its maximum in August and

coincides in time with the maximum H'_{ster}, and the minimum occurs a month earlier than H'_{ster} – in February. For the seasonal cycle of the manometric component of sea level, according to GRACE data, good agreement was obtained with the seasonal cycle of the Black Sea freshwater balance, calculated from hydrometeorological observations.

The maximum difference in the steric level H'_{ster} between the periphery and the center of the sea was about 15 cm. The regions of the maximum range of the seasonal cycle in the steric level have been identified. These areas correspond to the areas of maximum seasonal vertical displacements of the main pycnocline. A comparison of the mean annual values of steric sea level (deviations from the basin mean) in the 0–50 m layer and in the 50–300 m layer shows that, despite the opposite directional decadal trends in temperature and salinity, the spatial distribution of the long-term mean values in these layers is qualitatively consistent.

The steric level H_{ster} reconstructed from satellite data is characterized by significant interannual variability with periods of various oscillation modes with timescale about 3 years and amplitude changes from 5 to 15 cm. In 2010–2011 and 2013–2015, there was a violation of the quasi-regularity of steric oscillations and a decrease in their amplitude under 5 cm. The estimate of the linear trend of the reconstructed steric level has a negative sign and amounts to -0.59 ± 0.21 cm/year. The steric level was also calculated from Argo floats CTD profiles, which provided an independent instrumental estimate confirming the general trend of interannual changes in the reconstructed steric level H_{ster}. The range of steric oscillations according to Argo floats is approximately twice smaller than that of H_{ster}, and, accordingly, the negative trend coefficient is smaller (-0.22 ± 0.05 cm/year). The general negative trend in the steric component of the Black Sea level indicates that among the thermohaline properties impacts on the sea level, the contribution of an increase in salinity prevails over the contribution of an increase in water temperature. In addition to the regional heat and water balance, changes in the thermohaline structure of waters and the steric component of sea level are affected by the inflow of saline and warm waters into the Black Sea through the system of Turkish straits. In the future, it seems possible to estimate water exchange through the Bosphorus using the discussed approach of combining altimetry and gravimetric measurements.

REFERENCES

1. Malinin, V.N., Gordeeva, S.M. and Shevchuk, O.I., 2019. Changes in the Global Sea Level in the Current Century. *Sovremennye Problemy Distantsionnogo Zondirovaniya Zemli iz Kosmosa = Current Problems in Remote Sensing of the Earth from Space*, 16(5), pp. 9–22 (in Russian).
2. Gregory, J.M., Griffies, S.M., Hughes, C.W., Lowe, J.A., Church, J.A., Fukimori, I., Gomez, N., Kopp, R.E., Landerer, F. [et al.], 2019. Concepts and Terminology for Sea Level: Mean, Variability and Change, both Local and Global. *Surveys in Geophysics*, 40, pp. 1251–1289. doi:10.1007/s10712-019-09525-z
3. Ponte, R.M., 1999. A Preliminary Model Study of the Larger-Scale Seasonal Cycle in Bottom Pressure over the Global Ocean. *Journal of Geophysical Research: Oceans*, 104(C1), pp 1289–1300. doi:10.1029/1998JC900028

4. Arkhipkin, V.S. and Berezhnoi, V.Yu., 1995. Steric Oscillations of the Black Sea Level. *Oceanology*, 35(6), pp. 735–741.
5. Stanev, E.V., Peneva E. and Chtirkova, B., 2019. Climate Change and Regional Ocean Water Mass Disappearance: Case of the Black Sea. *Journal of Geophysical Research: Oceans*, 124(7), pp. 4803–4819. doi:10.1029/2019JC015076
6. Knysh, V.V., Korotaev, G.K., Moiseenko, V.A., Kubryakov, A.I., Belokopytov, V.N. and Inyushina, N.V., 2011. Seasonal and Interannual Variability of Black Sea Hydrophysical Fields Reconstructed from 1971–1993 Reanalysis Data. *Izvestiya, Atmospheric and Oceanic Physics*, 47(3), pp. 399–411. doi:10.1134/S000143381103008X
7. Polonsky, A.B., Shokurova, I.G. and Belokopytov, V.N., 2013. The Decadal Variability of Temperature and Salinity in the Black Sea. *Morskoy Gidrofizicheskiy Zhurnal*, (6), pp. 27–41 (in Russian).
8. Miladinova, S., Stips, A., Garcia-Gorriz, E. and Macias Moy, D., 2017. Black Sea Thermohaline Properties: Long-Term Trends and Variations. *Journal of Geophysical Research: Oceans*, 122(7), pp. 5624–5644. doi:10.1002/2016JC012644
9. Belokopytov, V.N., 2018. Retrospective Analysis of the Black Sea Thermohaline Fields on the Basis of Empirical Orthogonal Functions. *Physical Oceanography*, 25(5), pp. 380–389. doi:10.22449/1573-160X-2018-5-380-389
10. Roquet, F., Madec, G., McDougall, T. and Barker, P., 2015. Accurate Polynomial Expressions for the Density and Specific Volume of Seawater using the TEOS-10 Standard. *Ocean Modelling*, 90, pp. 29–43. doi:10.1016/j.ocemod.2015.04.002
11. Simonov, A.I. and Altman, E.N., 1991. [*Hydrometeorology and Hydrochemistry of Seas of the USSR. Vol. 4. The Black Sea. Iss. 1. Hydrometeorological Conditions*]. Saint Petersburg: Gidrometeoizdat, 429 p. (in Russian).
12. Avsar, N.B., Jin, S. and Kutoglu, S.H., 2018. Recent Sea Level Changes in the Black Sea from Satellite Gravity and Altimeter Measurements. In: T. Tanzi, M. Chandra, O. Altan and F. Sunar, eds., 2018. *The International Archives of the Photogrammetry, Remote Sensing and Spatial Information Sciences. 18–21 March 2018, Istanbul, Turkey.* Istanbul. Vol. XLII-3/W4, pp. 83–85. doi:10.5194/isprs-archives-XLII-3-W4-83-2018
13. Lemeshko, E.E., Lemeshko, E.M. and Novitskaya, V.P., 2021. Influence of the Arctic Oscillation on the Formation of Water Circulation Regimes in the Sector of the North, Norwegian and Barents Seas. *Ecological Safety of Coastal and Shelf Zones of Sea*, (2), pp. 47–64. doi:10.22449/2413-5577-2021-2-47-64 (in Russian).
14. Volkov, D.L. and Landerer, F.W., 2015. Internal and External Forcing of Sea Level Variability in the Black Sea. *Climate Dynamics*, 45(9–10), pp. 2633–2646. doi:10.1007/s00382-015-2498-0
15. Loomis, B.D., Luthcke, S.B. and Sabaka, T.J., 2019. Regularization and Error Characterization of GRACE Mascons. *Journal of Geodesy*, 93(9), pp. 1381–1398. doi:10.1007/s00190-019-01252-y
16. Fenoglio-Marc, L., Rietbroek, R., Grayek, S., Becker, M., Kusche, J. and Stanev, E., 2012. Water Mass Variation in the Mediterranean and Black Seas. *Journal of Geodynamics*, 59–60, pp. 168–182. doi:10.1016/j.jog.2012.04.001
17. Podymov, O.I., Zatsepin, A.G. and Ocherednik, V.V., 2021. Increase of Temperature and Salinity in the Active Layer of the North-Eastern Black Sea from 2010 to 2020. *Physical Oceanography*, 28(3), pp. 257–265. doi:10.22449/1573-160X-2021-3-257-265

Submitted 21.04.2023.; accepted after review 15.06.2023;
revised 28.06.2023; published 25.09.2023

About the authors:

Victoria P. Novitskaya, Senior Research Engineer, Marine Hydrophysical Institute of the Russian Academy of Sciences (299011, Russia, Sevastopol, Kapitanskaya St., 2), **SPIN code: 9079-6274; ResearcherID; Scopus Author ID;** *doronina.viktori@mail.ru*

Evgeny M. Lemeshko, Senior Research Associate, Marine Hydrophysical Institute of RAS (2 Kapitanskaya St., Sevastopol, 299011, Russian Federation), Ph.D. (Phys.-Math.), **SPIN code**: **3836-5786**, **ResearcherID**: **S-7815-2018**, **Scopus Author ID**: **6508300982**, *evgeny.lemeshko@mhi-ras.ru*

Vladimir N. Belokopytov, Head of the Department of Oceanography, Leading Researcher, Marine Hydrophysical Institute of the Russian Academy of Sciences (299011, Russia, Sevastopol, Kapitanskaya St., 2), Doctor of Geographical Sciences, **SPIN code: 5697-5700; ResearcherID: ABA-1230-2020; Scopus Author ID: 6602381894,** *v.belokopytov@gmail.com*

Contribution of the authors:

Victoria P. Novitskaya – publications review, processing of altimetry data for the study, analysis of the results and their interpretation, plotting, description of the study results.

Evgeny M. Lemeshko – general scientific guidance of research, formulation of objectives and tasks of the study, choice of data analysis methods, calculation of steric component of the sea level from satellite data, analysis of the study results, their interpretation, formula of conclusions.

Vladimir N. Belokopytov – calculation and analysis the Black Sea steric level and their thermosteric and halosteric components based on the archive of long-term hydrological data.

All the authors have read and approved the final manuscript.

Original article

Structure and Climatic Intra-Annual Variability of Water Mass Characteristics in the Powell Basin and on the Adjacent Antarctic Peninsula Shelf

Yu. V. Artamonov, E. A. Skripaleva *, N. V. Nikolskii

Marine Hydrophysical Institute of RAS, Sevastopol, Russia
** e-mail: sea-ant@yandex.ru*

Abstract

The paper analyzes the long-term average structure and climatic intra-annual variability of water mass characteristics in the Powell Basin and adjacent water areas based on monthly average potential temperature and salinity data for each year from 1958 to 2021 from *ECMWF ORA-S*5 reanalysis. It is shown that the Antarctic Shelf Water is observed not only over the shallow shelf of the Joinville Archipelago, but also over the continental slope in the northwestern Weddell Sea. It is revealed that the layer of Circumpolar Deep Water is divided into Upper and Lower modifications. The Deep and Bottom Waters of the Weddell Sea do not appear as separate extremes on the long-term average θ,*S*-curves. It is shown that in the center of the cyclonic gyre in the Powell Basin, the Antarctic Winter Water core is located in a layer of 25–55 m. In the Scotia Sea, the Hesperides Trough, and over the Philip Ridge, the Antarctic Winter Water core deepens to 60–85 m. The minimum depths of the cores of the Upper and Lower modifications of the Circumpolar Deep Water (250–300 m and 500–600 m, respectively) are observed in the central part of the Powell Basin and closer to the center of the Weddell Sea Gyre, the maximum depths (1000–1300 m and 1100–1500 m, respectively) are observed over the slopes of the depths of the Joinville shelf and the South Scotia, Philip, and Joinville Ridges. It is shown that seasonal changes in the θ-index of the Antarctic Surface Water are maximum (3.5–4°C) in the southern Scotia Sea and in the Hesperides Trough. Seasonal changes in the *S*-index are maximum (1.8–1.9 PSU) over the Philip Ridge and in the northern and southern parts of the Powell Basin. Intra-annual changes in the θ,*S*-indices of the Antarctic Shelf Water reach 1.6–1.8 °C and 1.5 PSU, respectively. The Weddell Sea Surface Water is characterized by weak changes in the θ-index, while changes in its *S*-index reach almost 1.8 PSU. Intra-annual changes in the θ,*S*-indices of Antarctic Winter Water are maximum in the central part of the Powell Basin (up to 1 °C and 1.1 PSU).

Keywords: Southern Ocean, Weddell Sea, Powell Basin, Antarctic shelf, water masses, potential water temperature, salinity, neutral density, spatiotemporal variability, vertical water structure

Acknowledgments: The work was carried out under FSBSI FRC MHI state assignment FNNN-2021-0004 «Fundamental studies of oceanological processes which determine the state and evolution of the marine environment influenced by natural and anthropogenic factors, based on observation and modeling methods» («Oceanological processes» code).

For citation: Artamonov, Yu.V., Skripaleva, E.A. and Nikolskii, N.V., 2023. Structure and Climatic Intra-Annual Variability of Water Mass Characteristics in the Powell Basin and on the Adjacent Antarctic Peninsula Shelf. *Ecological Safety of Coastal and Shelf Zones of Sea*, (3), pp. 22–39.

Структура и климатическая внутригодовая изменчивость характеристик водных масс в котловине Пауэлл и на прилегающем шельфе Антарктического полуострова

Ю. В. Артамонов, Е. А. Скрипалева *, Н. В. Никольский

Морской гидрофизический институт РАН, Севастополь, Россия

* *e-mail: sea-ant@yandex.ru*

Аннотация

По среднемесячным значениям потенциальной температуры и солености для каждого года с 1958 по 2021 г. из реанализа *ECMWF ORA-S*5 проанализированы среднемноголетняя структура и климатическая внутригодовая изменчивость характеристик водных масс котловины Пауэлл и прилегающих акваторий. Показано, что антарктическая шельфовая вода наблюдается не только над мелководным шельфом архипелага Жуэнвиль, но и над свалом глубин в северо-западной части моря Уэдделла. Выявлено, что слой циркумполярной глубинной воды разделяется на верхнюю и нижнюю модификации. Глубинная и донная воды моря Уэдделла в виде отдельных экстремумов на среднемноголетних θ,*S*-кривых не проявляются. Показано, что в центре циклонического круговорота в котловине Пауэлл ядро антарктической зимней воды располагается в слое 25–55 м. В море Скоша, желобе Гесперид и над хребтом Филипп оно заглубляется до 60–85 м. Минимальные глубины залегания ядер верхней и нижней модификаций циркумполярной глубинной воды (соответственно 250–300 и 500–600 м) наблюдаются в центральной части котловины Пауэлл и ближе к центру круговорота моря Уэдделла, максимальные глубины (соответственно 1000–1300 и 1100–1500 м) – над свалами глубин шельфа Жуэнвиль и хребтов Южный Скоша, Филипп и Жуэнвиль. Показано, что сезонные изменения θ-индекса антарктической поверхностной воды максимальны (3.5–4 °С) в южной части моря Скоша и в желобе Гесперид, *S*-индекса (1.8–1.9 ЕПС) – над хребтом Филипп и в северной и южной частях котловины Пауэлл. Внутригодовые изменения θ,*S*-индексов антарктической шельфовой воды достигают 1.6–1.8 °С и 1.5 ЕПС соответственно. Поверхностная вода моря Уэдделла характеризуется слабыми изменениями θ-индекса, тогда как изменения ее *S*-индекса достигают почти 1.8 ЕПС. Внутригодовые изменения θ,*S*-индексов антарктической зимней воды максимальны в центральной части котловины Пауэлл (до 1 °С и 1.1 ЕПС).

Ключевые слова: Южный океан, море Уэдделла, котловина Пауэлл, антарктический шельф, водные массы, потенциальная температура морской воды, соленость, нейтральная плотность, пространственно-временная изменчивость, вертикальная структура вод

Благодарности: работа выполнена в рамках государственного задания ФГБУН ФИЦ МГИ по теме FNNN-2021-0004 «Фундаментальные исследования океанологических процессов, определяющих состояние и эволюцию морской среды под влиянием естественных и антропогенных факторов, на основе методов наблюдения и моделирования» (шифр «Океанологические процессы»).

Для цитирования: *Артамонов Ю. В., Скрипалева Е. А., Никольский Н. В.* Структура и климатическая внутригодовая изменчивость характеристик водных масс в котловине Пауэлл и на прилегающем шельфе Антарктического полуострова // Экологическая безопасность прибрежной и шельфовой зон моря. 2023. № 3. С. 22–39. EDN ZDFRLB.

Introduction

Water masses and their boundaries (hydrological fronts) are the most important abiotic factors that determine the level of bioproductivity of water, influencing the spatial distribution of nutrients [1–7]. The most bioproductive area is the southwestern part of the Southern Ocean Atlantic sector, where the Antarctic krill spawn on the vast Antarctic Peninsula shelf. The krill transported from spawning grounds along the western periphery of the Weddell Sea Gyre (WSG) accumulate in the Powell Basin [8–10]. Further, the main transfer of the krill aggregations occurs along the northern periphery of the WSG, passing along the Philip and South Scotia Ridges that bound the Powell Basin from the north [2, 3, 5]. The commercial significance of the shelf areas of the Antarctic Peninsula, the northwestern Weddell Sea, and the Powell Basin led to the appearance of a number of works devoted to the study of the processes of formation, modification and distribution of water masses in this region [1)] [2, 10–21].

The research results show that, in general, the vertical structure of the local waters is characterized by the following features [1)] [1, 2, 11–14, 17–20].
In the upper layer, there are Antarctic Surface Waters (AASW) consisting of two modifications. They are relatively warm and desalinated well-mixed Summer Waters (AASSW) and colder and saltier Winter Waters (AASWW). Deeper down, there is a subsurface layer of the Antarctic Winter Water (AAWW) characterized by the minimum temperature and representing the remnants of the previous winter upper mixed layer of the AASWW. Below, a layer of circumpolar deep water (CDW) lies, which, to the south of the Antarctic Circumpolar Current (ACC) system, is called “warm deep water” (WDW) according to the terminology of some authors [12, 14, 15, 20]. In the upper part of the layer, the CDW is determined by the maximum temperature (Upper CDW), and at intermediate depths – by the maximum salinity (Lower CDW). It should be noted that some authors believe that in the WSG region, it is impossible to divide the CDW layer into Upper and Lower modifications [2]. Other authors [18] believe that to the south of the ACC system, the entire CDW layer is occupied by its Lower modification characterized by the maximum salinity.

[1)] Sarukhanyan, E.I. and Smirnov, N.P., 1986. [*Water Masses and Circulation of the South Ocean*]. Leningrad: Gidrometeoizdat, 288 p. (in Russian).

In [20], three modifications of the WDW with different thermohaline characteristics were identified in the Powell Basin: Upper, Middle, and Lower. Underneath the CDW layer, a layer of Weddell Sea Deep Water (WSDW) lies, under which a layer of Weddell Sea Bottom Water (WSBW) is located. The WSDW from the Powell Basin penetrates north into the Hesperides Trough and into the Scotia Sea through the deep-sea passages of the surrounding bottom uplifts [2, 15–18], while the WSBW does not spread beyond the WSG boundaries [17, 22].

The Antarctic Shelf Waters (AAShW) with temperatures close to the sea water freezing point are formed on the shallow shelves surrounding the Powell Basin as a result of powerful autumn-winter convection, leading to thermal uniformity throughout the entire layer, from the surface to the bottom. These waters are characterized by low salinity in summer when sea ice melts over the Antarctic shelf, and high salinity in winter when the sea ice is formed [1] [1, 2, 11–14, 17, 19, 20].

It should be noted that most studies that analyze the structure of water masses in the region under consideration are based on the data provided by irregular synoptic hydrological measurements, carried out due to severe weather conditions mainly in the warm period and not always coinciding in space. Analysis and identification of water masses based on data from scattered synoptic surveys at individual sections and hydrological stations lead to the fact that the amount of water masses does not coincide with their modifications in the works of various authors [2, 18, 20].

Currently, constant replenishment of factual databases and increase in the length of time series of remote measurements contribute to the introduction of modern versions of oceanic reanalyses, which assimilate all available data from contact and satellite measurements. The use of such reanalyses makes it possible to clarify the long-term average spatial structure of waters and provide estimates of intra-annual changes in the characteristics of water masses, which is necessary to interpret the structural features of waters obtained from the results of actual field measurements [9, 10, 19, 20, 23].

The purpose of this work is to use the *ECMWF ORA-S5* oceanic reanalysis data to analyze the long-term average spatial structure of water masses and study the climatic intra-annual variability of their characteristics in the Powell Basin and adjacent waters (the eastern shelf of the Antarctic Peninsula and the northwestern Weddell Sea).

Materials and methods

The research examines the region of the Southern Ocean east of the Antarctic Peninsula, located between 60° and 65° south and 56° and 47.5° west. It includes the shelf of the Joinville Archipelago, the Powell Basin, the northwestern Weddell Sea, and the southwestern Scotia Sea. The Powell Basin is separated from the main basin of the Weddell Sea by the Joinville Ridge, and from the Scotia Sea by the South Scotia and Philip Ridges (Fig. 1, *a*). When constructing the bottom topography diagram, the data from *General Bathymetric Chart of the Oceans* (*GEBCO*) (URL: http://www.gebco.net/data_and_products/gridded_bathymetry_data/) were used with a spatial resolution of 15 arcseconds.

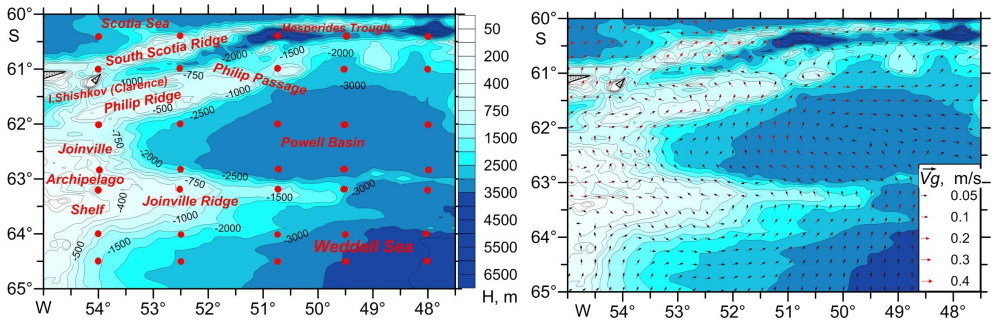

F i g . 1 . Study area (*a*) and distribution of long-term average vectors of geostrophic currents (*b*). The red dots show the grid nodes for which examples of θ,*S*-curves are presented in Fig. 3

Analysis of the thermohaline structure of waters and identification of water masses were carried out in accordance with *European Centre for Medium-Range Weather Forecasts OCEAN*5 *system* (*ECMWF ORAS*5) (URL: https://cds.climate.copernicus.eu/cdsapp#!/dataset/reanalysis-oras5?tab=form) reanalysis data. The reanalysis contains monthly averages of potential temperature θ (°C) and salinity *S* (PSU) at grid points of approximately 0.25° × 0.25° at 75 vertical levels in *sigma*-coordinates for each year within the period from 1958 to 2021. These values are derived from the *Nucleus for European Modelling of the Ocean* (*NEMO*) ocean model and the *NEMOVAR* ocean assimilation system adopting surface and subsurface temperature, salinity, sea ice concentration, and sea level anomalies [24]. Based on the initial data, long-term and climatic monthly average values of potential temperature and salinity were calculated. To identify the cores of water masses and their thermohaline indices, long-term and climatic monthly average θ,*S*-curves were constructed at each grid node. According to the classical *T*,*S*-analysis, the amount of water masses was determined on the θ,*S*-curve by the number of extrema plus two end points [2), 3)] [25]. To clarify the vertical structure of the waters, we analyzed the vertical distributions of neutral density γ^n (kg/m^3), which is a function of salinity, in situ temperature, pressure, longitude and latitude [26] and indirectly reflects the position of the boundaries of water masses. When assessing the seasonal variability of thermohaline indices of water masses, the spatial distributions of intra-annual root-mean-square deviations (RMSD) of temperature and salinity were analyzed.

The spatial distributions of water mass characteristics were interpreted against the background of the geostrophic circulation of water. The long-term

---

[2)] Mamayev, O.I., 1975. *Temperature-Salinity Analysis of World Ocean Waters*. Amsterdam: Elsevier Scientific Publishing, 374 p.

[3)] Bulgakov, N.P., 1975. [*Convection in the Ocean*]. Moscow: Nauka, 272 p. (in Russian).

average structure of currents was analyzed using the *Copernicus Marine Environment Monitoring Service* (*CMEMS*) (URL: http://marine.copernicus.eu/?option=com_csw&view=details&product_id=SEA-LEVEL_GLO_PHY_L4_REP_OBSERVATIONS_008_047) reanalysis data containing average daily values of geostrophic velocity components at regular grid nodes with a step of 0.25° from 1993 to 2020. These values were used when calculating the long-term average values of the velocity modulus $\vec{V}g$ and the direction of current vectors (Fig. 1, *b*).

Main results

Distributions of long-term average values of potential temperature and salinity on vertical meridional sections and long-term average θ,*S*-curves, examples of which are presented in Figs. 2 and 3, showed that the structure of waters in the studied water areas differing in orographic conditions also differentiates significantly.

In deep-water areas of the water area, such as the southern Scotia Sea, the Hesperides Trough, the Powell Basin, the northwestern Weddell Sea, adjacent to the Antarctic shelf, the Antarctic type of vertical water structure can be observed. In the distributions of temperature (Fig. 2, *a*, *c*, *e*) and long-term average θ,*S*-curves (Fig. 3) north of the shelf and the Joinville Ridge in a layer of approximately 25–150 m, subsurface minimum θ characterizing the Antarctic Winter Water is clearly visible. Temperature values in the Antarctic Winter Water layer decrease significantly in the deep-sea areas between the South Scotia and Philip Ridges and over the slopes of the depths of the Joinville Ridge (θ < −1.5 °C) and increase (θ < −1 °C) in the Scotia Sea, Hesperides Trough, and central part of the Powell Basin (Figs. 2, *a*, *c*, *e*; 3). The distribution of neutral density isolines γ^n shows that isopycnic line 27.95 can be conventionally taken as the lower boundary of the Antarctic Winter Water. In the open Weddell Sea, the subsurface minimum corresponding to the Antarctic Winter Water is not observed in the long-term average temperature field, and the entire near-surface layer is occupied by the coldest (θ < −1.6 °C) and low-salinity (*S* < 33.6 PSU) Antarctic Surface Water of the high-latitude modification, which is called the Weddell Sea Surface Water (WSSW) in accordance with [2] (Figs. 2, *c* – *f*; 3, *b*, *c*).

Under the Antarctic Winter Water layer in the southern Scotia Sea, temperature increase is observed, and at the depths of 400–1000 m its intermediate maximum (θ ~ 1–1.2 °C) can be found, which is typical for the Circumpolar Deep Water Upper modification (UCDW) (Figs. 2, *a*; 3, *a*). Under the temperature maximum layer at the depths of 700–1400 m, weak salinity maximum (34.7–34.705 PSU) is observed, which characterizes the CDW Lower modification (LCDW) (Figs. 2, *b*; 3, *a*). The upper boundary of the UCDW layer qualitatively corresponds to the position of isopycnic line 28.05, the upper boundary of the LCDW layer corresponds qualitatively to the position of isopycnic line 28.1, which is consistent with the results of [18]. At the same time, the identification of two CDW modifications (Upper and Lower) in the southern Scotia Sea clarifies the results of this work, according to which the entire CDW layer is occupied by its Lower modification to the south of the ACC system. To the south of the South Scotia Ridge, over the deep slopes of the depths of the Philip Ridge and the Joinville shelf, temperature increase is observed, corresponding to the UCDW, which can be monitored almost to the bottom (Fig. 2, *a*).

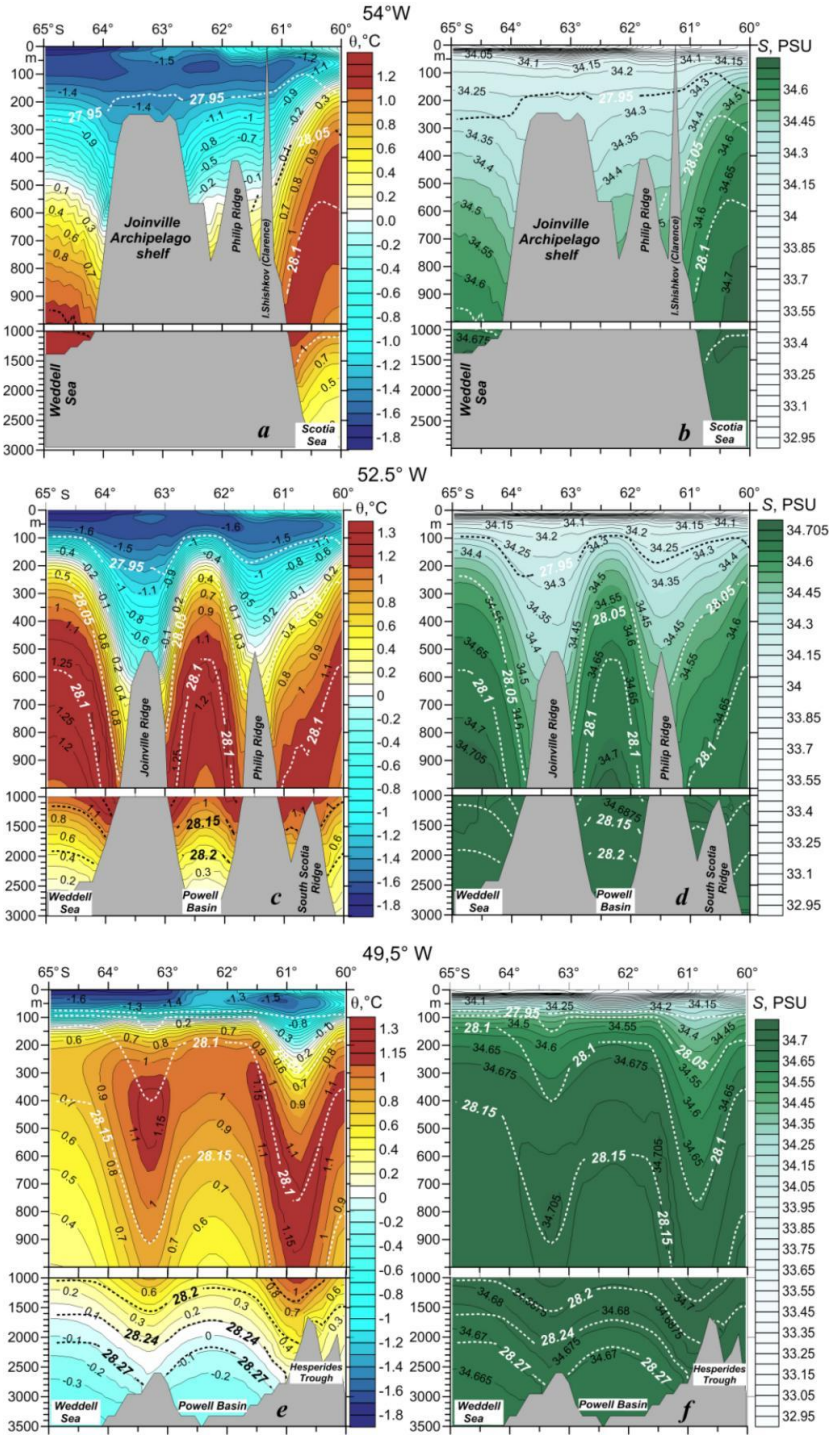

Fig. 2. Vertical distributions of long-term average potential temperature (*a*, *c*, *e*) and salinity (*b*, *d*, *f*) at sections along 54° W (*a*, *b*), 52.5° W (*c*, *d*) and 49.5° W (*e*, *f*). The dashed line shows neutral density γ^n isolines

Deeper than the LCDW layer in the southern Scotia Sea, monotonous temperature decrease is observed with uniform salinity distribution, corresponding to colder (θ < 0.5 °C) and less saline (S < 34.7 PSU) WSDW (Figs. 2, *a*, *b*; 3, *a*). According to the distribution of vectors of geostrophic currents (see Fig. 1, *b*) and the results shown in [2, 15–18], the WSDW penetrates into the Scotia Sea from the Weddell Sea and the Powell Basin through the deep-sea passages of the Philip and South Scotia Ridges. The upper WSDW boundary here corresponds approximately to the position of isopycnic line 28.15 (Figs. 2, *a*, *b*; 3, *a*).

To the east, in deep-water areas located between the Southern Scotia, Philip and Joinville Ridges (the Scotia Sea, the Powell Basin, the Weddell Sea), due to the cyclonic direction of the currents (see Fig. 1, *b*), a noticeable rise of the CDW layer is observed closer to the surface (Fig. 2, *c* – *f*).

In the central part of the Powell Basin and in the deep-sea part of the Weddell Sea, closer to the WSG center, the upper and lower boundaries of the UCDW and LCDW are located approximately 500–600 m higher than over the slopes of the depths, judging by the position of layers of intermediate temperature and salinity maxima and neutral density γ^n isopycnic lines 28.05, 28.1, and 28.15 (Figs. 2, *e*, *f*; 3, *c*). Due to the intense rise of colder waters, the intermediate temperature maximum weakens, the temperature in the UCDW layer decreases by approximately 0.2–0.3 °C (Fig. 2, *e*). It should be noted that in the Weddell Sea, in the lower part of the CDW layer, a weak maximum of salinity can be observed, which, in contrast to [2], makes it possible to divide the CDW layer into Upper and Lower modifications.

Under the CDW layer, deeper than 1500–2000 m, monotonous temperature decrease and uniform salinity distribution corresponding to the WSDW and WSBW can be observed (Fig. 2, *c* – *f*). There are no clearly expressed extrema on the long-term average θ,*S*-curves that would make it possible to separate these water masses (Fig. 3, *b*, *c*). According to [18], the WSBW layer is separated from the Weddell Sea deep water layer by the position of the isolines of neutral density γ^n > 28.24–28.27. This boundary is clearly visible in vertical sections of temperature and salinity passing over the deep-sea parts of the Powell Basin and the Weddell Sea, with the temperature and salinity values in the WSBW layer decreasing noticeably compared to their WSDW layer values, respectively, to −0.5…0.1 °C and 34.66–34.675 PSU (Fig. 2, *e*, *f*). We identify the end point on the θ,*S*-curves in these areas as the WSBW core, and the WSDW core is not clearly identified as an extremum (Fig. 3, *c*).

Over the shallow shelf of the Joinville Archipelago with depths less than 300 m, the long-term average vertical stratification of waters has its own characteristics. Here, the AAShW is characterized by weak subsurface temperature increase of approximately 0.1–0.2 °C in a layer of 20–30 m (Figs. 2, *a*; 3, *a*) and gradual salinity increase with depth (Fig. 2, *b*). Weak temperature inversion in the subsurface layer with a positive vertical salinity gradient in coastal shelf areas was noted earlier in [27]. It should be noted that the AAShW traces with the inversion of θ up to 0.15 °C in the subsurface layer of 15–25 m are observed over the slopes of the depths in the northwestern Weddell Sea (Fig. 3, *b*). To the south of 64° S, temperature and salinity increase monotonically with depth to the bottom (Fig. 2, *a*, *b*). At the same time, the distribution of isopycnic lines of neutral density γ^n shows that isopycnic line 28.05 is located at the depths of 950–1100 m, corresponding to the UCDW upper boundary.

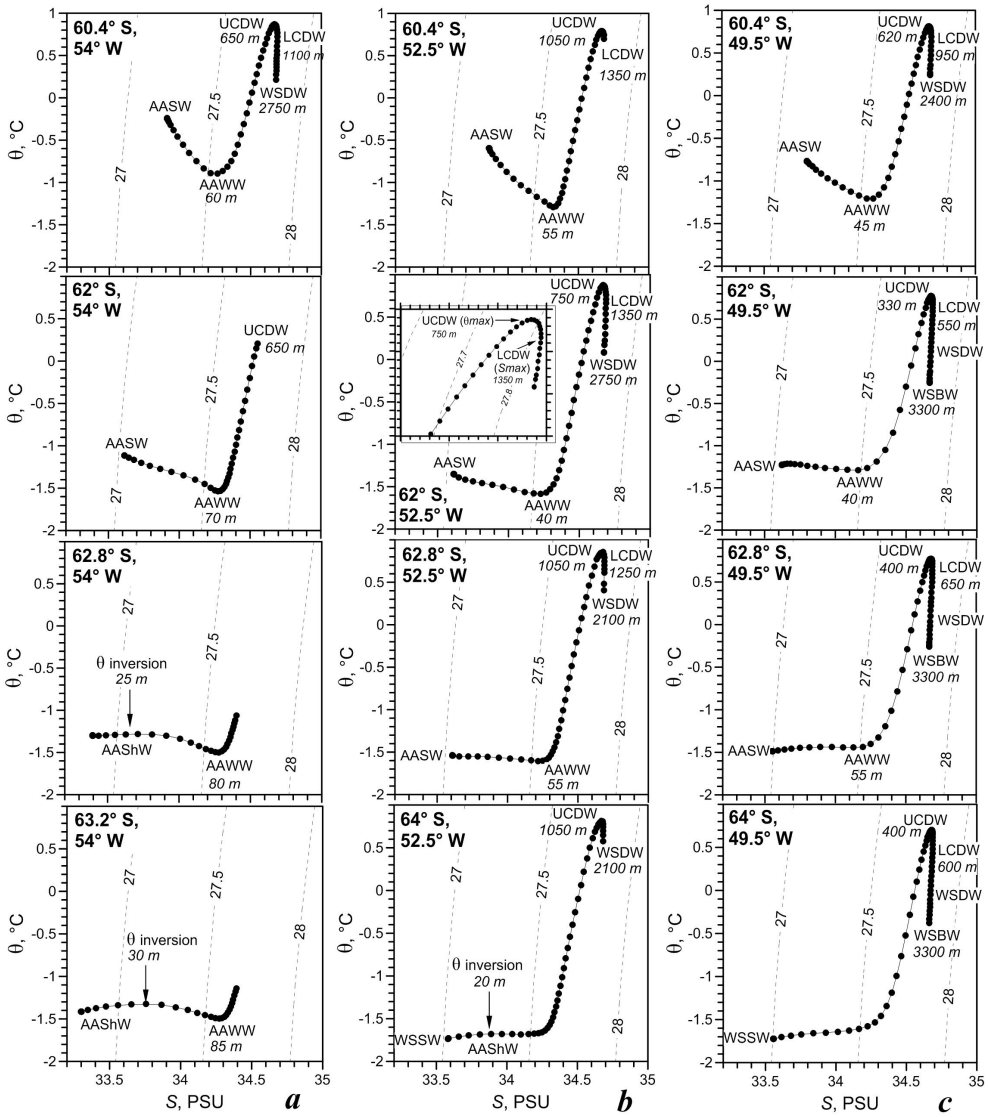

F i g . 3 . Examples of long-term average θ,*S*-curves in separate grid nodes located at 54° W (*a*), 52.5° W (*b*) and 49.5° W (*c*). The numbers next to the curves are the depths of the water mass cores (m). The dashed lines are isopycnic lines of conditional density σ_t. The inset shows an enlarged fragment of the θ,*S*-curve showing the presence of intermediate temperature and salinity maxima

The distributions of the thermohaline indices of the UCDW and LCDW cores, defined as intermediate maxima of temperature and salinity, respectively, and the depths of their occurrence (Fig. 4) illustrate clearly the qualitative connection of their spatial variability with the features of the bottom topography and the main elements of circulation. The minimum values of the UCDW θ-index are observed over the seaward edge of the shelves of the Joinville Archipelago and the Philip Ridge with the depths of less than 800 m, as well as in the Weddell Sea closer to the WSG center, where they make 0.4–0.5 °C and 0.5–0.7 °C, respectively. The UCDW core temperature decrease (1.05–1.1 °C) associated both with the cyclonic rise of waters and with the penetration of colder waters from the Weddell Sea (Fig. 1, *b*) is noted in the deep-sea part of the Powell Basin. In the southern Scotia Sea and over the slopes of the depths of the Jouinville Archipelago and Philip Ridge shelves with the depths of more than 1500 m, the θ-index values increase to 1.15–1.35 °C (Fig. 4, *a*). The range of spatial variability of the LCDW θ-index is

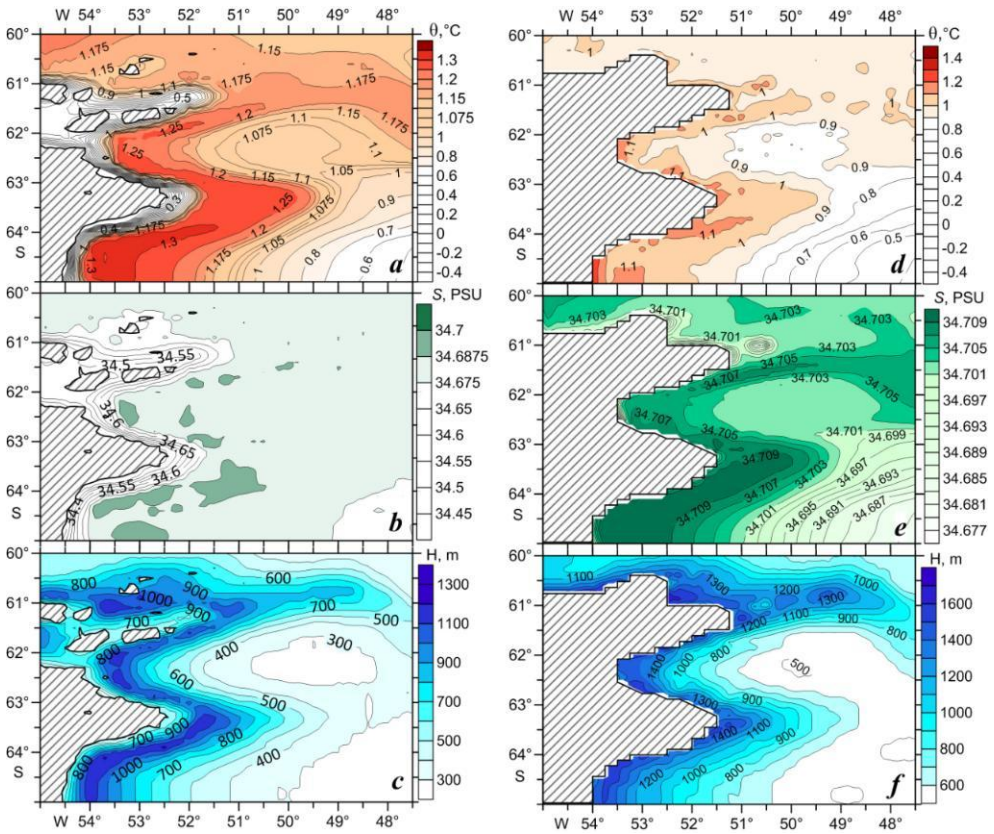

F i g . 4 . Spatial distributions of θ-indices (*a*, *d*), *S*-indices (*b*, *e*) and core depths *H* (*c*, *f*) of the Upper (*a*–*c*) and Lower (*d*–*f*) modifications of CDW. The areas, where UCDW and LCDW are absent, are shaded

significantly lower than that of the UCDW θ-index. At the same time, there is also a tendency towards a decrease in the values of the LCDW θ-index in the WSG area (0.5–0.7 °C) and in the central part of the Powell Basin (0.85–0.9 °C) and an increase over the slopes of the depths (to 1–1.1 °C) (Fig. 4, *d*).

The spatial variability of the UCDW *S*-index in most water area (in the Scotia and Weddell Seas, Powell Basin, Hesperides Trough) is small with its values varying within 34.675–34.69 PSU (Fig. 4, *b*). A significant decrease in the values of the UCDW *S*-index to 34.4–34.65 PSU, as well as its θ-index, is observed over the shelf edge with the depths less than 800 m. The low values of the UCDW θ,*S*-index here can be explained by the UCDW transformation due to its mixing with colder and fresher shelf water. Spatial changes in the values of the LCDW *S*-index (Fig. 4, *e*), which is its distinctive feature, are characterized by the same changes as in the UCDW θ-index. Decreased values of the UCDW *S*-index, as well as the UCDW θ-index, are observed in the WSG area (34.685–34.697 PSU) and in the central part of the Powell Basin (34.701–34.703 PSU), and increased ones (34.707–34.709 PSU) – over the slopes of the depths and in the southern Scotia Sea (Fig. 4, *e*).

The minimum depths of the UCDW core (less than 300 m) are observed in the areas of cyclonic gyres – in the central part of the Powell Basin and the Weddell Sea. Over the slopes of the depths, the UCDW core decreases to 1000–1300 m (Fig. 4, *c*). Similar spatial variability was revealed for the depth of the LCDW core. It is minimal (500–600 m) in the central part of the Powell Basin and the Weddell Sea and increases sharply (up to 1100–1500 m) over the slopes of the depths (Fig. 4, *f*). Qualitatively similar spatial features of the distribution of principal characteristics of the CDW Upper (θ-index) and Lower (*S*-index) modifications, as well as the depth of their cores, reflect the influence of the bottom topography and water circulation on the entire water layer occupied by the CDW.

Analysis of the distributions of intra-annual RMSD of potential temperature and salinity showed that the level of seasonal variability of these parameters varied noticeably over space (Fig. 5).

Intra-annual changes decrease significantly over the depth of 60–70 m in the temperature field (Fig. 5, *a – c*) and over the depth of 20–30 m in the salinity field (Fig. 5, *d – f*). The maximum level of intra-annual temperature variability is observed in the upper 20–30 m layer in the northern part of the water area (in the Scotia Sea, the Hesperides Trough, and over the South Scotia Ridge), where the θ RMSD values reach 1–1.6 °C (Fig. 5, *a – c*). The θ RMSD values decrease southward and amount to 0.6–0.8 °C in the Powell Basin (Fig. 5, *b*, *c*), 0.4–0.5 °C over the Joinville shelf (Fig. 5, *a*). The minimum level of intra-annual temperature variability is observed in the Weddell Sea, where the θ RMSD values do not exceed 0.2 °C (Fig. 5, *a – c*).

The spatial distribution of the intra-annual salinity RMSD differs significantly from the distribution of the temperature RMSD. The maximum *S* RMSD values are observed in the areas of intense ice formation and melting – over the Philip Ridge, the Joinville shelf and Ridge (0.5–0.8 PSU) (Fig. 5, *d*, *e*), as well as in the deep Weddell Sea (0.6–0.7 PSU) (Fig. 5, *f*).

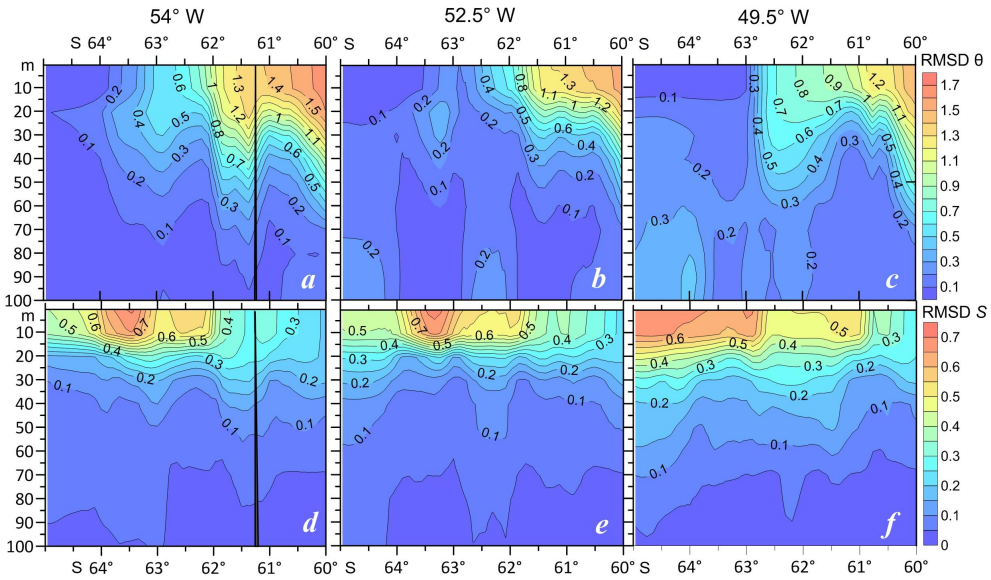

F i g . 5 . Vertical distributions of intra-annual RMSD of potential temperature (*a*–*c*) and salinity (*d*–*f*) along 54° W (*a*, *d*), 52.5° W (*b*, *e*) and 49.5° W (*c*, *f*). The dark band in Fig. 5, *a*, *d* is Shishkov Island

Over the slopes of the depths in the northwestern Weddell Sea and in the western part of the Powell Basin, the *S* RMSD values make 0.45–0.6 PSU (Fig. 5, *d*, *e*), and in the central deep-sea part of the Powell Basin they decrease to 0.4–0.5 PSU (Fig. 5, *f*). Minimum level of intra-annual salinity variability (*S* RMSD < 0.2–0.4 PSU) is observed in the areas of maximum intra-annual temperature variability – in the Scotia Sea and the Hesperides Trough (Fig. 5, *d* – *f*).

Spatial changes in the level of intra-annual variability of thermohaline parameters are reflected in climatic seasonal changes in θ,*S*-indices of water masses. Analysis of average monthly θ,*S*-curves showed that the greatest intra-annual changes in thermohaline indices characterized water masses of the upper 60–70 m ocean layer, in which the maximum seasonal variations of thermohaline fields were observed (Figs. 5; 6, *a*; 7). The maximum intra-annual changes in thermohaline indices are observed for the Antarctic Surface Water characterized by its Winter (AASWW) and Summer (AASSW) modifications (Fig. 6, *a*). The maximum seasonal changes in the ASW temperature index are observed in the southern Scotia Sea, where they reach almost 4 °C. In the Hesperides Trough, the θ-index changes make 3.5 °C. Over the Philip Ridge and in the northern and central parts of the Powell Basin, they decrease to 2–2.5 °C, and in its southern part – to 1–1.1 °C (Fig. 6, *b*). The AASW *S*-index intra-annual changes are maximum over the Philip Ridge and in the northern and southern parts of the Powell Basin, where they reach almost 1.9 PSU. In the Scotia Sea, the Hesperides Trough, and in the central part of the Powell Basin, the AASW *S*-index seasonal changes decrease to 0.8–1 PSU (Fig. 6, *c*).

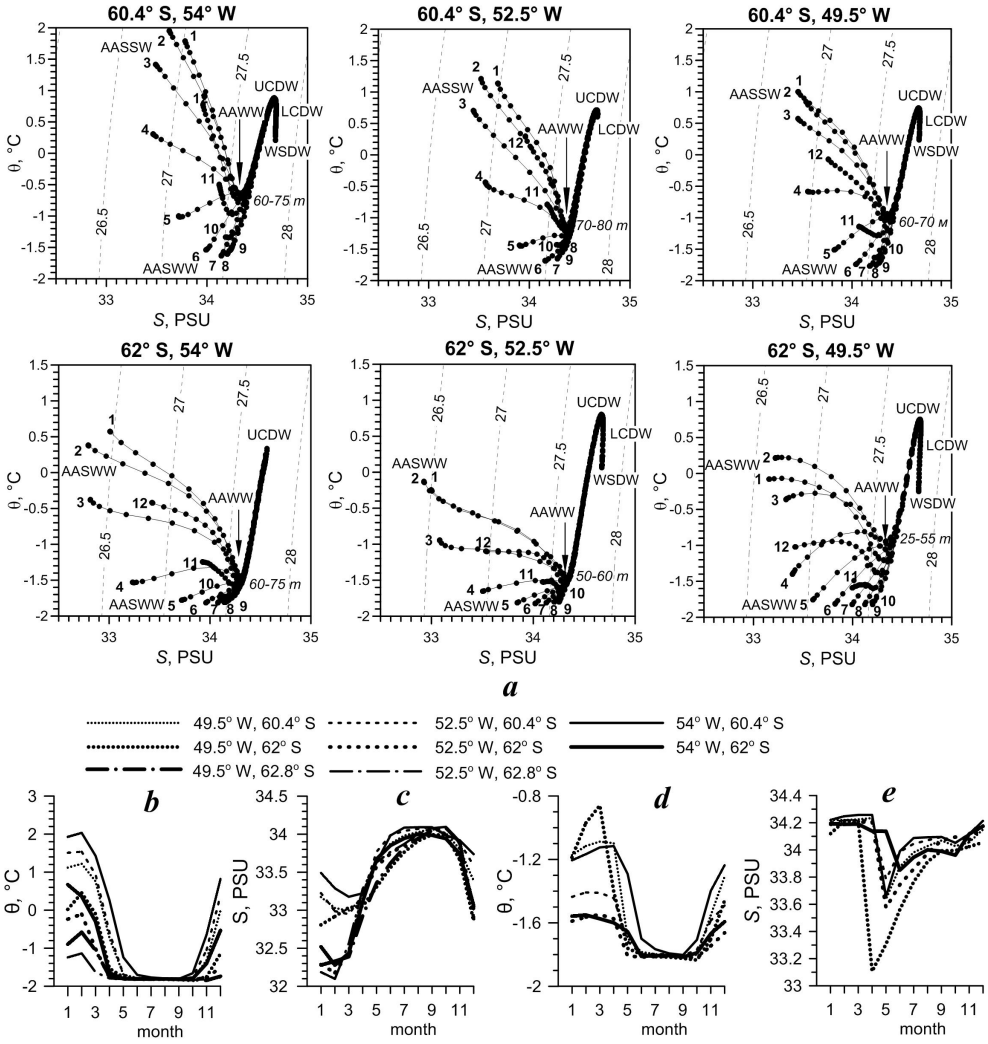

Fig. 6. Examples of monthly average θ,*S*-curves in separate grid nodes (*a*) and graphs of the intra-annual cycle of the θ-index (*b*, *d*) and *S*-index (*c*, *e*) of the ASW (*b*, *c*) and AWW (*d*, *e*). The numbers at the curves in Figs. 6, *a* – months and depths of the AWW core (m)

It should be noted that the value of the amplitude of intra-annual changes in the AASW θ,*S*-indices and its spatial variability depend mainly on the changes in the θ,*S*-indices of the AASW Summer modification. Throughout the entire water area, there are almost no changes in the values of the AASW Winter modification θ,*S*-indices, which amount to −1.8…−1.6 °C and 34–34.1 PSU in the period from May to October (Fig. 6, *b*, *c*). The values of the AASW Summer modification θ-index in January–March make 1.2–2 °C in the Scotia Sea and the Hesperides Trough, 0.6–0.8 °C over the Philip Ridge and decrease to −0.2…0.4 °C

in the northern and central parts of the Powell Basin and to −1.1…−0.6 °C in its southern part (Fig. 6, *b*). The values of the AASSW *S*-index make 32.1–32.5 PSU over the Philip Ridge in the northern and southern parts of the Powell Basin, 32.8–33 PSU in its central part, 33.2–33.5 PSU in the Scotia Sea and the Hesperides Trough (Fig. 6, *c*).

In the Weddell Sea, the temperature index of the AASW high-latitude modification – WSSW – varies throughout the year from −1.85...−1.8 °C in winter to −1.2...−1.1 °C in summer. The WSSW *S*-index intra-annual changes make almost 1.8 PSU (from 34.2–34.3 PSU in winter to 32.5–32.8 PSU in summer) (Fig. 7).

The AAWW can be observed in the subsurface layer throughout the year in the southern Scotia Sea, in the Hesperides Trough, over the Philip Ridge, in the northern and central parts of the Powell Basin (Fig. 6, *a*). Intra-annual changes in the AAWW θ,*S*-indices are maximum in the central part of the Powell Basin (up to 1 °C and 1.1 PSU), where the AAWW core is located closer to the surface in a 25–55 m layer due to the rise of water in the center of the cyclonic circulation. Minimum changes in the AAWW θ,*S*-indices, not exceeding 0.4 °C and 0.3 PSU, are observed in the Scotia Sea, the Hesperides Trough, and over the Philip Ridge, where the AAWW core deepens to 60–85 m (Fig. 6, *d*, *e*).

In the southern part of the studied water area, the AAWW is observed only for a part of the year due to the intense convection during the cold period (Fig. 7). Over the Joinville shelf, the AAWW is observed from September–November to May–June, in the southern part of the Powell Basin – from November–December to April, in the Weddell Sea – from December to March–April. In these areas, the AAWW θ,*S*-indices show poor spatiotemporal variability and amount to −1.8…−1.4 °C and 34.1–34.2 PSU, respectively. A slight increase in the AAWW θ-index (up to −1.4…−1.1 °C) is noted in the southern part of the Powell Basin (Fig. 7).

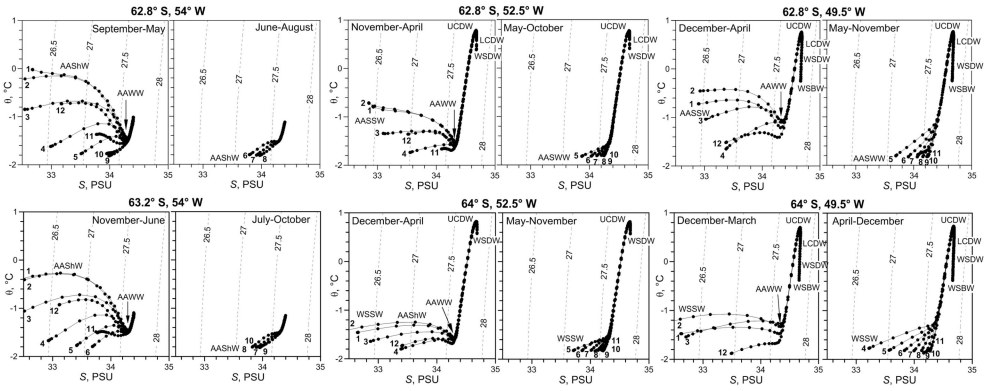

Fig. 7. Examples of monthly average θ,*S*-curves in separate grid nodes. The numbers at the curves are months.

The AAShW, like the AASW, is characterized by significant changes in thermohaline indices. Over the Joinville shelf, intra-annual changes in the AAShW θ-index reach 1.6–1.8 °C (from −1.8 °C in winter to −0.2…0 °C in summer), changes in the *S*-index amount to almost 1.5 PSU (from 33.9–34 to 32.5–32.6 PSU in summer) (Fig. 7).

Conclusions

Based on the *ECMWF ORAS*5 reanalysis data for the period from 1958 to 2021, the long-term average structure and climatic intra-annual variability of water mass characteristics in the Powell Basin and adjacent water areas are analyzed. The AASW and its colder and less saline modification, the Weddell Sea surface water, were identified as well as the AAShW, AAWW, CDW, WSDW, and WSBW. It is shown that the AAShW is observed not only over the shallow shelf of the Joinville Archipelago, but also over the continental slope in the northwestern Weddell Sea. It is revealed that in deep water areas, the CDW layer is divided into Upper and Lower modifications characterized by intermediate temperature and salinity maximums, respectively. The WSDW and WSBW do not appear in the form of separate extrema on the long-term average θ,*S*-curves.

It is shown that due to the rise of water in the center of the cyclonic gyre in the Powell Basin, the Antarctic Winter Water core is located closer to the surface in a layer of 25–55 m. In the Scotia Sea, the Hesperides Trough, and over the Philip Ridge, it deepens to 60–85 m. The minimum UCDW and LCDW core depths (250–300 m and 500–600 m, respectively) are also observed in the central part of the Powell Basin and in the Weddell Sea, closer to the WSG. The maximum UCDW and LCDW core depths (1000–1300 m and 1100–1500 m, respectively) are observed over the slopes of the depths of the Joinville shelf and the South Scotia, Philip, and Joinville Ridges.

An increase in the values of the UCDW θ-index and the LCDW *S*-index is revealed (up to 1.15–1.35 °C and 34.707–34.709 PSU, respectively) in the southern Scotia Sea and over the slopes of the depths of the shelf of the Joinville Archipelago and the Philip Ridge with the depths of more than 1500 m. A decrease in temperature in the UCDW core and salinity in the LCDW core is also observed in the Weddell Sea (0.5–1 °C and 34.685–34.699 PSU) and in the deep-sea part of the Powell Basin (1.05–1.1 °C and 34.701–34.703 PSU). The minimum values of the UCDW θ-index (0.4–0.7 °C) are observed over the edge of the shelves of the Joinville Archipelago and the Philip Ridge with the depths less than 800 m.

The maximum intra-annual changes in thermohaline indices characterize the AASW with its Winter and Summer modifications. Seasonal changes in the AASW θ-index are maximum in the southern Scotia Sea, where they reach almost 4 °C, and in the Hesperides Trough they are 3.5 °C, over the Philip Ridge and in the northern and central parts of the Powell Basin they decrease to 2–2.5 °C, and in its southern part – to 1–1.1 °C. Intra-annual changes in the AASW *S*-index are maximum over the Philip Ridge and in the northern and southern parts of the Powell Basin, where they reach almost 1.9 PSU. In the Scotia Sea, the Hesperides Trough, and in the central part of the Powell Basin, seasonal changes in the AASW *S*-index decrease to 0.8–1 PSU.

The WSSW is characterized by weak changes in the θ-index throughout the year (from −1.85…−1.8 °C in winter to −1.2…−1.1 °C in summer), while changes in its *S*-index reach almost 1.8 PSU (from 34.2–34.3 PSU in winter to 32.5 –32.8 PSU in summer).

The AAShW, like the AASW, is characterized by significant changes in thermohaline indices. Intra-annual changes in the AAShW θ-index reach 1.6–1.8 °C (from −1.8 °C in winter to −0.2…0 °C in summer), changes in the *S*-index amount to almost 1.5 PSU (from 33.9–34 to 32.5–32.6 PSU in summer).

Intra-annual changes in the AAWW θ,*S*-indices are maximum in the central part of the Powell Basin (up to 1 °C and 1.1 PSU), minimal (up to 0.4 °C and 0.3 PSU) in the Scotia Sea, the Hesperides Trough, and above the Philip Ridge. In the southern part of the water area, the AAWW is not visible in all months. Over the Joinville shelf, the AAWW is observed from September–November to May–June, in the southern part of the Powell Basin – from November–December to April, in the Weddell Sea – from December to March–April. In these areas, the AAWW θ,*S*-indices vary slightly both in space and time.

REFERENCES

1. Dubravin, V.F., 2001. [*Surface Water Masses and the Formation of Zones of Biological Productivity of the Atlantic Ocean*]. Saint Petersburg: Gidrometeoizdat, 115 p. (in Russian).
2. Maslennikov, V.V., 2003. *Climatic Variability and Marine Ecosystem of the Antarctic*. Moscow: VNIRO Publishing, 295 p. (in Russian).
3. Shulgovsky, K.E., 2005. [*Large-Scale Variability of Oceanological Conditions in the Western Part of the Atlantic Sector of the Antarctic and its Influence on the Distribution of Krill*]. Kaliningrad: AtlantNIRO, 148 p. (in Russian).
4. Venables, H., Meredith, M.P., Atkinson, A. and Ward, P., 2012. Fronts and Habitat Zones in the Scotia Sea. *Deep-Sea Research Part II: Topical Studies in Oceanography*, 59–60, pp. 14–24. doi:10.1016/j.dsr2.2011.08.012
5. Arzhanova, N.V. and Artamonova, K.V., 2014. Hydrochemical Structure of Water Masses in Areas of the Antarctic Krill (*Euphausia superba Dana*) Fisheries. *Trudy VNIRO*, 152, pp. 118–132 (in Russian).
6. Lohmann, R. and Belkin, I.M., 2014. Organic Pollutants and Ocean Fronts across the Atlantic Ocean: A Review. *Progress in Oceanography*, 128, pp. 172–184. doi:10.1016/j.pocean.2014.08.013
7. Chapman, C.C., Lea, M.-A., Meyer, A., Sallée, J.-B. and Hindell, M., 2020. Defining Southern Ocean Fronts and their Influence on Biological and Physical Processes in a Changing Climate. *Nature Climate Change*, 10, pp. 209–219. doi:10.1038/s41558-020-0705-4
8. Siegel, V. and Watkins, J.L., 2016. *Distribution, Biomass and Demography of Antarctic Krill, Euphausia superba*. In: V. Siegel, ed., 2016. Biology and Ecology of Antarctic Krill. Cham: Springer, pp. 21–100. doi:10.1007/978-3-319-29279-3_2
9. Spiridonov, V.A., Zalota, A.K., Yakovenko, V.A. and Gorbatenko, K.M., 2020. Composition of Population and Transport of Juveniles of Antarctic Krill in Powell Basin Region (Northwestern Weddell Sea) in January 2020. *Trudy VNIRO*, 181, pp. 33–51. doi:10.36038/2307-3497-2020-181-33-51 (in Russian).

10. Morozov, E.G., Spiridonov, V.A., Molodtsova, T.N., Frey, D.I., Demidova, T.A. and Flint, M.V., 2020. Investigations of the Ecosystem in the Atlantic Sector of Antarctica (Cruise 79 of the R/V Akademik Mstislav Keldysh). *Oceanology*, 60(5), pp. 721–723. https://doi.org/10.1134/S0001437020050161
11. Orsi, A.H., Nowlin Jr., W.D. and Whitworth III, Th., 1993. On the Circulation and Stratification of the Weddell Gyre. *Deep-Sea Research Part I: Oceanographic Research Papers*, 40(1), pp. 169–203. doi:10.1016/0967-0637(93)90060-G
12. Fahrbach, E., Rohardt, G., Scheele, N., Schröder, M., Strass, V. and Wisotzki, A., 1995. Formation and Discharge of Deep and Bottom Water in the Northwestern Weddell Sea. *Journal of Marine Research*, 53(4), pp. 515–538. doi:10.1357/0022240953213089
13. Artamonov, Yu.V., Popov, Yu.I. and Trotsenko, B.G., 1997. Water Masses in Antarctic Sector of South-Western Atlantic in February-April 1997. In: UAC, 1997. *UAC Bulletin*. Kyiv. Iss. 1, pp. 125–131 (in Russian).
14. Naveira Garabato, A.C., McDonagh, E.L., Stevens, D.P., Heywood, K.J. and Sanders, R.J., 2002. On the Export of Antarctic Bottom Water from the Weddell Sea. *Deep-Sea Research Part II: Topical Studies in Oceanography*, 49(21), pp. 4715–4742. https://doi.org/10.1016/S0967-0645(02)00156-X
15. Franco, B.C., Mata, M.M., Piola, A.R. and Garcia, C.A.E., 2007. Northwestern Weddell Sea Deep Outflow into the Scotia Sea during the Austral Summers of 2000 and 2001 Estimated by Inverse Methods. *Deep Sea Research Part I: Oceanographic Research Papers*, 54(10), pp. 1815–1840. doi:10.1016/j.dsr.2007.06.003
16. Thompson, A.F. and Heywood, K.J., 2008. Frontal Structure and Transport in the Northwestern Weddell Sea. *Deep Sea Research Part I: Oceanographic Research Papers*, 55(10), pp. 1229–1251. doi:10.1016/j.dsr.2008.06.001
17. Tarakanov, R.Yu., 2009. Antarctic Bottom Water in the Scotia Sea and the Drake Passage. *Oceanology*, 49(5), pp. 607–621. doi:10.1134/S0001437009050026
18. Palmer, M., Gomis, D., del Mar Flexas, M., Jordà, G., Jullion, L., Tsubouchi, T. and Naveira Garabato, A.C., 2012. Water Mass Pathways and Transports over the South Scotia Ridge West of 50°W. *Deep Sea Research Part I: Oceanographic Research Papers*, 59, pp. 8–24. doi:10.1016/j.dsr.2011.10.005
19. Morozov, E.G., Frey, D.I., Polukhin, A.A., Krechik, V.A., Artemiev, V.A., Gavrikov, A.V., Kasian, V.V., Sapozhnikov, F.V., Gordeeva, N.V. and Kobylyansky, S.G., 2020. Mesoscale Variability of the Ocean in the Northern Part of the Weddell Sea. *Oceanology*, 60(5), pp. 573–588. https://doi.org/10.1134/S0001437020050173
20. Fedotova, A.A. and Stepanova, S.V., 2021. Water Mass Transformation in the Powell Basin. In: E. G. Morozov, M. V. Flint and V. A. Spiridonov, eds., 2021. *Antarctic Peninsula Region of the Southern Ocean*. Cham: Springer, pp. 115–129. doi:10.1007/978-3-030-78927-5_8
21. Mukhametyanov, R.Z. and Frey, D.I., 2021. [Mesoscale Variability of the Characteristics of Water Masses and Currents in the Northern Weddell Sea (Powell Basin)]. In: IO RAS, 2021. *Complex Investigations of the World Ocean.* Proceedings of the VI Russian Scientific Conference of Young Scientists, Moscow, April 18–24, 2021. Moscow: Shirshov Institute of Oceanology RAS, p. 139. doi:10.29006/978-5-6045110-3-9 (in Russian).
22. Orsi, A.H., Whitworth III, Th. and Nowlin Jr., W.D., 1995. On the Meridional Extent and Fronts of the Antarctic Circumpolar Current. *Deep Sea Research Part I: Oceanographic Research Papers*, 42(5), pp. 641–673. doi:10.1016/0967-0637(95)00021-W

23. Morozov, E.G., Flint, M.V., Orlov, A.M., Frey, D.I., Molodtsova, T.N., Krechik, V.A., Latushkin, A.A., Salyuk, P.A., Murzina, S. A. [et al.], 2022. Oceanographic and Ecosystem Studies in the Atlantic Sector of Antarctica (Cruise 87 of the Research Vessel Akademik Mstislav Keldysh). *Oceanology*, 62(5), pp. 721–723. https://doi.org/10.1134/S0001437022050150
24. Zuo, H., Balmaseda, M.A., Tietsche, S., Mogensen, K. and Mayer, M., 2019. The ECMWF Operational Ensemble Reanalysis-Analysis System for Ocean and Sea Ice: A Description of the System and Assessment. *Ocean Science*, 15(3), pp. 779–808. doi:10.5194/os-15-779-2019
25. Dobrovolskii, A.D., 1961. On the Estimation of Water Masses. *Oceanology*, 1(1). pp. 12–24 (in Russian).
26. Jackett, D.R. and McDougall, T.J., 1997. A Neutral Density Variable for the World's Oceans. *Journal of Physical Oceanography*, 27(2), pp. 237–263. doi:10.1175/1520-0485(1997)027<0237:ANDVFT>2.0.CO;2
27. Artamonov, Yu.V., Bulgakov, N.P., Lomakin, P.D. and Skripaleva, E.A., 2004. Vertical Thermohaline Structure, Water Masses, and Large-Scale Fronts in the South-West Atlantic and Neighboring Antarctic Water Areas. *Physical Oceanography*, 14(3), pp. 161–172. https://doi.org/10.1023/B:POCE.0000048898.31072.cc

Submitted 29.04.2023; accepted after review 18.05.2023;
revised 28.06.2023; published 25.09.2023

About the authors:

Yuri V. Artamonov, Leading Research Associate, Marine Hydrophysical Institute of RAS (2 Kapitanskaya St., Sevastopol, 299011, Russian Federation), Dr.Sci. (Geogr.), **ResearcherID: AAC-6651-2020**, *artam-ant@yandex.ru*

Elena A. Skripaleva, Senior Research Associate, Marine Hydrophysical Institute of RAS (2 Kapitanskaya St., Sevastopol, 299011, Russian Federation), Ph.D. (Geogr.), **ResearcherID: AAC-6648-2020,** *sea-ant@yandex.ru*

Nikolay V. Nikolskii, Junior Research Associate, Marine Hydrophysical Institute of RAS (2 Kapitanskaya St., Sevastopol, 299011, Russian Federation), **ResearcherID: AAC-7723-2020**, *nikolsky.geo@gmail.com*

Contribution of the authors:

Yuri V. Artamonov – general scientific supervision of the study, statement of the study aims and objectives, method development, qualitative analysis of the results and their interpretation, discussion of the work results, formulation of conclusions

Elena A. Skripaleva – review of literature on the study problem, qualitative analysis of the results and their interpretation, processing and description of the study results, discussion of the work results, formulation of conclusions, preparation of the manuscript, text refinement

Nikolay V. Nikolskii – development and debugging of computer programmes for data processing, algorithm programming, graph plotting, participation in discussion of the article materials

All the authors have read and approved the final manuscript.

Original article

Prospects for Radar Monitoring of Wind Speed, Wind Wave Spectra and Velocity of Currents from an Oceanographic Platform

Yu. Yu. Yurovsky, V. V. Malinovsky, A. E. Korinenko *, L. A. Glukhov, V. A. Dulov

Marine Hydrophysical Institute of RAS, Sevastopol, Russia
** e-mail: korinenko.alex@mhi-ras.ru*

Abstract

The article aims to present the prospects of radar monitoring of the marine environment from an oceanographic platform located near the village of Katsiveli on the South coast of Crimea at the Black Sea hydrophysical sub-satellite test site of the Marine Hydrophysical Institute of the Russian Academy of Sciences. Operation of the radar station from the platform in Katsiveli would allow continuous round-view mode recording of the wind speed fields, wind wave spectra, and a current velocity vector in the water area of a 1 km radius with a resolution of up to 100 meters. The paper describes approaches and problems in estimating wind speed fields, wind wave spectra, and current velocity vectors using a navigation radar. It is shown that the already known methods developed in satellite and ship radar are suitable for the reconstruction of the mentioned fields from the radar signal if we use the results of wind wave-breaking studies carried out from the Katsiveli platform. The approaches were tested in autumn 2022 from the Katsiveli platform using radar stations MRS-1011 (X-band, electromagnetic wavelength 3 cm) and MRS-3000 (Ka-band, electromagnetic wavelength 8 mm). Both stations have power and Doppler channels, horizontal polarizations of emission and reception, and perform all-around scanning of the water area at grazing angles to the sea surface not exceeding 10°. The specialized experiment included the radar operation simultaneously with the standard equipment of the platform, and data processing was based on the described recovery algorithms. As a result of the experiment, it is shown that the recovered frequency spectra of wind waves agree with the spectra measured with a conventional string wave recorder, the recovered spatial fields of wind and currents meet the traditional concepts, and the field of currents agrees qualitatively with the Doppler channel data. The data obtained with radar stations demonstrate the possibility of recovery of wind speed fields, vectors of the velocity of currents, and wave frequency spectra in a water area with a radius of about 1 km with a spatial resolution of tens of meters. Radar monitoring from the Katsiveli platform provides a technical base for studies of air-sea interactions and wave-current interactions and for the development and validation of satellite technologies and regional models of the marine environment.

Keywords: radar, sea surface, normalized radar cross-section, Doppler spectrum, scatterometry, wave spectra, current velocity, in situ measurements, monitoring, oceanographic platform

Acknowledgments: The work was performed under state assignment of MHI RAS on topics no. FNNN-2021-0005 and no. FNNN-2021-0004.

For citation: Yurovsky, Yu.Yu., Malinovsky, V.V., Korinenko, A.E., Glukhov, L.A. and Dulov, V.A., 2023. Prospects for Radar Monitoring of Wind Speed, Wind Wave Spectra and Velocity of Currents from an Oceanographic Platform. *Ecological Safety of Coastal and Shelf Zones of Sea*, (3), pp. 40–54.

Перспективы радиолокационного мониторинга скорости ветра, спектров ветровых волн и скорости течения с океанографической платформы

Ю. Ю. Юровский, В. В. Малиновский, А. Е. Кориненко *, Л. А. Глухов, В. А. Дулов

Морской гидрофизический институт РАН, Севастополь, Россия
** e-mail: korinenko.alex@mhi-ras.ru*

Аннотация

Цель статьи – представить перспективы радиолокационного мониторинга морской среды с океанографической платформы, расположенной вблизи поселка Кацивели на Южном берегу Крыма на Черноморском гидрофизическом подспутниковом полигоне Морского гидрофизического института РАН. Работа радиолокационной станции с платформы в Кацивели позволила бы регистрировать в непрерывном режиме кругового обзора поля скорости ветра, спектров ветровых волн и вектора скорости течения в акватории радиуса 1 км с разрешением до 100 м. Описаны подходы и проблемы при оценке полей скорости ветра, спектров ветровых волн и вектора скорости течения с помощью навигационного радара. Показано, что для восстановления перечисленных полей по сигналу радара пригодны уже известные методы, развитые в спутниковой и корабельной радиолокации, если воспользоваться результатами исследований обрушений ветровых волн, проведенных с платформы в Кацивели. Апробация подходов выполнена осенью 2022 г. с платформы в Кацивели на основе радиолокационных станций *MRS*-1011 (*X*-диапазон, длина электромагнитной волны 3 см) и *MRS*-3000 (*Ka*-диапазон, длина электромагнитной волны 8 мм). Обе станции имеют мощностные и доплеровские каналы, горизонтальные поляризации излучения и приема и осуществляют круговой обзор акватории под скользящими углами к морской поверхности, не превышающими 10°. Специализированный эксперимент включал работу радара одновременно со штатным оборудованием платформы, а обработка данных основывалась на описанных алгоритмах восстановления. В результате эксперимента показано, что восстановленные частотные спектры ветровых волн согласуются со спектрами, измеренными традиционным струнным волнографом, восстановленные пространственные поля ветра и течений отвечают традиционным представлениям, причем поле течений согласуется на качественном уровне с данными доплеровского канала. Данные, полученные с помощью радиолокационных станций, демонстрируют возможности восстановления полей скорости ветра, векторов скорости течения и частотных спектров волнения в акватории

радиусом около километра с пространственным разрешением в десятки метров. Радиолокационный мониторинг с платформы в Кацивели предоставляет техническую базу для исследований взаимодействия океана и атмосферы, взаимодействия ветровых волн и течений, для отработки и валидации спутниковых технологий и региональных моделей морской среды.

Ключевые слова: радиолокатор, морская поверхность, удельная эффективная площадь рассеяния, доплеровский спектр, скаттерометрия, спектры волн, скорость течения, натурные измерения, мониторинг, океанографическая платформа

Благодарности: работа выполнена в рамках госзадания МГИ РАН по темам № FNNN-2021-0005 и № FNNN-2021-0004.

Для цитирования: Перспективы радиолокационного мониторинга скорости ветра, спектров ветровых волн и скорости течения с океанографической платформы / Ю. Ю. Юровский [и др.] // Экологическая безопасность прибрежной и шельфовой зон моря. 2023. № 3. С. 40–54. EDN OFYNOG.

1. Introduction

From the stationary oceanographic platform near the village of Katsiveli (hereinafter referred to as "the Katsiveli platform"), both specialized marine experiments and continuous monitoring of the coastal zone (see, for example, the collection [1)] and the papers [1–5]), are traditionally carried out [6]. The platform and its surrounding water area form an experimental test site (the Black Sea hydrophysical sub-satellite test site (BHSTS) of Marine Hydrophysical Institute of the Russian Academy of Sciences), where standard measuring equipment operates [6], and some measurement data are displayed in real time on publicly accessible websites (see, for example, current information about the state of the sea on a constantly working website http://dvs.net.ru/mhiplatform/index.shtml). Over decades of research, extensive archival data on the characteristics of the marine environment at the test site and their variability have been accumulated [1, 6]. Thus, there are ample opportunities both for optimal planning of experimental work at the test site and for expanded control of external conditions during experiments. Therefore, the conditions for carrying out work at the test site are similar to those in the laboratory. Today, this kind of "*in situ* laboratories" is necessary primarily for the developing and tuning the regional models of the marine environment and validation of satellite technologies for ocean monitoring.

A natural step to strengthen the measuring capabilities of the "*in situ* laboratory" in Katsiveli would be to carry out continuous radar monitoring of the water area surrounding the platform with a radius of about 1 km (Fig. 1). Such monitoring could provide fields of surface currents, surface wind speed and wind wave spectra with a spatial resolution of up to tens of meters. A suitable device for such purposes is a coherent navigation radar, capable of, in addition

---

[1)] Ivanov, V.A., ed., 2010. *Ecological Safety of Coastal and Shelf Zones and Comprehensive Use of Shelf Resources. To 30th Years Anniversary of the Oceanographic Platform in Kaciveli – Results and Perspectives*. Sevastopol: MHI. Iss. 21, 265 p. (in Russian).

to the standard reflection power, recording the signal phase (Doppler frequency shift), and therefore the speed of the irradiated surface.

Fig. 1, *a* shows a schematic monitoring area; Fig. 1, *b* shows a real radar image of its fragment; Fig. 1, *c*, *d* shows domestic radar stations (radars), purchased by MHI to perform such work. The image (Fig. 1, *b*) shows the signal power, in the field of which wind waves are clearly distinguishable. Each pixel in the image can be considered as a "virtual station" where a time series of signal characteristics is recorded. A set of "virtual stations", shown schematically in Fig. 1, *a*, provides detailed spatiotemporal fields of the studied characteristics of the marine environment.

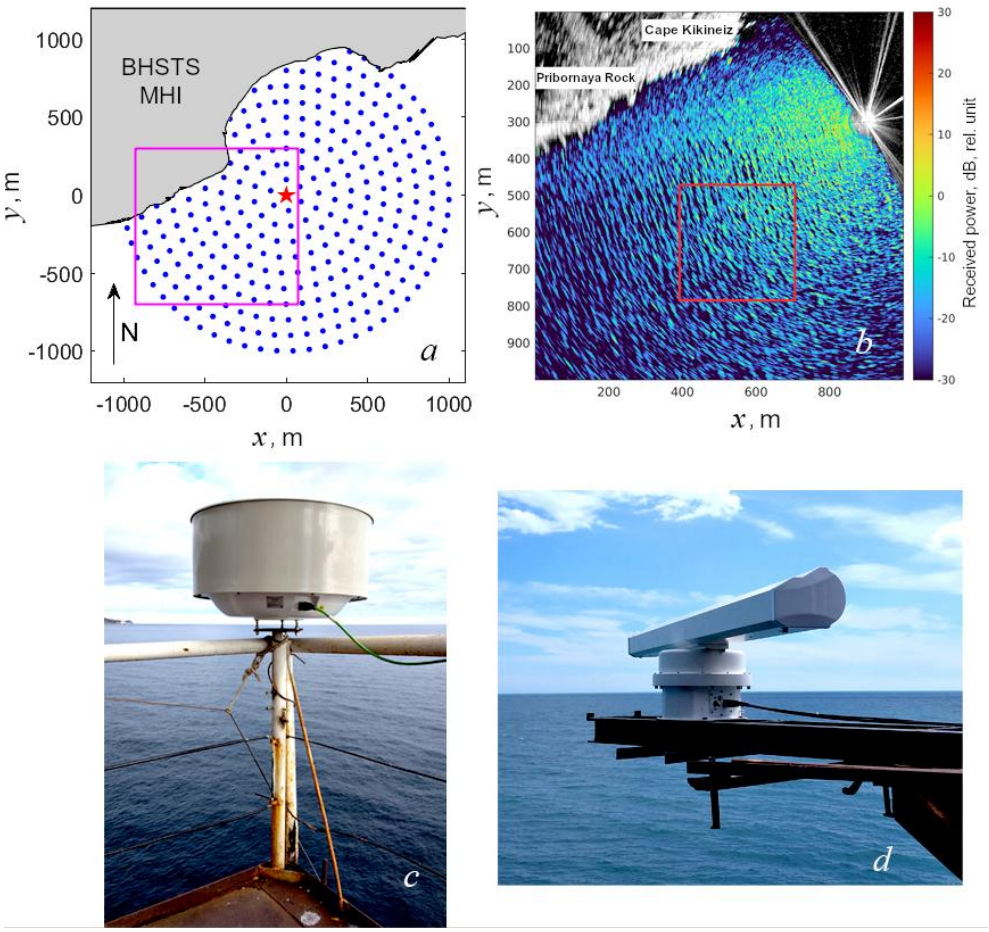

Fig. 1. Radar monitoring from the Katsiveli platform: *a* – monitoring area (the star denotes the platform location, the dots are virtual stations); *b* – radar image of the rectangular area selected in Fig. 1, *a*; *c* – MRS-3000 radar; *d* – MRS-1011 radar

Radar monitoring from the Katsiveli platform would provide an experimental basis for carrying out relevant studies of the ocean-atmosphere interaction, wind waves and currents interaction, conducting satellite experiments, developing and validating of the regional marine environment models. At the same time, the methods developed in recent decades for reconstructing wind speed, wind wave spectra, and current speed from satellite measurements provide a theoretical basis for the implementation of the project.

Radar measurements of the sea surface at small grazing angles not exceeding 10°, characteristic of coastal or marine radars, have backscattering features which are determined not by the resonant Bragg scattering, but by reflection from the breaking crests of wind waves (see, e.g. [7] and the references therein).

To solve applied problems, in particular, to restore wind speed, the geophysical model functions (GMFs) constructed from radar data are used. In the paper [8], it was proposed to use a third-order GMF to estimate wind speed from marine radars. At wind speeds of ~ 4 and 22 m/s, the speed reconstruction errors were ~ 0.8 and ~ 0.1 m/s, respectively. An empirical GMF, taking into account the grazing angle and the observation azimuth, is given in [5], where it is shown that the dependence of the normalized radar cross-section on wind speed is described by a power function with an exponent of 2.8.

Marine navigation radars are also widely used to determine marine environment characteristics [9, 10]. To estimate the surface current velocity and sea depth from the deformation of the dispersion curve, a technique was proposed for analyzing sequences of images of a radar plan-position indicator [11], subsequently improved to a commercial product [12]. In the same vein, other methods for restoring sea surface monitoring are being developed. An example is the WaMos system [13], which combines subsystems for observing waves, ice conditions, oil spills, as well as its Russian analogue also known as SeaVision [14]. A new source of information, but one that has not yet fully revealed its potential, is the Doppler velocity of scatterers, the measurement of which has become relatively simple with the introduction of solid-state coherent radars [15].

The purpose of this article is to discuss the use of marine radars for monitoring surface wind speed fields, wind wave spectra and surface currents from the Katsiveli platform. Below, the radar equipment installed on the platform is described, the ideology of obtaining estimates of the listed fields is presented, and preliminary results of the *in situ* proof-of-concept experiments in the autumn 2022 are presented.

2. Data and methods

2.1. Equipment and general description of work

In the autumn of 2022, MRS-1011 and MRS-3000 radars were installed on the Katsiveli platform (Fig. 1). Both stations operate on horizontal transmit/receive polarization providing a 360-degree view of the water area at grazing angles. The MRS-1011 station operates in the *X*-band (electromagnetic wavelength 3 cm), generally accepted for marine radars. The MRS-3000 station operates in the Ka-band (electromagnetic wavelength 8 mm), which is currently considered promising for improving the spatial resolution of satellite radars [16]. Data collection is carried out on media located on the platform, and work management and control of its correctness are carried out remotely via the Internet.

During the experiment , signals from an array of string wave gauges were continuously registered from the platform. A detailed description of the equipment used and the signal processing is given in sections 2.3 and 3.4 of the monograph [6]. Wind speed and direction, air temperature and humidity, water temperature in the upper 1-m layer were continuously recorded by a DavisVantagePro weather station installed on the platform.

2.2. The ideology of wind speed recovery

The speed and direction of the surface wind for almost the entire World Ocean are reconstructed using the data from satellite scatterometers using geophysical model functions, which are estimated experimentally from sub-satellite oceanographic buoy data. Analogs of the GMF for a radar operating from a platform can be obtained using the same method, accumulating an array of simultaneous measurements of the radar signal and wind speed using standard equipment installed on the platform. However, unlike satellite scatterometers, a navigation radar operates at grazing angles to the sea surface. This determines the GMF specificity, since the observed radar scattering is formed only by the highest wave crests visible from the radar location [17]. At wind speeds above 5 m/s, when the radar signal from the sea surface is strong enough to operate the radar, such crests typically correspond to breaking waves. The results of the studies of wave breaking statistics obtained in recent years [18, 19], including the Katsiveli platform [1, 4, 6], make it possible to predetermine the GMF shape for a radar operating at grazing angles.

The wave breaking contribution to the normalized radar cross-section (NRCS) of the sea surface is presented in the following form

$$\sigma_{wb} \propto \int \sigma_{0wb} dq, \qquad (1)$$

where σ_{0wb} is NRCS of the breaking zones; dq is the sea surface portion covered by breaking. According to O. Phillips [20] and numerous studies based

on his approach (see, for example, [4, 18, 19]), $dq \infty k^{-1} \Lambda(k)\, dk$, where $\Lambda(k)\, dk$ is the length of the breaking crests per unit surface area in the range of wave numbers (k, k + dk). Following [21], we will describe the length of the crests of breaking waves as

$$\Lambda(k,\varphi) = \frac{1}{2k} \frac{B(k,\varphi)}{\alpha}^{n+1}, \quad (2)$$

where $B(k, \varphi) = k^{-4} S(k, \varphi)$ is the wind wave saturation spectrum associated with the elevation spectrum $S(k, \varphi)$; α and n are dimensionless parameters; φ is the direction of wave propagation. From expression (1) taking into account $B(k, \varphi) \infty (U^2/c^2)^{1/n}$ and formula (2), we obtain the relation for NRCS at grazing angles

$$\sigma_{wb} \infty \int \sigma_{0wb} \left(\frac{U^2}{c^2} \right)^{\frac{n+1}{n}} dk d\varphi, \quad (3)$$

where c is the phase wave speed; U is the wind speed. The power of the radar signal received is described by the well-known radar equation

$$P = C\sigma_{wb} R^{-3}, \quad (4)$$

where C is the radar parameter; R is the distance to the scatterer. From here, taking into account (3), a general expression for (4) follows, which is a proxy for GMF:

$$P = C(\varphi_r) U^m, \quad (5)$$

where φ_r is the azimuth of radar observations, measured from the wind direction.

The constant m and the function $C(\varphi_r)$ in (5) are determined experimentally from arrays of simultaneous measurements of wind speed and radar signal. Such an array was accumulated during measurements from the Katsiveli platform with a radar with characteristics similar to the MRS-1011 station, as part of the work supported by the state assignment of MHI RAS No. 0827-2014-0010 presented in the paper [5]. A summary of these data for a range of 200 m, chosen as an example, is shown in Fig. 2. Functions $C(\varphi_r)$ for various wind speeds have maximum values when measured against the wind, φ = 90° (Fig. 2, *a*). Dependence of signal power on wind speed at φ = 90°is shown in Fig. 2, *b*, where a solid line shows the power-law dependence of PU^m at m = 2.8. Using expression (5) and the obtained dependences of the signal power on the observation azimuth, we estimate wind speed using the following formula:

$$U = \left(P / C(\varphi_{up}) \right)^{1/m}, \quad (6)$$

where φ_{up} is the radar-to-wind direction.

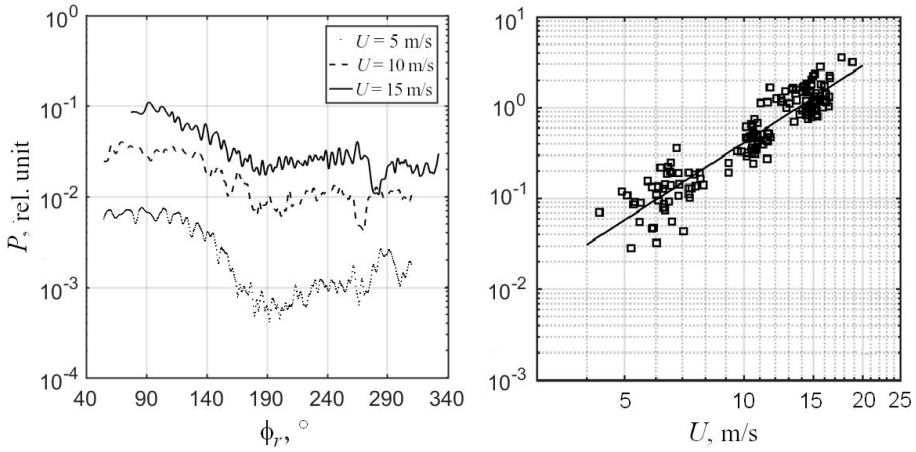

Fig. 2. Radar signal power depending on the observation azimuth (*a*) and wind speed (*b*)

As follows from formula (6), the values of U are satisfactorily described by a power function $U = (13.2 \pm 0.4) \cdot P^{0.30 \pm 0.02}$. The error in determining wind speed obtained from the data presented in Fig. 2, *b*, is $U = \pm 0.1U$. Thus, for example, at $U = 15$ m/s, the accuracy of wind speed reconstruction is ±1.5 m/s.

2.3. The ideology of recovering the spectra of wind waves and surface current velocities

The ideology of estimating the spectra of wind waves and the velocity of near-surface currents from radar images of the ocean surface has been known for a relatively long time [22]. The characteristics of wind waves can be restored by Fourier transform of the radar image fragments, as follows from Fig. 1, *b*, where the waves are clearly visible. The resulting radar spectrum $S_R(k_x, k_y)$, where k_x, k_y are the wave vector components, is related to the spectrum of sea surface elevations $S(k_x, k_y)$, as

$$S_R(k_x, k_y) = \mathrm{M}(U, k, \phi) S(k_x, k_y), \qquad (7)$$

where $\mathrm{M}(U, k, \phi)$ is the modulation transfer function (MTF); k is the wave vector magnitude, and ϕ is its direction, measured from the wind direction [23]. This approach is similar to the reconstruction of wave spectra from ocean images obtained by optical scanners [1, 24]. The three-dimensional function $\mathrm{M}(U, k, \phi)$ for the case of radar at grazing angles was discussed in [14, 17, 23]. In principle, its form can be obtained experimentally by performing simultaneous assessments of wave spectra using a radar and an array of string wave recorders at known wind speeds. With a known $\mathrm{MTFM}(U, k, \phi)$, the two-dimensional spectrum $S(k_x, k_y)$ can be simply restored using formula (7).

However, this approach requires extremely long expeditionary work. A simplified approach is to replace the MTF with a constant M_0 for the region of the spectral peak of wind waves. Then the frequency spectrum of elevations $S(f)$, where f is the wave frequency, measured in Hz, can be found from as

$$S_R(f) = M_0 S(f),$$

where $S_R(f) = \oint S_R(k \cdot \cos(\phi), k \cdot \sin(\phi)) k (dk/df) d\phi$, and dk/df is determined from the dispersion relation for surface waves

$$2\pi f = \sqrt{gk \tanh(kH)} + k_x V_x + k_y V_y, \quad (8)$$

where g is the acceleration of gravity; H is the sea depth at observation point; V_x and V_y are the current velocity components. Within the framework of a simplified approach for estimating wave spectra during measurements from a stationary platform, the current speed can be set to zero. For the case of measurements from the Katsiveli platform, when the wind wavelengths do not exceed the double depth, the deep-water approximation can be used. Then the dispersion relation (8) is reduced to $2\pi f = \sqrt{gk}$ and in this form is used to recalculate $S_R(f, k_x, k_y)$. A simplified approach has recently been validated using both measurements from a wave buoy and calculations using the WaveWatch-3 wave model [14].

The ideology of reconstructing the velocity of the near-surface current from a sequence of radar images [22] is similar to the ideology of reconstructing currents from optical images from satellites (see, for example, [25]) and video recordings from an unmanned aerial vehicle [26]. Since a radar enables one to observe variability of the wave field in space and time, by the three-dimensional Fourier transform of a sequence of radar images it is possible to estimate the radar spatiotemporal spectra $S_R(f, k_x, k_y)$. Since wind waves obey the dispersion relation (8), the parameters f, k_x, k_y of the spectrum $S_R(f, k_x, k_y)$ also satisfy equation (8). Having a large set of points (f, k_x, k_y), we find the current velocity components from the overdetermined system of equations (8). This approach, using video recordings instead of radar image sequences, has recently been thoroughly validated in a laboratory setup [27]. For radar monitoring from the Katsiveli platform, this approach provides a radar estimate of the current velocity vector, regardless of the mechanism of wave manifestation in the radar signal.

Measuring the radar signal phase makes it possible to estimate the Doppler spectra of the sea surface $S_D(f)$ formed by moving scatterers [2, 3]. The gravity center of the Doppler spectrum, "Doppler centroid",

$$f_D = \int f S_D(f) df \Big/ \left(\int S_D(f) df \right), \quad (9)$$

contains information about the average value of the velocity component of scatterers along the radar beam V_D: $f_D = k_R V_D/\pi$, where k_R is the wave number of an electromagnetic wave [28]. The f_D field measured from satellites gives

a qualitatively correct picture of the main ocean currents [28], which initiated special projects SKIM (European Space Agency) and WaCM/DopplerScatt (NASA) to develop satellite missions for Doppler current measurements [16]. However, in addition to currents, a significant contribution to V_D is made by the slopes and orbital velocities of energy-containing wind waves and wave breaking. Moreover, during a strong storm, the raindrop fraction in the air distorts the Doppler signal [3, 16, 28, 29]. The studies of Doppler shifts within the framework of radar monitoring from the Katsiveli platform will make it possible, on the one hand, to solve fundamental issues of the current reconstructing from space, on the other hand, they will provide alternative estimates of current velocity in addition to the estimates obtained by the dispersion relation analysis method.

Results

Fig. 3 demonstrates the radar monitoring capabilities confirmed during radar testing. Fig. 3, *a*, *b* shows the spatiotemporal variability of the reconstructed wind speed fields. In this case, a katabatic wind ("coastline") was observed with an average speed of 12 m/s. The areas of increased wind speed over a kilometer in length, oriented approximately parallel to the coastline, were transported with the wind speed towards the open sea. The figures show the same structure with a time shift of about a minute.

Fig. 3, *c* corresponds to the situation of rain in light wind conditions. The radar signal is determined by volumetric scattering on raindrops, and the reduced field shows horizontal distribution of the raindrop fraction in a layer of driving air with a thickness of about the height of the radar installation (~ 10 m) [3]. This distribution clearly shows a vortex structure. Radars make it possible to observe frontal and vortex structures with scales from hundreds of meters to a kilometer, evolving in the near-water layer of the atmosphere. Observations of such structures using a line of optical sensors are described in [30].

Fig. 3, *d* shows an example of the reconstructed wave frequency spectrum. The spectrum was estimated for the image fragment highlighted in Fig. 1, *b* with a pink rectangle. Although the simplified method described above was used for the calculation, comparison with the spectrum estimated from the wave gauge record shows good agreement in the region of energy-carrying waves (Fig. 3, *d*).

Fig. 3, *e* shows an example of the reconstructed field of current velocity vectors. An alongshore jet with a current velocity of 30–35 cm/s and a direction coinciding with the direction of the wind and waves is deteced. The current weakens in the wind shadow zone near the shore and on the seaward side. Fig. 3, *f* shows the simultaneously recorded Doppler centroid field f_D (9). Despite the f_D artifacts in the northern part, associated with the signal registration peculiarities, both fields have a similar spatial structure. This can be considered as a confirmation at a qualitative level of the assessment of the current field, performed on the basis of fundamentally different data – using dispersion analysis of the radar signal power.

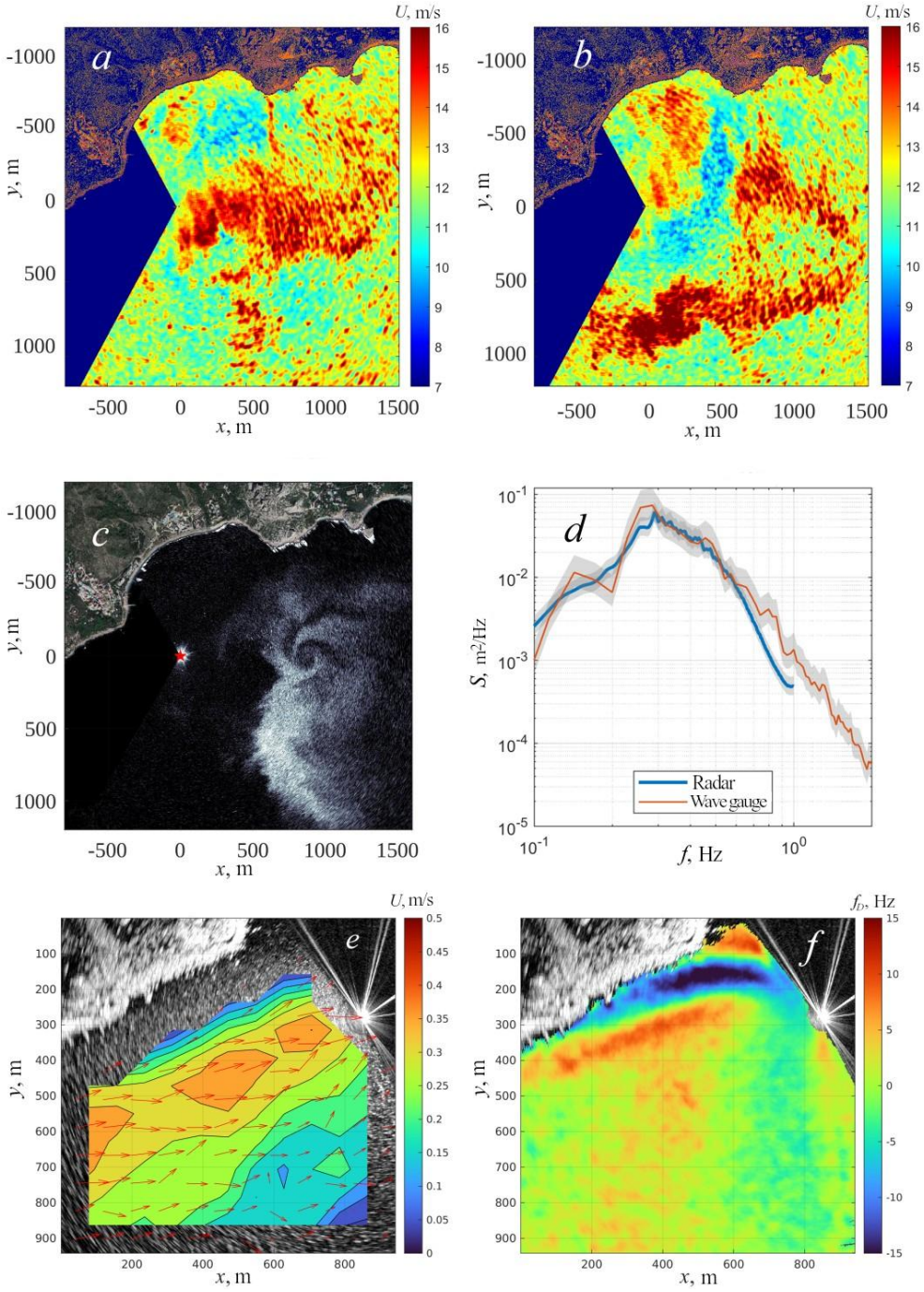

Fig. 3. Radar-derived recovered fields of wind speed (*a*, *b*), raindrop fraction field (qualitatively) (*c*), wave frequency spectrum estimated from radar signal and wave gauge measurements (*d*), recovered field of current velocity vectors (*e*), Doppler frequency shift (*f*) corresponding to the field of currents (*e*)

4. Conclusion

This paper presents a project to equip the oceanographic platform in Katsiveli with a radar station based on a marine radar in order to significantly expand research capabilities of the "*in situ* laboratory" at the Black Sea hydrophysical sub-satellite test site. Operation of the station will make it possible to monitor wind speed fields, wind wave spectra and current velocity vector in a water area with a radius of 1 km with a resolution of up to 100 m. The study of these fields is obviously of independent interest. However, when conducting experimental work on the interaction of the ocean and the atmosphere, wind waves and currents, as well as when developing and validating satellite technologies and regional models of the marine environment, detailed information about the current fields of wind speed and current velocity vector, as well as spectra of wind waves will greatly enhance reliability and validity of experimental conclusions.

The article shows that recovery of the listed fields from a radar signal is based on the already known methods developed for satellite and marine radar processing, as well as on the results of studies of wind wave breaking conducted from the Katsiveli platform. In order to test field restoration in the autumn of 2022, a special experiment was carried out from the Katsiveli platform using two new MRS-1011 and MRS-3000 marine radars, operating at electromagnetic wavelengths of 3 cm and 8 mm. The approaches to estimating wind speed fields, wind wave spectra, and current velocity vectors described in the article were applied to the reconstruction of the listed fields.

A preliminary data analysis showed:

– The wind speed field contains propagating frontal and vortex structures with scales from hundreds of meters to a kilometer, evolving in the surface layer of the atmosphere, which were previously observed by other methods.

– The reconstructed frequency spectra of wind waves are consistent with the spectra measured by a traditional string wave gauge.

– The current field contains an alongshore jet with maximum velocity values reaching 35 cm/s; its direction coincides with the direction of wind and waves. This current picture is qualitatively confirmed by the Doppler signal field obtained from the radar.

The results of the work carried out demonstrate the prospects for continuous radar monitoring at the Black Sea hydrophysical sub-satellite test site and the associated new capabilities of the "*in situ* laboratory" in Katsiveli.

REFERENCES

1. Bondur, V., Dulov, V., Kozub, V., Murynin, A., Yurovskaya, M. and Yurovsky, Yu., 2022. Validation of the Satellite Method for Measuring Spectra of Spatially Inhomogeneous Sea Waves. *Journal of Marine Science and Engineering*, 10(10), 1510. doi:10.3390/jmse10101510
2. Panfilova, M., Ryabkova, M., Karaev, V. and Skiba, E., 2020. Retrieval of the Statistical Characteristics of Wind Waves from the Width and Shift of the Doppler Spectrum of the Backscattered Microwave Signal at Low Incidence Angles. *IEEE Transactions on Geoscience and Remote Sensing*, 58(3), pp. 2225–2231. doi:10.1109/TGRS.2019.2955546

3. Yurovsky, Yu.Yu., Kudryavtsev, V.N., Grodsky, S.A. and Chapron, B., 2022. Ka-Band Doppler Scatterometry: A Strong Wind Case Study. *Remote Sensing*, 14(6), 1348. doi:10.3390/rs14061348
4. Korinenko, A.E., Malinovsky, V.V., Kudryavtsev, V.N. and Dulov, V.A., 2020. Statistical Characteristics of Wave Breakings and their Relation with the Wind Waves' Energy Dissipation Based on the Field Measurements. *Physical Oceanography*, 27(5), pp. 472–488. doi:10.22449/1573-160X-2020-5-472-488
5. Malinovsky, V.V., Korinenko, A.E. and Kudryavtsev, V.N., 2018. Empirical Model of Radar Scattering in the 3-cm Wavelength Range on the Sea at Wide Incidence Angles. *Radiophysics and Quantum Electrinics*, 61, pp. 98–108. https://doi.org/10.1007/s11141-018-9874-7
6. Ivanov, V.A. and Dulov, V.A., eds., 2014. *Monitoring of the Coastal Zone in the Black Sea Experimental Sub-Satellite Testing Area*. Sevastopol: ECOSI-Gidrofizika, 526 p. (in Russian).
7. Ermoshkin, A.V., Bakhanov, V.V. and Bogatov, N.A., 2015. Development of an Empirical Model for Radar Backscattering Cross Section of the Ocean Surface at Grazing Angles. *Sovremennye Problemy Distantsionnogo Zondirovaniya Zemli iz Kosmosa = Current Problems in Remote Sensing of the Earth from Space*, 12(4), pp. 51–59 (in Russian).
8. Vicen-Bueno, R., Horstman, J., Terril, E., de Paolo, T. and Dannenberg, J., 2013. Real-Time Ocean Wind Vector Retrieval from Marine Radar Image Sequences Acquired at Grazing Angle. *Journal Atmospheric and Oceanic Technology*, 30(1), pp. 127–139. doi:10.1175/JTECH-D-12-00027.1
9. Robinson, I.S., Ward, N.P., Gommenginger, C.P. and Tenorio-Gonzales, M.A., 2000. Coastal Oceanography Applications of Digital Image Data from Marine Radar. *Journal Atmospheric and Oceanic Technology*, 17(5), pp. 721–735. doi:10.1175/1520-0426(2000)017<0721:COAODI>2.0.CO;2
10. Huang, W., Liu, X. and Gill, E.W., 2017. Ocean Wind and Wave Measurements Using X-Band Marine Radar: A Comprehensive Review. *Remote Sensing*, 9(12), 1261. doi:10.3390/rs9121261
11. Young, I.R., Rosenthal, W. and Ziemer, F., 1985. A Three-Dimensional Analysis of Marine Radar Images for the Determination of Ocean Wave Directionality and Surface Currents. *Journal of Geophysical Research: Oceans*, 90(C1), pp. 1049–1059. doi:10.1029/JC090iC01p01049
12. Senet, C.M., Seeman, J., Flampouris, S. and Ziemer, F., 2007. Determination of Bathymetric and Current Maps by the Method DiSC Based on the Analysis of Nautical X-Band Radar Image Sequences of the Sea Surface (November 2007). *IEEE Transactions on Geoscience and Remote Sensing*, 46(8), pp. 2267–2279. doi:10.1109/TGRS.2008.916474
13. Hessner, K.G., Nieto-Borge, J.C. and Bell, P.S., 2008. Nautical Radar Measurements in Europe: Applications of WaMoS II as a Sensor for Sea State, Current and Bathymetry. In: V. Barale and M. Gade, eds., 2008. *Remote Sensing of the European Seas*. Dordrecht, The Netherlands: Springer, pp. 435–446. https://doi.org/10.1007/978-1- 4020-6772-3_33
14. Tilinina, N., Ivonin, D., Gavrikov, A., Sharmar, V., Gulev, S., Suslov, A., Fadeev, V., Trofimov, B., Bargman, S. [et al.], 2022. Wind Waves in the North Atlantic from Ship Navigational Radar: SeaVision Development and its Validation with the Spotter Wave Buoy and WaveWatch III. *Earth System Science Data*, 14(8), pp. 3615–3633. doi:10.5194/essd-14-3615-2022

15. Veremeev, V.I., Zacepin, A.G., Kulikova, D.U., Gorbunov, I.G., Kukleev, S.B. and Telegin V.A., 2019. On Measuring the Characteristics of the Sea Surface using a Coherent Microwave Radar. In: MIREA, 2019. [*Actual Problems and Perspectives for the Development of Radio Engineering and Infocommunication (Radioinfocom 2019): Proceedings of the 4th International Scientific and Practical Conference*]. Moscow: RTU MIREA, pp. 8–13 (in Russian).
16. Arduhin, F., Aksenov, Ye., Benetazzo, A., Bertino, L., Brandt, P., Caubet, E., Chapron, B., Collard, F., Cravatte, S. [et al.], 2018. Measuring Currents, Ice Drift, and Waves from Space: the Sea Surface Kinematics Multiscale Monitoring (SKIM) Concept. *Ocean Science*, 14(3), pp. 337–354. doi:10.5194/os-14-337-2018
17. Nieto Borge, J., RodrÍguez, G.R., Hessner, K. and González, P.I., 2003. Inversion of Marine Radar Images for Surface Wave Analysis. *Journal of Atmospheric and Oceanic Technology*, 21(8), pp. 1291–1300. doi:10.1175/1520-0426(2004)021<1291:IOMRIF>2.0.CO;2
18. Kleiss, J.M. and Melville, W.K., 2010. Observations of Wave Breaking Kinematics in Fetch-Limited Seas. *Journal of Physical Oceanography*, 40(12), pp. 2575–2604. doi:10.1175/2010JPO4383.1
19. Sutherland, P. and Melville, W.K., 2013. Field Measurements and Scaling of Ocean Surface Wave-Breaking Statistics. *Geophysical Research Letters*, 40(12), pp. 3074–3079. doi:10.1002/grl.50584
20. Phillips, O.M., 1985. Spectral and Statistical Properties of the Equilibrium Range in Wind-Generated Gravity Waves. *Journal of Fluid Mechanics*, 156, pp. 505–531. doi:10.1017/S0022112085002221
21. Kudryavtsev, V., Hauser, D., Caudal, G. and Chapron, B., 2003. A Semiempirical Model of the Normalized Radar Cross-Section of the Sea Surface. 1. Background Model. *Journal of Geophysical Research: Oceans*, 108(C3), 8054. doi:10.1029/2001JC001003
22. Young, I.R., Rosenthal, W. and Ziemer, F., 1985. A Three-Dimensional Analysis of Marine Radar Images for the Determination of Ocean Wave Directionality and Surface Currents. *Journal of Geophysical Research: Oceans*, 90(C1), pp. 1049–1059. doi:10.1029/JC090iC01p01049
23. Plant, W.J., 1989. The Modulation Transfer Function: Concept and Applications. In: G. J. Komen and W. A. Oost, eds., 1989. *Radar Scattering from Modulated Wind Waves.* Dordrecht: Springer, pp. 155–172. https://doi.org/10.1007/978-94-009-2309-6_13
24. Kudryavtsev, V., Yurovskaya, M., Chapron, B., Collard, F. and Donlon, C., 2017. Sun Glitter Imagery of Ocean Surface Waves. Part 1: Directional Spectrum Retrieval and Validation. *Journal of Geophysical Research: Oceans*, 122(2), pp. 1369–1383. doi:10.1002/2016JC012425
25. Yurovskaya, M.V., Kudryavtsev, V.N. and Stanichny, S.V., 2019. Reconstruction of Surface Wave Kinematic Characteristics and Bathymetry from Geoton-L1 Multichannel Optical Images from Resurs-P Satellite. *Sovremennye Problemy Distantsionnogo Zondirovaniya Zemli iz Kosmosa = Current Problems in Remote Sensing of the Earth from Space*, 16(2), pp. 218–226. doi:10.21046/2070-7401-2019-16-2-218-226 (in Russian).
26. Yurovsky, Yu.Yu., Kubryakov, A.A., Plotnikov, E.V. and Lishaev, P.N., 2022. Submesoscale Currents from UAV: An Experiment over Small-Scale Eddies in the Coastal Black Sea. *Remote Sensing*, 14(14), 3364. doi:10.3390/rs14143364
27. Smeltzer, B.K., Æsøy, E., Ådnøy, A. and Ellingsen, S.Å., 2014. An Improved Method for Determining Near-Surface Currents from Wave Dispersion Measurements. *Journal of Geophysical Research: Oceans*, 124(12), pp. 8832–8851. doi:10.1029/2019JC015202

28. Chapron, B., Collard, F. and Ardhuin, F., 2005. Direct Measurements of Ocean Surface Velocity from Space: Interpretation and Validation. *Journal of Geophysical Research: Oceans*, 110(C7), C07008. doi:10.1029/2004JC002809

29. Yurovsky, Yu.Yu., Kudryavtsev, V.N., Chapron, B. and Grodsky, S.A., 2018. Modulation of Ka-band Doppler Radar Signals Backscattered from the Sea Surface. *IEEE Transactions on Geoscience and Remote Sensing*, 56(5), pp. 2931–2948. doi:10.1109/TGRS.2017.2787459

30. Titov, V.I., Artamonov, A.Yu., Bakhanov, V.V., Ermakov, S.A., Luchinin, A.G., Repina, I.A. and Sergievskaya, I.A., 2014. Monitoring of Sea Surface with Optional Technique. *Issledovanie Zemli iz Kosmosa*, (5), pp. 3–14. doi:10.7868/S0205961414050078 (in Russian).

Submitted 15.05.2023; accepted after review 08.06.2023;
revised 28.06.2023; published 25.09.2023

About the authors:

Yury Yu. Yurovsky, Senior Research Associate, Marine Hydrophysical Institute of RAS (2 Kapitanskaya St., Sevastopol, 299011, Russian Federation), Ph.D. (Phys.-Math.), **Scopus Author ID: 24377122700**, **ORCID ID: 0000-0002-9995-3965**, **SPIN-код: 8482-5777**, *yyyurovsky@gmail.com*

Vladimir V. Malinovsky, Senior Research Associate, Marine Hydrophysical Institute of RAS (2 Kapitanskaya St., Sevastopol, 299011, Russian Federation), Ph.D. (Phys.-Math.), **ORCID ID: 0000-0002-5799-454X**, **ResearcherID: F-8709-2014**, **SPIN-код: 9206-3020**, **Scopus Author ID: 23012976200**, *vladimir.malinovsky@mhi-ras.ru*

Aleksandr E. Korinenko, Research Associate, Marine Hydrophysical Institute of RAS (2 Kapitanskaya St., Sevastopol, 299011, Russian Federation), Ph.D. (Phys.-Math.), **Scopus Author ID: 23492523000**, **ORCID ID: 0000-0001-7452-8703**, **SPIN-код: 7288-8023**, *korinenko.alex@mhi-ras.ru*

Lev A. Glukhov, Junior Research Associate, Marine Hydrophysical Institute of RAS (2 Kapitanskaya St., Sevastopol, 299011, Russian Federation)

Vladimir A. Dulov, Chief Research Associate, Marine Hydrophysical Institute of RAS (2 Kapitanskaya St., Sevastopol, 299011, Russian Federation), Dr.Sci. (Phys.-Math.), **ORCID ID: 0000-0002-0038-7255**, **ResearcherID: F-8868-2014**, **SPIN-код: 8303-6244**, **Scopus Author ID: 6602725409**, *dulov@mhi-ras.ru*

Contribution of the authors:

Yury Yu. Yurovsky – development of methods and conduction of experimental studies, processing, analysis, and description of the study results, preparation of the manuscript

Vladimir V. Malinovsky – problem statement, participation in discussion of the article materials, preparation of the manuscript

Aleksandr E. Korinenko – development of methods and conduction of experimental studies, processing, analysis, and description of the study results, participation in discussion of the article materials

Lev A. Glukhov – review of literature on the study problem, qualitative analysis of the results and their interpretation, discussion of the work results

Vladimir A. Dulov – general scientific supervision of the study, problem statement, analysis and description of the study results, preparation of the manuscript

All the authors have read and approved the final manuscript.

Научная статья
УДК 551.435.32 (265)
EDN SAIMZC

Динамика аккумулятивных берегов Юго-Западного Крыма

Ю. Н. Горячкин *, В. В. Долотов

Морской гидрофизический институт РАН, Севастополь, Россия
** e-mail: yngor@mhi-ras.ru*

Аннотация
В связи с проблемой развития рекреационной инфраструктуры города федерального значения Севастополя рассмотрена динамика аккумулятивных берегов вблизи устьев рек Качи и Бельбека. Цель статьи – определить количественные характеристики изменчивости береговой линии. В анализ был включен также пляж микрорайона Учкуевка, имеющий большое рекреационное значение. Использовались данные оцифровки береговых линий из космических снимков сервиса *Google Earth* для периода 2011–2021 гг. и материалы полевых наблюдений Морского гидрофизического института РАН. Установлено, что рассмотренные берега в последнее десятилетие находятся в динамическом равновесии. Значимых трендов изменений среднего положения береговой линии не обнаружено. Отмечено, что ранее береговая линия пляжей претерпела значительные изменения, связанные с антропогенной деятельностью (сокращение твердого стока, добыча песка, строительство берегозащитных сооружений). В каждом из рассмотренных пляжей выделены районы с максимальными и минимальными изменениями береговой линии за последнее десятилетие, приводятся количественные характеристики. Рассмотрена межгодовая изменчивость среднего по длине пляжей положения береговой линии. Показано, что внутригодовые изменения положения береговой линии могут превышать межгодовые. Во избежание ложных выводов рекомендуется при анализе спутниковых данных использовать не только снимки, полученные в крайние даты, а всю совокупность имеющихся изображений. Приводятся данные о динамике аккумулятивных берегов других причерноморских стран в сходных природных условиях.

Ключевые слова: береговая линия, космические снимки, устья рек, пляж, антропогенное воздействие, Черное море

Благодарности: работа выполнена в рамках темы государственного задания ФГБУН ФИЦ МГИ FNNN-2021-0005.

Для цитирования: *Горячкин Ю. Н., Долотов В. В.* Динамика аккумулятивных берегов Юго-Западного Крыма // Экологическая безопасность прибрежной и шельфовой зон моря. 2023. № 3. С. 55–70. EDN SAIMZC.

Dynamics of Accumulative Shores of South-Western Crimea

Yu. N. Goryachkin *, V. V. Dolotov

Marine Hydrophysical Institute of RAS, Sevastopol, Russia
** e-mail: yngor@mhi-ras.ru*

Abstract

In connection with the problem of developing the recreational infrastructure of the federal city of Sevastopol, the paper considers the dynamics of accumulative banks near the mouths of the Kacha and Belbek Rivers. The purpose of the article is to determine the quantitative characteristics of the coastline variability. The analysis also included the beach of the Uchkuevka microdistrict, which is of great recreational importance. We used data from the digitization of coastlines of space images from the Google Earth service for 2011–2021 and materials of field observations of Marine Hydrophysical Institute of the Russian Academy of Sciences. It is established that the considered coasts have been in a dynamic equilibrium in the last decade. Significant trends in changes in the average position of the coastline were not found. It is noted that earlier the coastline of the beaches underwent significant changes associated with anthropogenic activities (reduction of solid runoff, sand mining, construction of coastal protection structures). In each of the considered beaches, areas are identified with the maximum and minimum range of changes in the coastline over the past decade, and quantitative characteristics are given. The interannual variability of the coastline position averaged over beach length is considered. It is shown that intra-annual changes in the coastline position can exceed interannual ones in magnitude. To avoid false conclusions, when analyzing satellite data it is recommended not to use the images obtained on the first and last dates of observations, but the entire set of available images. The paper provides data on the dynamics of accumulative shores in other Black Sea countries in similar natural conditions.

Keywords: coastline, space images, river mouths, beaches, anthropogenic impact

Acknowledgments: The work was carried out under state assignment no. FNNN-2021-0005.

For citation: Goryachkin, Yu.N. and Dolotov, V.V., 2023. Dynamics of Accumulative Shores of South-Western Crimea. *Ecological Safety of Coastal and Shelf Zones of Sea*, (3), pp. 55–70.

Введение

В настоящее время на различных административных уровнях рассматриваются проекты развития рекреационной инфраструктуры города федерального значения Севастополя. Протяженность его береговой линии составляет около 170 км (для сравнения: береговая линия Румынии – 225 км, Болгарии – 300 км). Наиболее населенный и протяженный участок региона (около 73 км) – собственно севастопольские бухты с немногочисленными пляжами – мало пригоден для развития рекреации, поскольку плотно застроен и увеличение пляжной территории здесь практически невозможно. При этом к настоящему времени вследствие антропогенной деятельности здесь сохранилось только 0.3 погонных км или 10 % от ранее существовавших наиболее ценных песчаных пляжей [1].

Южное побережье от м. Херсонес до м. Святого Николая (около 72 км) представляет собой гористую местность с немногочисленными прислоненными валунно-галечными пляжами, опасными из-за обвалов и оползней. Рекреационный потенциал находящейся на этом участке побережья бухты Ласпи почти исчерпан. Поэтому не удивительно, что внимание администрации и инвесторов обращено на северную часть региона – побережье от м. Тюбек до м. Коса Северная (около 26 км). Однако и здесь бóльшая часть побережья, хотя и имеет относительно широкие пляжи, вместе с тем является обвало- и оползнеопасной, тут неоднократно фиксировались несчастные случаи. Тем существеннее значение, которое приобретают аккумулятивные пляжи полного профиля, расположенные в долинном понижении приустьевых участков рек Качи и Бельбека. Еще один пляж неполного профиля расположен у микрорайона Учкуевка. Все три пляжа занимают 20 % побережья и имеют большое рекреационное значение ввиду хорошей транспортной доступности (рис. 1).

Антропогенное воздействие на береговую зону Крыма и Севастополя в последнее время возрастает. Освоение берегов, к сожалению, зачастую сопровождается негативными последствиями (вплоть до утраты пляжей). Как правило, они возникают вследствие недостатка знаний о динамике береговой зоны, которые необходимы при определении влияния реализации различных хозяйственных проектов на изменение состояния берегов, обосновании схем берегозащиты и при решении ряда других задач. Это особенно актуально, поскольку администрацией Севастополя подписано соглашение о строительстве крупного рекреационного кластера стоимостью 15 млрд. рублей в районе пляжа вблизи устья р. Бельбек.

Р и с . 1 . Пляжи северной части Севастопольского региона: *1* – близ с. Орловка; *2*– в микрорайоне Любимовка; *3* – в микрорайоне Учкуевка

F i g . 1 . Beaches in the northern Sevastopol area: *1* – near the village of Orlovka; *2* – in the microdistrict of Lyubimovka; *3* – in the microdistrict of Uchkuevka

Ранее в литературе в основном рассматривалась динамика песчаного пляжа в устье р. Бельбек [2–4]. Так, в работе [2] на основании анализа натурных наблюдений в 2007 и 2009 гг. было показано, что наиболее значительная межгодовая изменчивость положения береговой линии характерна для северного и центрального участков, где размах смещения достигал 20 м. На южном участке было отмечено некоторое выдвижение линии уреза воды в сторону моря. В [3] сравнивались космические

снимки 1966 г. и первого десятилетия XXI в. Отмечено, что за этот период береговая линия на южном участке выдвинулась в сторону моря приблизительно на 20–40 м. В [4] на основе анализа космических снимков за 2009–2014 гг. отмечалось, что пляж в районе устья р. Бельбек в целом отступал со средней скоростью 1.4 м/год. В южной части наблюдалась аккумуляция, при этом пляж выдвинулся в среднем на 10 м. В центральной и северной частях пляж отступил в среднем на 15 м. Там же отмечено, что типичные значения межгодовых колебаний составляли около 12 м, минимальные – 5 м, максимальные – до 30 м, наибольшим изменениям был подвержен центральный участок. В работе, посвященной состоянию морских берегов Севастополя на основе сопоставления топографической карты 1955 г. и космического снимка 2014 г., делается вывод, что «аккумулятивный берег в долине Качи отступает со скоростью до 5 м в год!» [5, с. 241].

К настоящему времени накоплен значительный массив космических снимков, позволяющий провести более обоснованный анализ изменений положения береговой линии во времени. Цель данной работы – определить на основе космических снимков количественные характеристики межгодовой изменчивости береговой линии аккумулятивных берегов, прилежащих к устьям рек Качи и Бельбека. Кроме этого, в анализ был включен пляж микрорайона Учкуевка, который находится в пределах абразионно-оползневого берега и имеет большое рекреационное значение.

Материалы и методы исследования

В работе использовались данные оцифровки береговых линий на космических снимках сервиса *Google Earth* для периода 2011–2021 гг. и спутниковый снимок США, сделанный в 1966 г. для *United States Geological Survey* (*USGS*). При наличии нескольких снимков за год выбирался снимок с максимальной детализацией. Почти все снимки (9 из 11) относились к теплому периоду года.

После создания соответствующих снимкам цифровых массивов и загрузки их в ГИС визуально отмечалось искажение линейных структур, обусловленное погрешностями, порожденными в процессе генерирования непрерывных снимков. Последние состоят из тайловых массивов различного разрешения, являющихся основой технологии создания картографических сервисов [1), 2)] [6, 7]. Используемый в работе сервис *Google Maps* позволяет выполнять векторную прорисовку интересующих объектов с достаточно высокой точностью. Этому способствовали дополнительно еще два фактора: незначительная абсолютная высота большинства объектов в прибрежной зоне и расположение линий уреза воды в горизонтальной плоскости. Для дополнительной коррекции искажений выполнялась привязка оцифрованных линий к неподвижным объектам, в качестве которых чаще всего выбирались угловые точки бетонных бун.

[1)] *Лабутина И. А., Балдина Е. А.* Использование данных дистанционного зондирования для мониторинга экосистем ООПТ. Москва, 2011. 88 с.

[2)] *Малышева Н. В.* Автоматизированное дешифрование аэрокосмических изображений лесных насаждений. Москва : Изд-во Московского государственного университета леса, 2012. 151 с.

Для дальнейшего анализа использовались основные расчетные алгоритмы, описанные в модуле *DSAS*[3]. Модуль выполняет построение серии линий поперечных сечений пляжа от условной линии, принятой за базовую через заданное расстояние. С учетом протяженности пляжей и желаемой детализации поперечные сечения для всех трех пляжей проводились через 20 м. В дальнейшем расстояния от базовой линии до линий уреза воды для каждого сечения сводились в электронную таблицу, средствами которой вычислялись максимальные отклонения (положительные значения размаха, независимые от даты) и расстояния между двумя линиями, соответствующими крайним датам (результирующие смещения). Графики смещения береговой линии построены на двунаправленной оси абсцисс, при этом направление влево соответствует выдвижению берега в сторону моря, т. е. в западном направлении. Кроме спутниковых данных, нами использовались материалы полевых наблюдений Морского гидрофизического института РАН.

Результаты и обсуждение

Аккумулятивный берег в районе устья р. Качи. Протяженность пляжа в этом районе около 1.4 км, с южной стороны имеются два участка с перпендикулярными берегу каменными набросками. С учетом этого для расчетов длина принималась равной 1.2 км.

Ширина пляжа, сложенного хорошо сортированным среднезернистым песком с мелкой галькой, в настоящее время составляет от 30 до 50 м. Тыловую границу пляжа на ряде участков выделить сложно, поскольку здесь расположены волноотбойная стенка (построена в 2009 г.), искусственный вал и некоторые другие объекты. Устьевая зона сформирована аллювием с преобладанием глин и песков. Геологическое строение свидетельствует о том, что на этом месте ранее располагался лиман, заполненный впоследствии аллювием[4].

Естественный гидрологический режим р. Качи сильно изменен. На реке сооружены два крупных водохранилища – Бахчисарайское (6.9 млн. м³, построено в 1934 г.) и Загорское (27.8 млн. м³, 1975 г.), что наряду с отбором воды на хозяйственные нужды привело к значительному сокращению твердого стока реки. В настоящее время сток реки даже в период интенсивных атмосферных осадков незначителен (рис. 2).

При заполнении прудов, расположенных в приустьевом участке, в отдельные периоды сток близок к нулю. Место впадения реки в море изменяется только в пределах полосы пляжа в обе стороны, в основном до 100 м, в более редких случаях – до 250 м от среднего положения. Иногда устье не соприкасается непосредственно с морем, а образует небольшую лагуну, параллельную береговой линии и отчлененную волноприбойным валом, через который вода фильтруется в море.

---

[3] URL: https://www.usgs.gov/centers/whcmsc/science/digital-shoreline-analysis-system-dsas (date of access: 07.09.2023).

[4] *Зенкович В. П.* Морфология и динамика советских берегов Черного моря. Москва : Изд-во АН СССР, 1958. Т. 1. 187 с.

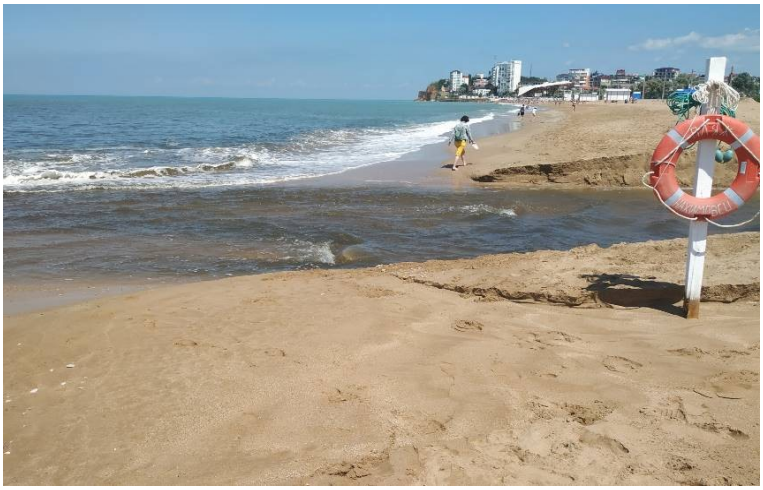

Р и с . 2 . Вид на устье р. Качи с юга в период сильного паводка 19 июня 2021 г.

F i g . 2 . View of the Kacha River mouth during a strong freshet, 19 June 2021

Для определения динамики береговой линии использовались 62 поперечных сечения пляжа (рис. 3). Анализ показал, что наибольший максимальный размах смещения положения береговой линии характерен для участка к северу от устья р. Качи, где он достигает 26 м при среднем значении 20 м. Только в северной части, примыкающей к клифу на протяжении 200 м, среднее значение смещения уменьшается до 13 м при максимальном 16 м.

На участке южнее устья р. Качи максимальный размах смещения уменьшается до 16 м, а средний до 13 м. Если брать изменения между крайними датами (2011–2021 гг.), то обнаруживается другая картина. За указанный период половина участка к северу от устья выдвинулась в сторону моря на расстояние до 10 м (в среднем на 6 м), а другая половина, примыкающая к устью, отступила до 15 м (в среднем на те же 6 м). Другими словами, на этом участке изменилась конфигурация берега. Участок же южнее устья в целом, за небольшим исключением, выдвинулся в сторону моря в среднем на расстояние до 5 м при максимуме 11 м.

Из анализа видно, что максимальный размах смещения существенно больше почти по всей протяженности пляжа, чем значения смещения за рассматриваемый период. Это говорит о том, что при анализе тенденций изменения береговой линии нужно учитывать межгодовую изменчивость. Несомненно, что необходимо также учитывать и сезонную изменчивость, однако имеющееся в настоящее время количество снимков в течение года не позволяет это сделать. В нашей работе до некоторой степени эта проблема снимается использованием снимков, сделанных в теплый период года, когда изменчивость береговой линии минимальна.

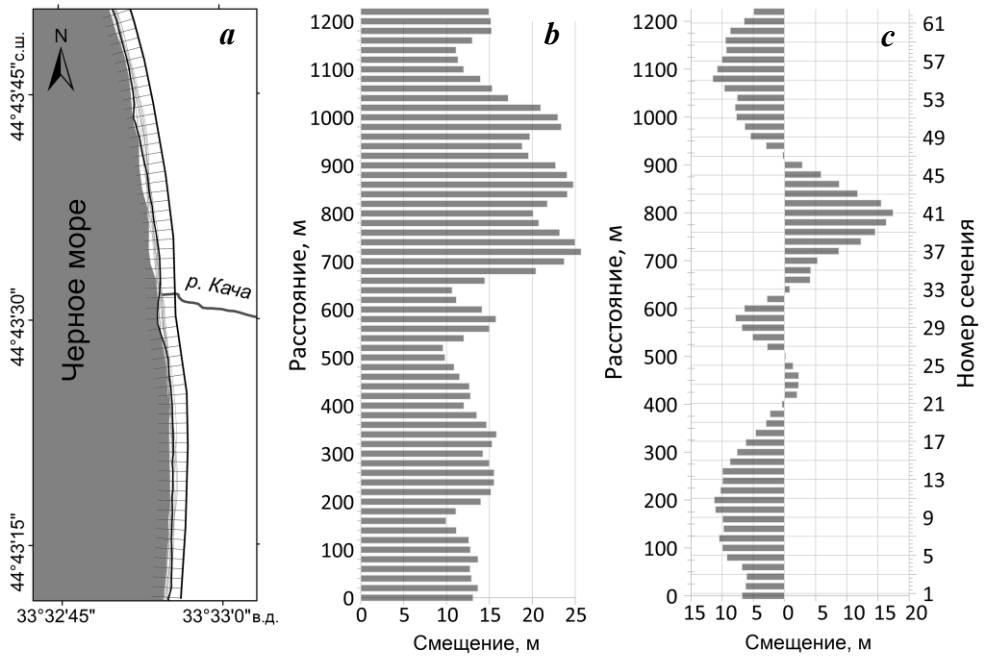

Р и с . 3 . Схема сечений на пляже вблизи устья р. Качи (*a*); размах смещений береговой линии за весь период (*b*); итоговые смещения береговой линии между крайними датами (*c*)

F i g . 3 . Map of transects on the beach near the Kacha River mouth (*a*); coastline displacement span for the whole period (*b*); resulting coastline displacements between the first and last dates of observations (*c*)

На рис. 4 приведена межгодовая изменчивость береговой линии, рассчитанная по всей длине пляжа. Из него видно, что на фоне небольшого отрицательного тренда (отступания берега на 0.38 м/год) наблюдаются колебания с размахом до 10 м, особенно выраженные с 2017 г. Сравнение береговых линий 1966 г. и 2021 г. показало, что в северной части пляжа суммарное отступание составило 15–20 м, а в южной – до 40 м. Факт отступания можно связать со значительным сокращением поступления твердых наносов р. Качи, вызванным вводом в эксплуатацию Загорского водохранилища. Необходимо также отметить: в работе [5] показано, что на месте ранее выровненного берега сейчас образовалась вогнутость береговой линии, совпадающая с пляжем в устье р. Качи. Действительно, такая тенденция прослеживается, однако автор относит это к периоду после 1985 г., из чего делает неверный вывод, что пляж отступает скоростью 5 м/год. Нет сомнений, что ранее пляж испытал значительное отступание, вызванное, во-первых, добычей песка, которая проводилась на расстоянии около 200 м от берега рефулерами в течение 1950-х гг. (месторождение «Севастопольский»), а во-вторых, из-за сокращения твердого стока в результате зарегулирования реки. Однако имеющие данные не позволяют количественно оценить отступание береговой линии из-за этих факторов.

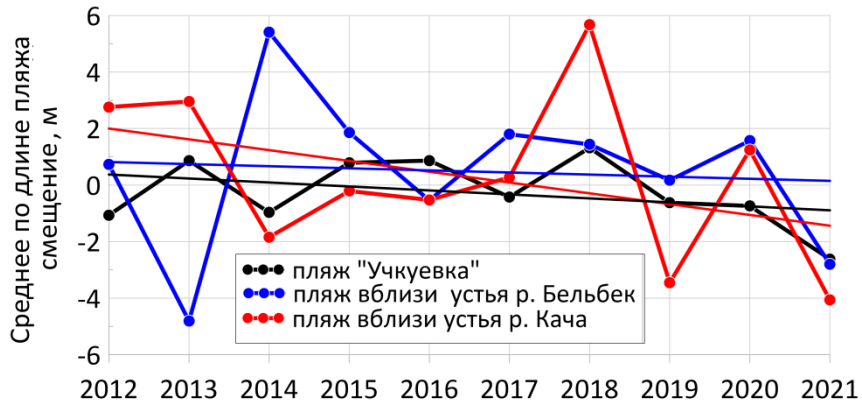

Р и с . 4 . Межгодовая изменчивость среднего по длине пляжей положения береговой линии. Прямые линии – линейные тренды

F i g . 4 . Interannual variability of the coastline position averaged over beach length. The straight lines are linear trends

Строительство поперечной каменной наброски в южной части пляжа значительно повлияло на его динамику. По нашим наблюдениям, при южных и юго-западных штормах, когда движение донных наносов направлено к северу, здесь наблюдаются явления низового размыва. Несколько таких случаев зафиксировано и на спутниковых снимках. Отступание берега в районе каменной наброски может достигать 10–20 м. При этом затяжные штормы могут угрожать целостности прибрежных строений, так как расстояние до них от уреза сокращается до 10 м, что явно недостаточно для эффективного гашения волновой энергии.

Аккумулятивный берег в районе устья р. Бельбек. Пляж полного профиля микрорайона Любимовка, незадернованная часть которого имеет ширину до 70–80 м при протяженности 1.1 км, расположен в устье р. Бельбек. Он сложен преимущественно песчаным материалом, а непосредственно вблизи уреза воды – гравийно-галечным. Примыкающий к нему с юга участок бывшего абразионного обвально-оползневого берега в конце 1970-х гг. был террасирован. Тогда же там было построено берегозащитное сооружение, состоящее из набережной, подпорной стены и системы из шести бун, что привело к частичной блокировке вдольберегового потока наносов. К северу от пляжа полного профиля расположен прислоненный к глинистому клифу и такой же по вещественному составу пляж шириной 25–40 м. Оба пляжа относятся к одной литодинамической ячейке. Северной ее границей является южная граница Большого Любимовского оползня [8], южной – северная буна вышеупомянутой системы из шести бун. Так же, как и на р. Качe, ранее на месте пойменной долины существовал лиман, впоследствии перекрытый сверху аллювием [4)].

Бельбек – самая полноводная река Крыма. К настоящему времени после окончания строительства в 1964 г. трех водохранилищ общим объемом более 12 млн. м^3 зарегулировано всего 20 % ее стока. Поступление аллювия в течение года крайне неравномерно. Формирование бюджета пляжеобразующего

материала и соответствующие изменения в динамике береговой линии в наибольшей степени определяются перераспределением объемов наносов во вдольбереговом направлении и поступлением аллювия с твердым стоком р. Бельбек. Другой источник поступления материала – береговая и донная абразия. Вклад последней в бюджет наносов из-за отсутствия наблюдений остается дискуссионным вопросом. Особенностью этого района побережья является существование направленного с севера на юг результирующего за год потока наносов.

После сильных штормов в прибойной зоне образуется волноприбойный вал, запирающий устье, при этом речные воды поступают в море, фильтруясь через этот вал. По нашим наблюдениям, для его образования необходимы два основных условия: сильный и продолжительный фронтальный западный шторм и слабое течение реки. При юго-западных штормах устье обычно отклоняется вправо, и в этом случае течение реки направлено параллельно берегу на расстоянии до 200 м. При северо-западных штормах устье ранее аналогичным образом отклонялось влево. В критических случаях с помощью бульдозеров прорывали искусственное русло реки.

В 2010 г. южнее устья для защиты пляжа была построена буна из каменной наброски, ступенчатым сооружением укреплен левый берег устья. Угол наклона буны в сторону моря составляет около 3° и равен естественному уклону пляжа. Пляж покрыл буну сверху песком и стабилизировался в течение первых трех лет после строительства. После окончания работ устье реки стало смещаться только вправо, к северу. В настоящее время верхняя часть буны обнажается только после сильного и продолжительного шторма с быстрым затуханием до первого шторма с медленным затуханием. В период катастрофического паводка в июне 2021 г. сильным течением реки отмыло только небольшую часть сооружения, которая затем в течение нескольких дней опять покрылась песком.

Анализ изменения береговой линии показывает, что формирование пляжа на значительной площади центрального участка пляжа ранее происходило в результате меандрирования устья р. Бельбек в обоих направлениях от устья. После строительства берегозащитного сооружения, которое исключило поворот устья реки в южном направлении, влияние этого фактора на конфигурацию береговой линии в северной части резко возросло. В результате паводков неоднократно наблюдался прорыв реки вдоль берега параллельно береговому валу в северном направлении на расстояние до 400 м, образование основных и вторичных валов. Это сопровождалось разрушением береговых построек, подмывом клифа и другими негативными последствиями. В период очень сильных паводков на протяжении до 200 м пляж может сильно размываться, однако после уменьшения стока довольно быстро восстанавливается (рис. 5).

Для определения динамики береговой линии использовались 105 поперечных сечений пляжа (рис. 6). Из рисунка видно, что наибольший размах смещения береговой линии характерен для короткого участка к северу от устья р. Бельбек протяженностью 260 м. Здесь максимальная величина составляет 30 м при среднем значении 20 м. К северу от этого участка на протяжении 900 м до северной границы пляжа максимальные значения составляют 13 м при среднем 8 м. К югу от устья реки значения несколько выше: максимальные

Р и с . 5 . Вид на устье р. Бельбек с юга в период сильного паводка 19 июня 2021 г.

F i g . 5 . View of the Belbek River from south during a strong freshet, 19 June 2021

до 23 м, а средние по этому участку 14 м. Необходимо отметить, что наиболее высокие значения размаха смещения выделяются в узкой зоне протяженностью 60 м, примыкающей к буне на южной границе пляжа, у которой происходит, в зависимости от направления вдольберегового движения наносов, попеременно размыв или аккумуляция пляжного материала.

Изменения между крайними датами (2011–2021 гг.) относительно невелики. К северу от устья р. Бельбек пляж в этот период оставался относительно стабильным, с небольшими смещениями в пределах ±5…8 м. В южной же части по всей длине наблюдалось выдвижение берега на расстояние в среднем до 10 м. График межгодовой изменчивости среднего по длине положения береговой линии показывает статистически незначимый тренд (−0.07 м/год) на фоне межгодовых колебаний до 9 м (2013–2014 гг.). Можно отметить, что после этого периода межгодовые изменения были крайне малы – 1…4 м (рис. 4). Ранее проведенные нами тахеометрические измерения показали, что внутригодовые изменения достигали 20 м [2].

Если брать период 1966–2021 гг., то в целом за 55 лет зафиксировано выдвижение береговой линии в южной части пляжа, величина которого в среднем составила 30 м, или 0.5 м/год. В северной части, где расположен клиф, наблюдалось отступание уреза на 10–20 м с увеличением к северу, или в среднем 0.3 м/год. Вместе с тем бóльшая часть изменений произошла между 1966 и 2005 гг. [3]. Вероятнее всего, этот период еще меньше, однако имеющиеся данные не позволяют сделать более обоснованный вывод. Мы связываем эти изменения со строительством набережной длиной 600 м и шести бун длиной 65 м каждая на южной границе пляжа, которое было начато в 1982 г. и завершено в 1989 г. Как известно, поперечные гидротехнические сооружения способствуют накоплению пляжевого материала или размыву.

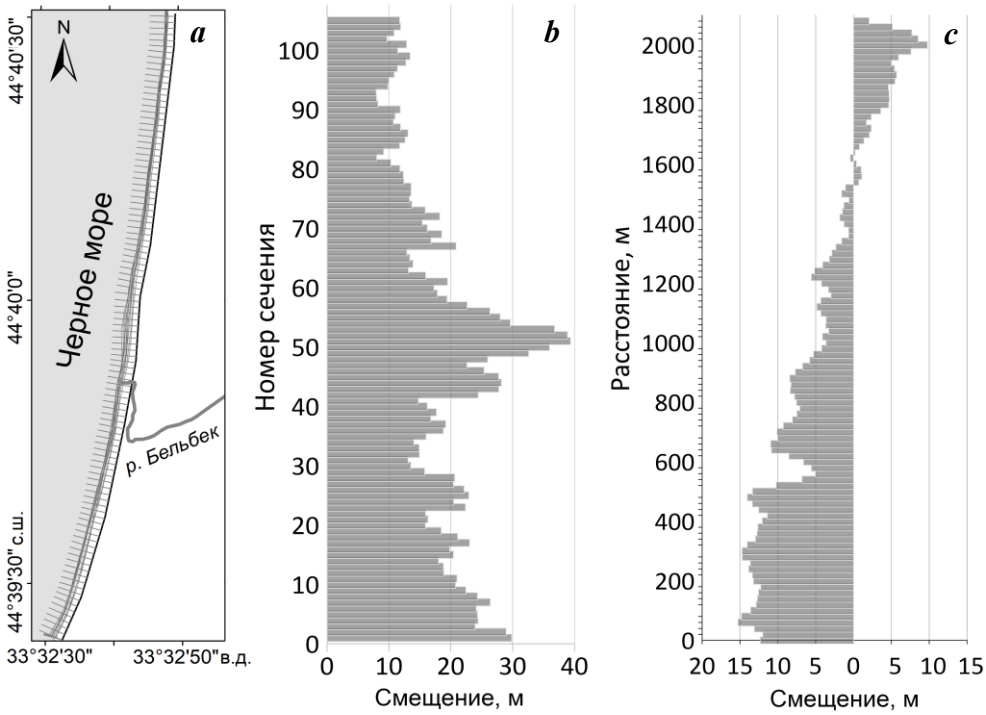

Р и с . 6 . Схема сечений на пляже вблизи устья р. Бельбек (*a*); размах смещений береговой линии за весь период (*b*); итоговые смещения береговой линии между крайними датами (*c*)

F i g . 6 . Map of transects on the beach near the Belbek River mouth (*a*); coastline displacement span for the whole period (*b*); resulting coastline displacements between the first and last dates of observations (*c*)

Наши наблюдения показали, что накопление здесь выражается не только в выдвижении берега, но и в увеличении вертикальной мощности пляжа, при этом избыточный материал даже перебрасывается через гребень бун.

В заключение отметим, что в 2021 г. в районе с. Верхнесадовое на р. Бельбек был построен водозабор. Первый год эксплуатации показал, что в бетонном ложе русла реки по длине сооружения очень быстро накапливаются наносы. Это требует периодической очистки, в результате чего поступление наносов в пляжную зону будет уменьшаться.

Пляж Учкуевка. Границами пляжа микрорайона Учкуевка на севере можно считать безымянный мыс к югу от отмеченного выше берегозащитного сооружения из набережной и шести бун, на юге – другой безымянный мыс. Пляж имеет длину 1.2 км, ширина его от 20 до 50 м при типичной около 30 м. Пляж прислоненный, сложен хорошо сортированным песком с включениями мелкой гальки, в тылу пляжа набережная и разнообразные объекты, необходимые для его эксплуатации. Пляж является одним из основных рекреационных объектов г. Севастополя. Питание пляжа ранее осуществлялось за счет перемещения материала из устья р. Бельбек в южном направлении и продуктов разрушения существовавшего здесь до террасирования клифа. После сооружения набережной и бун к северу от пляжа этого источника не стало.

К сожалению, отсутствие хорошо выраженных ориентиров на снимках 1941 г. и 1966 г. не позволяет выполнить приемлемую по точности геопривязку, однако качественный анализ свидетельствует, по-видимому, об относительно небольшой многолетней изменчивости как площади, так и конфигурации пляжа за 80 лет (рис. 7). Можно отметить даже небольшое увеличение ширины пляжа в 1966 г. по сравнению с 1941 г.

Для определения динамики береговой линии использовались 60 поперечных сечений пляжа (рис. 8). Из рисунка видно, что в целом на бóльшей длине размах многолетних смещений береговой линии относительно невелик и лежит в пределах 6–13 м при среднем значении 9 м. Только на небольшом участке в северной части протяженностью 140 м он возрастает до 15–20 м. Изменения между крайними датами (2011–2021 гг.) относительно невелики. В южной половине пляжа они почти нулевые, а в северной – в среднем 7 м при максимуме 10 м. Межгодовые изменения среднего положения береговой линии крайне малы (рис. 3), они не превышают 1–2 м, линейный тренд статистически не значим (−0.1 м/год).

Вместе с тем, как показывают наши наблюдения, внутригодовые изменения могут быть более значительными. Так, в результате действия шторма редкой повторяемости (главным образом из-за его аномальной продолжительности) 18–19 октября 2013 г. в северной части пляжа на протяжении 360 м пляжные накопления были частично смыты (рис. 9).

Р и с . 7 . Район пляжа микрорайона Учкуевка – аэрофото 1941 г. (*a*), спутниковые снимки 1966 г. (*b*) и 2021 г. (*c*)

F i g . 7 . The beach area of the microdistrict of Uchkuevka – aerial photo dated 1941 (*a*), satellite images dated 1966 (*b*) and 2021 (*c*)

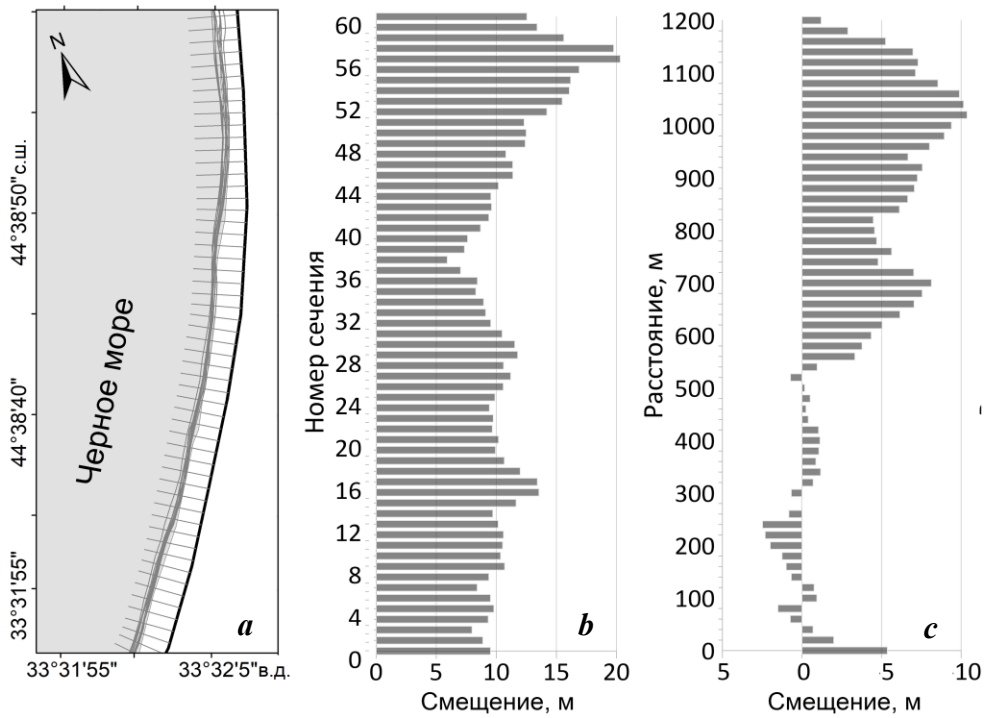

Рис. 8. Схема сечений на пляже Учкуевка (*a*); размах смещений береговой линии за весь период (*b*); итоговые смещения береговой линии между крайними датами (*c*)

Fig. 8. Map of transects on the beach near Uchkuevka Beach (*a*); coastline displacement span for the whole period (*b*); resulting coastline displacements between the first and last dates of observations (*c*)

В тыловой части пляжа образовался выраженный береговой уступ, возле уреза обнажились валуны, причем значительная часть материала была перемещена к югу. Объем песка и гравия, перемещенного к югу и вынесенного на глубину с одного погонного метра пляжа и подводного склона, оценивался нами в пределах от 20 до 35 м^3. Общий объем уменьшения пляжа в северной части составил около 10 тыс. м^3. Ширина пляжа в северной части уменьшилась на 5–10 м, на такую же примерно величину выдвинулся берег в южной части вплоть до безымянного мыса. На южной половине на участке берега протяженностью 550 м объем пляжного материала увеличился на 5–6 тыс. м^3, а около половины смытого в северной половине материала ушло на глубину. К апрелю – маю 2014 г. положение уреза почти восстановилось, однако вплоть до 2017 г. в северной части отмечалась нестабильность. Периодически берег отступал или выдвигался на 10–15 м, позже стал более устойчивым, однако прежний профиль пляжа не восстановился. Характерно, что, поскольку это событие зафиксировано в промежуток между снимками, оно никак не проявилось на графике межгодовой изменчивости средней ширины пляжа (см. рис. 3). Интересно сравнить динамику рассмотренных выше пляжей с динамикой аккумулятивных берегов в сходных природных условиях других причерноморских стран.

Р и с . 9 . Северная часть пляжа Учкуевка 18 октября 2010 г. (*a*), 2 ноября 2013 г. (*b*)

F i g . 9 . The northern Uchkuevka beach on 18 October 2010 (*a*), 2 November 2013 (*b*)

В настоящее время из общей длины береговой линии дельты Дуная более половины подвержено размыву, на 30 % отмечается аккумуляция, 15 % находятся в динамическом равновесии и относительно стабильны, типичные скорости размыва до 5–25 м/год [9]. Такое соотношение румынские ученые связывают со строительством плотин для гидроэнергетических целей, сооружением различных насыпей, спрямлением русла и другими гидротехническими работами в нижнем течении Дуная, в результате чего годовой сток наносов сократился вдвое [10, 11]. Проблемным является знаменитый пляж Мамая в Румынии. Имевший еще в 1960-х гг. ширину 100 м, к 1985 г. он уменьшился до 50 м. В последующие 15 лет пляж продолжал уменьшаться со средней скоростью 2.25 м/год. Причина – гидротехническое строительство, из-за которого был заблокирован вдольбереговой перенос наносов [12]. В 1980-х гг. в Варненском заливе (Болгария) была построена прибрежная дамба и система непроницаемых бетонных бун, из-за заносимости фарватеров регулярно проводилось дноуглубление. Кроме этого, в последние десятилетия практиковалось строительство зданий непосредственно на пляжах. Вся эта деятельность привела к нарушению естественных динамических процессов, а береговая линия Варненского залива была необратимо изменена. Так, до вмешательства человека пляж Аспарухово постоянно рос из-за разгрузки здесь двух встречных потоков наносов, а в настоящее время длина его уменьшилась на 800 м. В результате нарушения естественного питания прилегающих песчаных пляжей отдельные пляжи или исчезли, или существенно сократились[13–15].

Заключение

На основании вышеизложенного можно сделать следующие основные выводы.

1. Аккумулятивные берега в долинных понижениях рек Качи и Бельбека также, как и пляж Учкуевка, в последнее десятилетие (2011–2021 гг.) находятся в динамическом равновесии. Значимых трендов изменений среднего положения береговой линии для периода 2011–2021 гг. не обнаружено. Ранее пляжи испытали значительные изменения береговой линии, связанные с антропогенной деятельностью (сокращение твердого стока, добыча песка, строительство берегозащитных сооружений).

2. Наибольший максимальный размах смещения береговой линии в период 2011–2021 гг. характерен для участка к северу от устья р. Качи – 26 м при среднем значении 20 м. На участке южнее устья р. Качи максимальный размах смещения уменьшается до 16 м, а средний до 13 м.

3. Наибольший размах смещения положения береговой линии в период 2011–2021 гг. характерен для участка протяженностью 260 м к северу от устья р. Бельбек – 30 м при среднем значении 20 м. К северу от этого участка, на протяжении 900 м до северной границы пляжа, максимальные значения составляют 13 м при среднем 8 м. К югу от устья реки максимальные значения 23 м, а средние 14 м. Наиболее высокие значения размаха смещения выделяются в узкой зоне протяженностью 60 м, примыкающей к буне на южной границе пляжа, у которой наблюдается, в зависимости от направления вдольберегового движения наносов, попеременно размыв или аккумуляция.

4. На бóльшей длине пляжа Учкуевка в период 2011–2021 гг. размах многолетних смещений береговой линии относительно невелик и лежит в пределах 6–13 м при среднем значении 9 м. Только на небольшом участке в северной части протяженностью 140 м он возрастает до 15–20 м.

5. Максимальная межгодовая изменчивость среднего по длине положения береговой линии достигает 10 м для пляжей в устьях рек Качи и Бельбека, до 2 м для пляжа Учкуевка.

6. Внутригодовые изменения положения береговой линии по величине могут превышать межгодовые. При анализе спутниковых данных для определения динамики береговых линий необходимо использовать не только снимки, полученные в крайние даты, а всю совокупность имеющихся изображений.

Список литературы

1. *Ефремова Т. В., Горячкин Ю. Н*. Морфодинамика севастопольских бухт под воздействием антропогенной деятельности // Экологическая безопасность прибрежной и шельфовой зон моря. 2023. № 1. С. 31–47. EDN THAAMX. doi:10.29039/2413-5577-2023-1-31-47
2. *Удовик В. Ф., Долотов В. В.* Современное состояние и тенденции динамики береговой зоны в районе пляжа пос. Любимовка // Экологическая безопасность прибрежной и шельфовой зон и комплексное использование ресурсов шельфа. Севастополь : ЭКОСИ-Гидрофизика, 2009. Вып. 20. С. 92–99. EDN XCIVOL.
3. *Долотов В. В., Попова А. В.* Оценка долгопериодной динамики пляжа пос. Любимовка // Экологическая безопасность прибрежной и шельфовой зон и комплексное использование ресурсов шельфа. Севастополь : ЭКОСИ-Гидрофизика, 2014. Вып. 28. С. 31–41. EDN VBFSNV.
4. *Долотов В. В., Горячкин Ю. Н., Долотов А. В*. Статистический анализ изменений береговой линии пляжа поселка Любимовка // Экологическая безопасность прибрежной и шельфовой зон моря. 2017. № 1. С. 40–47.
5. *Луговой Н. Н.* Современное состояние морских берегов Севастополя // Теория и методы современной геоморфологии : Материалы XXXV Пленума Геоморфологической комиссии РАН. Т. 1. Симферополь, 2016. С. 241–245.
6. *Земсков В. Ф., Заичко В. А., Зайченко Ю.В.* Оценка геометрической точности космических снимков, получаемых системами дистанционного зондирования Земли в различных диапазонах электромагнитного спектра // Известия вузов. Приборостроение. 2018. Т. 61, № 7. С. 576–583. doi:10.17586/0021-3454-2018-61-7-576-583

7. О точности создания ортофотопланов по снимкам QuickBird / В. Н. Андров [и др.] // Геопрофи. 2005. № 6. С. 21–24.
8. *Горячкин Ю. Н., Федоров А. П.* Оползни Севастопольского региона. Часть 1. Северная сторона // Экологическая безопасность прибрежной и шельфовой зон моря. 2018. № 1. С. 4–12.
9. Danube Delta Coastline Evolution (1856–2010) / A. Vespremeanu-Stroe [et al.] // Landform Dynamics and Evolution in Romania. Cham : Springer, 2017. P. 551–564. https://doi.org/10.1007/978-3-319-32589-7_23
10. *Stanica A., Dan S., Ungureanu V. G.* Coastal changes at the Sulina mouth of the Danube River as a result of human activities // Marine Pollution Bulletin. 2007. Vol. 55, iss. 10–12. P. 555–563. https://doi.org/10.1016/j.marpolbul.2007.09.015
11. *Ungureanu Gh., Stanica A.* Impact of human activities on the evolution of the Romanian Black Sea beaches // Lakes & Reservoirs: Research and Management. 2000. Vol. 5, iss. 2. P. 111–115. https://doi.org/10.1046/j.1440-1770.2000.00105.x
12. Beach Erosion and Coastal Protection Plan along the Southern Romanian Black Seashore / K. Kuroki [et al.] // Coastal Engineering: proceedings of the 30th International Conference, San Diego, California, USA, 3–8 September 2006. World Scientific Publishing Co Pte Ltd., 2007. Vol. 5. P. 3788–3799. https://doi.org/10.1142/9789812709554_0318
13. Longshore sediment transport at Golden Sands (Bulgaria) / H. Nikolov [et al.] // Oceanologia. 2006. Vol. 48, iss. 3. P. 413–432.
14. *Дачев В. Ж.* Генезис и еволюция на централния плаж на град Варна // Трудове на Института по океанология. 2003. Т. 4. С. 74–82.
15. *Ефремова Т. В., Горячкин Ю. Н.* Антропогенное воздействие на литодинамику береговой зоны южного и западного побережий Черного моря (обзор) // Экологическая безопасность прибрежной и шельфовой зон моря. 2021. № 2. С. 5–29. doi:10.22449/2413-5577-2021-2-5-29

Поступила 1.05.2023 г.; одобрена после рецензирования 2023 г.;
принята к публикации 2023 г.; опубликована 2023 г.

Об авторах:

Горячкин Юрий Николаевич, главный научный сотрудник, Морской гидрофизический институт РАН (299011, Россия, Севастополь, ул. Капитанская, 2), доктор географических наук, **ORCID ID: 0000-0002-2807-201X, ResearcherID: I-3062-2015**, *yngor@mhi-ras.ru*

Долотов Вячеслав Валентинович, старший научный сотрудник, Морской гидрофизический институт РАН (299011, Россия, Севастополь, ул. Капитанская, 2), кандидат химических наук, **ORCID ID: 0000-0002-1485-2883**, **ResearcherID: E-5570-2016**, *dolotov_v_v@mhi-ras.ru*

Заявленный вклад авторов:

Горячкин Юрий Николаевич – постановка проблемы, обработка и анализ данных, подготовка текста статьи

Долотов Вячеслав Валентинович – обработка и анализ данных, подготовка текста статьи и иллюстративного материала

Все авторы прочитали и одобрили окончательный вариант рукописи.

Original paper

Approaches to Formation of the Ecological Framework of the Western Coast of Sevastopol

T. V. Pankeeva [1] *, N. V. Mironova [1], A. V. Parkhomenko [2]

[1] *Kovalevsky Institute of Marine Biological Research of RAS, Sevastopol, Russia*
[2] *Marine Hydrophysical Institute of RAS, Sevastopol, Russia*

* *e-mail: tatyanapankeeva@yandex.ru*

Abstract

For the first time, the paper proposes an outline of an ecological framework for the western coast of Sevastopol. An ecological framework is a network of protected areas and objects of different status represented by areal, linear and point elements. The studying of the bottom landscape structure and hydro-botanical survey of the coastal zone were carried out in summer 2020. Based on the obtained data, a map of underwater landscapes in the study water area was made. Six underwater landscapes dominated by key macrophyte species were identified in the landscape structure: *Ericaria crinita*, *Gongolaria barbata,* and *Phyllophora crispa*. For each underwater landscape, the phytocenosis is described, and quantitative and qualitative indicators of macrophytobenthos are calculated (species composition of macrophytes, presence of protected red-listed algae species, phytomass stock of macroalgae and its dominant species). Based on the landscape approach, spatial and functional conservation elements (key, transit, buffer and restorative) were identified taking into account the indicators of the vegetation component of underwater landscapes. It was revealed that for the coastal area under study the key water areas include underwater landscapes with "*Cystoseira*" phytocenosis, the transit ones include landscapes with "*Cystoseira*" – *Phyllophora* phytocenosis, and restorative ones include landscapes with *Phyllophora* phytocenosis. All elements of the ecological framework have different protection regimes and are of different types of nature management. The obtained results and proposed approach can be used to form an ecological framework of the marine areas of Sevastopol and the Republic of Crimea.

Keywords: underwater landscapes, macrophytobenthos, protected water areas, landscape approach, Black Sea.

Acknowledgments: This work was carried out under state assignment of A. O. Kovalevsky Institute of Biology of the Southern Seas of the Russian Academy of Sciences (no. 121030300149-0) and Marine Hydrophysical Institute of RAS no. FNNN-2021-0005. The authors are grateful to I. K. Evstigneeva and I. N. Tankovskaya for the determination of the species composition of algae and joint work on the processing of the collected material; divers I. Yu. Tamoikin for their help in sampling macrophytobenthos and taking photos and videos of underwater landscapes.

For citation: Pankeeva, T.V., Mironova, N.V. and Parkhomenko, A.V., 2023. Approaches to Formation of the Ecological Framework of the Western Coast of Sevastopol. *Ecological Safety of Coastal and Shelf Zones of Sea*, (3), pp. 71–85.

Подходы к формированию экологического каркаса западного прибрежья Севастополя

Т. В. Панкеева [1] *, **Н. В. Миронова** [1], **А. В. Пархоменко** [2]

[1] *ФГБУН ФИЦ Институт биологии южных морей имени А.О. Ковалевского РАН, Севастополь, Россия*
[2] *Морской гидрофизический институт РАН, Севастополь, Россия*
* *e-mail: tatyanapankeeva@yandex.ru*

Аннотация
Впервые предложена схема экологического каркаса для западного прибрежья Севастополя. Экологический каркас представляет собой сеть природоохранных территорий и объектов разного статуса, состоящих из площадных, линейных и точечных элементов. Работы по изучению ландшафтной структуры дна и гидроботаническая съемка прибрежной зоны проведены в летний период 2020 г. На основе полученных сведений составлена карта подводных ландшафтов исследуемой акватории. В ландшафтной структуре выделено шесть подводных ландшафтов с доминированием ключевых видов макрофитов: *Ericaria crinita*, *Gongolaria barbata* и *Phyllophora crispa*. Для каждого подводного ландшафта описан фитоценоз, рассчитаны количественные и качественные показатели макрофитобентоса (видовой состав макрофитов, наличие охраняемых краснокнижных видов водорослей, запас фитомассы макроводорослей и входящих в ее состав доминирующих видов). На основе ландшафтного подхода с учетом показателей растительной компоненты подводных ландшафтов выделены пространственно-функциональные природоохранные элементы (ключевые, транзитные, буферные и восстановительные). Выявлено, что на изучаемом прибрежье к ключевым акваториям относятся подводные ландшафты с «цистозировым» фитоценозом, к транзитным – с «цистозирово»-филлофоровым, к восстановительным – с филлофоровым. Все элементы экологического каркаса имеют разные режимы охраны и относятся к разным типам природопользования. Полученные результаты и предложенный подход могут быть использованы для формирования экологического каркаса морских акваторий Севастополя и Республики Крым.

Ключевые слова: подводные ландшафты, макрофитобентос, охраняемые акватории, ландшафтный подход, Черное море

Благодарности: исследование выполнено в рамках государственного задания Института биологии южных морей имени А.О. Ковалевского РАН (№ гос. регистрации 121030300149-0) и ФГБУН ФИЦ МГИ (№ гос. регистрации FNNN-2021-0005). Выражаем благодарность сотрудникам отдела биотехнологий фиторесурсов к. б. н., с. н. с. И. К. Евстигнеевой и м. н. с. И. Н. Танковской за определение видового состава водорослей и совместную работу по обработке собранного материала; дайверу И. Ю. Тамойкину за помощь в отборе проб макрофитобентоса и видеосъемку подводных ландшафтов.

Для цитирования: *Панкеева Т. В., Миронова Н. В., Пархоменко А. В*. Подходы к формированию экологического каркаса западного прибрежья Севастополя. // Экологическая безопасность прибрежной и шельфовой зон моря. 2023. № 3. С. 71–85. EDN YHYNCD.

Introduction

Specially protected natural reservations (SPNR) play an important role in preserving biological and landscape diversity. One of the recognized forms of territorial nature conservation is creation of ecological networks. Currently, the concept of ecological networks for land territories has been quite fully developed [1]. Models of regional ecological networks have been proposed for a number of constituent entities of the Russian Federation [2, 3]. However, the lack of a unified legislative framework, generally accepted methods and approaches makes it difficult to create regional and national ecological networks, especially for territories with anthropogenically transformed landscapes. In recent years, approaches [1), 2)] to the formation of marine ecological networks have been actively developed – mainly in regions where marine reserves have been created [4, 5]. Nevertheless, "the criteria for identifying and optimal areas of the main structural elements, and especially the issues of their connection into a functionally integral system" remain insufficiently developed [1, p. 134].

In 2008, a regional ecological network project was developed for the Autonomous Republic of Crimea and the city of Sevastopol. In addition, other schemes of ecological networks for Crimea are presented in the scientific literature [6, 7].

In the coastal waters of the Crimean Peninsula, 13 coastal elements of the eco-network have been identified (8 eco-centers and 5 eco-corridors). The SPNR of Sevastopol, which include marine protected areas (MPA), are located within the boundaries of the Heraclea and Aya Sarych seaside eco-centers, as well as the Kalamitskiy seaside eco-corridor [3)]. Most of the Crimean MPA are isolated, have a small area and have a low protection status, which does not allow them to fully carry out environmental protection tasks. The research carried out at the Crimean MPA shows that currently there is degradation of natural bottom complexes associated with an increased anthropogenic load [8].

In this regard, the ecological network elements of Crimea, including the city of Sevastopol, are in the need of developing an ecological framework of sustainability, consisting of interconnected spatial-functional environmental elements (key, transit, buffer and restoration) [9]. The works of a number of authors highlight the use of this approach to form ecological networks and their elements in land landscapes [10, 11]. With the landscape approach, attention is focused on "landscape diversity, environment-forming functions of geosystems, material and energy flows in the landscape" [1, p. 133]. The use of the landscape approach for marine ecological

---

[1)] Kelleher, G. and Recchia, C., 1998. Lessons from Marine Protected Areas around the World. *Parks,* 8(2), pp. 1–4. Available at: https://parksjournal.com/wp-content/uploads/2017/06/parks_8_2.pdf [Accessed: 12 September 2023].

[2)] Salm, R.V., Clark, J.R. and Sirila, E., 2000. *Marine and Coastal Protected Areas: A Guide for Planners and Managers*. Washington DC: IUCN, 371 p. Available at: http://seaknowledgebank.net/sites/default/files/marine-and-coastal-protected-areas-a-guide-for-planners-and-managers_0.pdf [Accessed: 12 September 2023]

[3)] TNU, 2008. [*Development of Regional Ecological Network Scheme of Autonomous Republic of Crimea: Report on Research Project*]. Simferopol, 312 p. (in Russian).

networks raises certain methodological difficulties due to poor development of theoretical foundations of underwater landscape science [9, 12].

One of the most important components of underwater landscapes is bottom vegetation, which is considered an indicator of morphological complexes of horizontal division of landscape structure. It is known that macrophytobenthos is the main production link of the Black Sea shelf and plays a leading role in stabilization and self-regulation of coastal ecosystems. Based on the fact that macrophytes actively respond to environmental changes, their quantitative and qualitative indicators can be used as criteria for identifying elements of an ecological network [8, 13].

The coastal zone of the western part of Sevastopol, which is distinguished by its biological and landscape diversity, was chosen as a model region. Currently, this zone is being actively developed – projects to develop infrastructure in the coastal zone are being implemented here. In this regard, it is relevant to develop recommendations for conservation of underwater coastal landscapes.

The purpose of this article is to develop an outline of the ecological framework of the western coastal area of Sevastopol.

Materials and research methods

The coastline length of the western coast of Sevastopol (Cape Kosa Severnaya – Cape Tubek) is about 26 km. The coastal waters are characterized by shallow depths and bottom slopes. On the bench, sandy and pebble bottom sediments are developed, replaced by a blocky pile [14]. The water area is located within the boundaries of the Kalamitskiy seaside eco-corridor of the ecological framework of the Crimean Peninsula. The SPNR is represented by the natural monument "Cape Lukull Coastal Aquatic Complex (CAC)", the length of its coastline reaches 3448.6 m, the width of the water area is 300 m. The total area of the natural monument is 128.5 ha, of which the territory area is 15.1 ha, and the water area is 113.4 ha.

The work to study the bottom landscape structure of the coastal zone was carried out on the basis of general provisions of the underwater landscape research program in the summer of 2020 [15]. The underwater landscaping work was carried out from small vessels using light diving equipment. When studying the structure of coastal landscapes, we used the method of landscape profiling with a description of profiles and key areas [16]. Landscape profiles were compiled for 10 profiles (Fig. 1). Landscape profiling made it possible to identify underwater landscapes and establish their boundaries. To create a landscape map, we used the QGIS 2.18.25 software package and the electronic basis of the navigation map. A combined analysis of bathygraphy, maps of lithological composition and diving survey data made it possible to extrapolate areas of the bottom with similar parameters to identify the boundaries of underwater landscapes. The results of generalization of studies of the landscape structure of the western coastal region of Sevastopol are reflected on the landscape map.

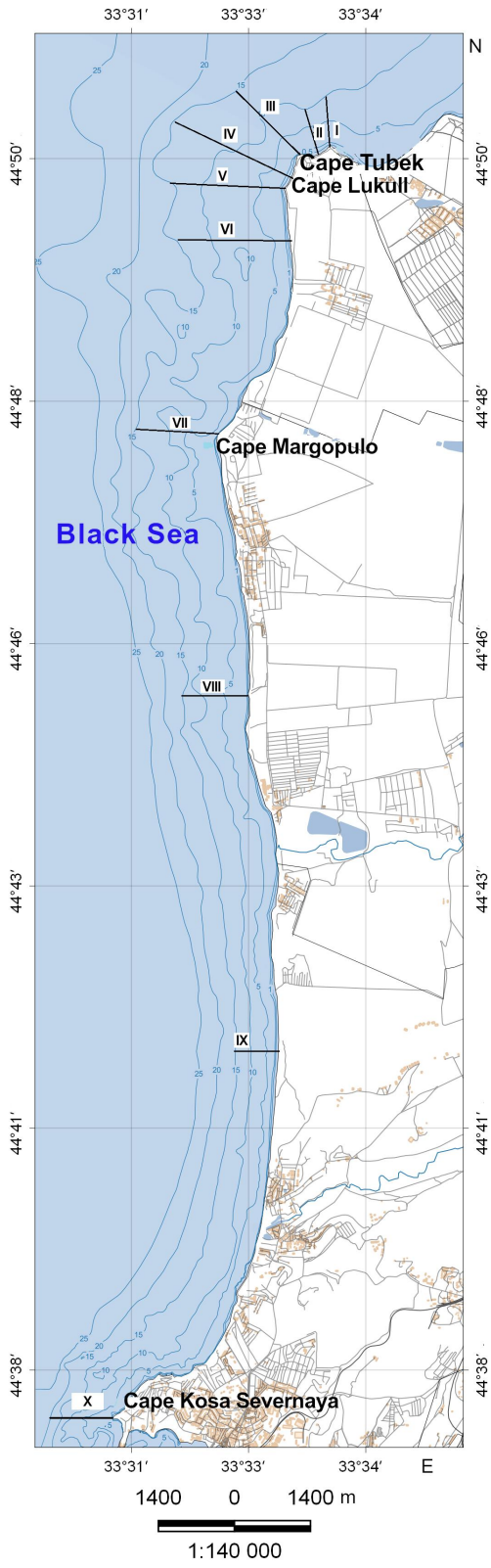

Fig. 1. Schematic map of the location of landscape and hydrobotanical profiles in the coastal zone Cape Kosa Severnaya – Cape Tubek (Roman numerals stand for profiles)

The study of bottom vegetation was carried out according to generally accepted methods [4]. To study the composition and structure of macrophytobenthos, we used materials from hydrobotanical surveys carried out on the same profiles. The sampling was carried out at depths of 0.5; 1; 3; 5; 10 and 15 m, where four counting areas measuring 25 × 25 cm were laid. The algae identification was carried out taking into account the latest nomenclature changes [5]. The resources of macroalgae (t, wet weight), the stock of phytomass of macrophytes and the key species of algae included in its composition ($t \cdot ha^{-1}$, wet weight) were calculated using a method modified for marine research [8]. The water area was determined using the QGIS program.

The criteria selected for identifying elements of the ecological network were quantitative and qualitative indicators of macrophytobenthos (species composition of macrophytes, presence of protected Red Book species of algae, stock of phytomass of macroalgae and its key species, share of *Ericaria crinita* (Duby) Molinari & Guiry = *Cystoseira crinita* and *Gongolaria barbata* (Stackhouse) Kuntze = *Cystoseira barbata* in the total reserves of macrophytes), characterizing the plant component of underwater landscapes. When working on the article, we used annotated lists of algae recorded in the area of the western coast and the natural monument "Cape Lukull Coastal Aquatic Complex (CAC)", given in the articles by I.K. Evstigneeva and I.N. Tankovskaya [17, 18].

Based on the mapping of underwater landscapes, qualitative and production characteristics of macrophytobenthos, a functional-areal distribution of the main elements of the ecological network (key environmental (protected cores), buffer protective, transit and restorative water areas) is proposed.

Results and discussion

In the landscape structure of the coastal zone, six underwater landscapes were identified with the participation of dominant species of macrophytes: *Ericaria crinita*, *Gongolaria barbata* and *Phyllophora crispa* (Hudson) P.S. Dixon (Fig. 2). The developed coastal landscape map is a cartographic basis for identifying water areas that form elements of the ecological framework.

For each landscape contour, quantitative and qualitative indicators of macrophytobenthos were calculated and presented in the table.

Based on the landscape approach, taking into account the values of the plant component of underwater landscapes, a map was drawn up and elements of the ecological framework of the western coast of Sevastopol were identified (Fig. 3).

The underwater landscapes located within the boundaries of the natural monument "Cape Lukull Coastal Aquatic Complex (CAC)" belong to **the key environmental water areas (protected cores) (KEWA)** (Fig. 3).

---

[4] Kalugina-Gutnik, A.A., 1969. [Study of the Black Sea Bottom Vegetation Using Lightweight Diving Equipment]. In: Academy of Sciences of the USSR, 1969. [*Marine Underwater Studies*]. Moscow: Nauka, pp. 105–113 (in Russian).

[5] Guiry, M.D. and Guiry, G.M. 2023. *AlgaeBase*. National University of Ireland, Galway. [online] Available at: http://www:algaebase.org [Accessed: 12 September 2023].

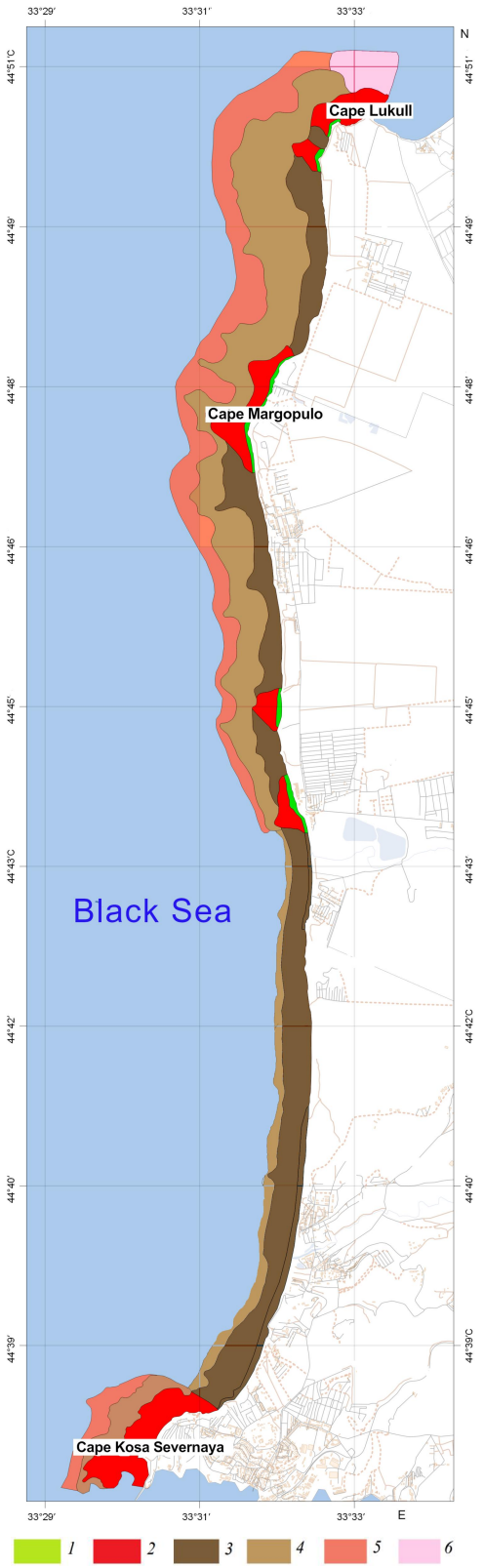

Fig. 2. Schematic map of the landscape structure of the coastal zone (Cape Kosa Severnaya – Cape Tubek): *1* – boulder benches with dominance of *Ericaria crinita* and *Gongolaria barbata*; *2* – upper shoreface consisting of psephitic sediments predominated by *Ericaria crinita* and *Gongolaria barbata*; *3* – upper shoreface consisting of sandy sediments with small ripple marks (riffles), devoid of bottom vegetation (species of *Ericaria crinita* and *Gongolaria barbata* or *Padina pavonica* and *Dictyota fasciola* dominate on some clumps); *4* – upper shoreface consisting of psephitic deposits predominated by *Gongolaria barbata* with mosaic alternation of pebble and gravel deposits and shell fragments predominated by *Phyllophora crispa*; *5* – gently dipping accumulation plain formed by psammitic deposits with inclusion of shell fragments predominated by *Phyllophora crispa*; *6* – gently dipping accumulation plain formed by sandy sediments, with no bottom vegetation

The landscape structure of this protected water area is dominated by underwater slopes dominated by *Cystoseira* species (*Ericaria crinita* and *Gongolaria barbata*), where the phytocenosis *Ericaria crinita*+*Gongolaria barbata* was recorded at depths of 0.5–5 m.

On the underwater slope at a depth of 0.5–1 m, ***a block-boulder bench with a predominance of Ericaria crinita and Gongolaria barbata (1)*** was recorded (Fig. 2). The plant component of this landscape is characterized by high species diversity (Table) – five species of algae listed in the Red Book of the Russian Federation, the Republic of Crimea and the city of Sevastopol are registered here (*Stilophora tenella* (Esper) P.C. Silva, *Laurencia coronopus* J. Ag, *Osmundea hybrida* (A.P. de Candolle), *Ericaria crinita* and *Gongolaria barbata*). The largest reserve of phytomass of macrophytes and their dominant species of *Cystoseira* (*Ericaria crinita* and *Gongolaria barbata*) is noted here (Table). The share of these algae in the total reserves of macrophytobenthos is maximum (86 %) (Table).

The underwater slope, composed of coarse sediments, dominated by Ericaria crinita and Gongolaria barbata (2), located at depths of 1–5 m, is distinguished by the greatest species diversity compared to other studied landscapes of the western coastal region (Table). The number of red-listed species of macrophytes reaches six (in addition to the above species, with the exception of *Osmundea hybrida*, *Phyllophora crispa* and *Osmundea pinnatifida* (Hudson) Stackhouse were discovered). The phytomass reserve of macrophytes, as well as *Ericaria crinita* and *Gongolaria barbata*, is slightly lower than at depths of 0.5–1 m (Table).

According to the information about the composition and structure of macrophytobenthos collected along the western coast of Sevastopol using a similar method by A.A. Kalugina-Gutnik and N.M. Kulikova [19] in 1964, we calculated the stock of *Cystoseira* phytomass in this selected landscape. Thus, a comparative analysis showed that at depths of 1–5 m the phytomass reserve of *Ericaria crinita* and *Gongolaria barbata* was 40.7 $t \cdot ha^{-1}$, which is approximately one and a half times lower than in 2020.

However, it is well known that at present, along the coast of Crimea, significant compaction of *Cystoseira* thickets is observed everywhere in the upper and middle sublittoral zone, while degradation and transformation of bottom vegetation is recorded in the lower zone [8]. Thus, over the past 56 years, the safety of the water area belonging to the KEWA has remained quite high.

In the rest of the coastal waters of the study region, the underwater landscapes dominated by *Cystoseira*, due to their environmental value, should be considered as **restorative water areas (RWA)**. In the future, in this part of the coastal zone it is expected to reduce the influence of anthropogenic impact, and in certain cases it is necessary to take special measures to restore biotopes and landscapes as a whole.

For ***an underwater slope composed of sandy sediments with small ripple marks (ripples), devoid of bottom vegetation, where individual blocks are dominated by the species of Ericaria crinita and Gongolaria barbata or Padina pavonica and Dictyota fasciola (3)***, at depths of 1–5 m the phytocenoses of

Ericaria crinita + *Gongolaria barbata* or *Padina pavonica* + *Dictyota fasciola* are characteristic. This landscape also shows high species diversity and the presence of red-listed species (Table). The phytomass reserve of macrophytes, *Ericaria crinita* and *Gongolaria barbata*, is significantly lower (Table). However, this isolated underwater landscape is characterized by an intensive exchange of material flows due to the movement of fine-clastic clay-sandy material by alongshore currents. In addition, this landscape provides the necessary connection between the underwater landscapes of the KEWA and RWA and provides an opportunity for distribution, migration and genetic exchange of aquatic species. Thus, this underwater landscape corresponds to the **transit water area (TWA)** of the coastal area under study, while in marine protected areas it must be included in the TWA.

Species composition and productivity of macrophytobenthos in the underwater landscapes of the western coast of Sevastopol

Species composition of algae					Number of protected algae species listed in Red Book of			Total biomass of, $t \cdot ha^{-1}$		
Underwater landscape	Total number	Green	Brown	Red	Sevastopol[6]	Republic of Crimea[7]	Russian Federation[8]	macrophytes	*Ericaria crinita* + *Gongolaria barbata*	*Phyllophora crispa*
1	40	12	7	21	1	4	1	78.8	67.8	0
2	49	8	8	29	2	6	2	69.1	49.1	0.1
3	40	9	8	23	1	5	0	17.1	13.1	0
4	43	8	8	27	2	6	1	40.2	20.1	2.4
5	30	6	7	17	1	3	1	39.4	13.0	3.1

Note: the numbering and description of underwater landscapes corresponds to the information presented in the text and in Fig. 2. Information on the algal species composition by depth is given in [17, 18].

[6] Dovgal, I.V. and Korzhenevskiy, V.V., eds., 2018. *The Red Data Book of Sevastopol*. Sevastopol: ROST-DOAFK, 432 p. (in Russian).

[7] Ivanov, S.P. and Fateryga, A.V., eds., 2015. *Red Book of the Republic of Crimea. Animals.* Simferopol: ARIAL, 440 p. (in Russian).

[8] Bardunov, L.V. and Novikov, V.S., eds., 2008. [*Red Data Book of the Russian Federation (Plants and Fungi)*]. Moscow: Tovarishchestvo Nauchnyh Izdaniy KMK, 885 p. (in Russian).

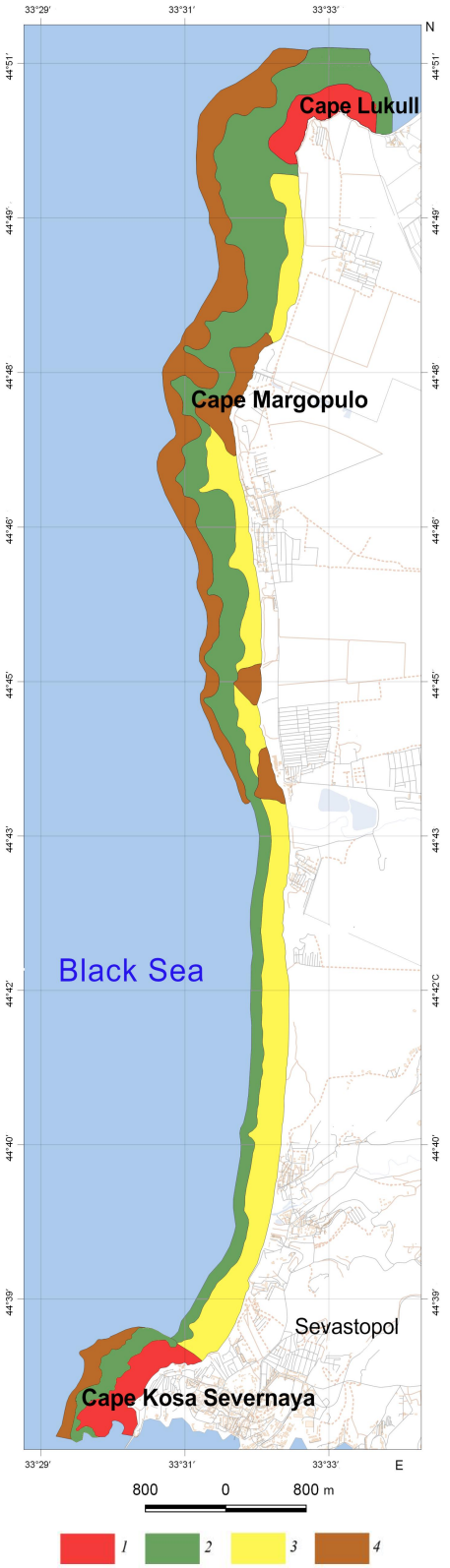

Fig. 3. Elements of the ecological framework of the Sevastopol western coast: *1* – key environmental water areas; *2* – buffer water areas; *3* – transit water areas; *4* – restorative water areas

It is characteristic that within the boundaries of the Kalamitskiy eco-corridor there is no sufficient number of natural cores, which is one of the prerequisites for the creation of the natural monument "Cape Kosa Severnaya Coastal Aquatic Complex (CAC)". Previously obtained research results in this coastal area indicate high floristic and landscape diversity in the depth range of 0.5–10 m [20]. The algal flora contains species of macrophytes included in the Red Book lists of the Russian Federation, the Republic of Crimea and Sevastopol (*Phyllophora crispa*, *Stilophora tenella*, *Ericaria crinita*, *Gongolaria barbata*, *Laurencia coronopus*, *Nereia filiformis* (J. Ag.) *Zanard.*). The indigenous phytocenoses of these underwater landscapes are characterized by a high degree of preservation, which makes it possible to recommend the water area near Cape Kosa Severnaya as promising for conservation and to include it in the KEWA.

The role of **a buffer water area (BWA)** is played by ***an underwater slope composed of coarse clastic sediments, dominated by Gongolaria barbata, mosaically alternating with pebble-gravel deposits with broken shells, dominated by Phyllophora crispa (4)*** (depth 5–10 m). The phytocenoses of *Gongolaria barbata* and *Phyllophora crispa* are described. This underwater landscape occupies the peripheral parts of the KEWA, RWA and TWA, and therefore performs a protective function of the water areas and ensures optimal functioning of protected species. Uniqueness of this underwater landscape lies in the fact that it represents a transitional strip where several perennial phytocenoses occur simultaneously at the same depth, and their distribution is determined by the peculiarities of bottom lithology. At these depths, there is a gradual change in the composition of bottom vegetation along the illumination gradient. The reserves of phytomass of macrophytes and *Cystoseira* are decreasing, but this indicator is increasing in *Phyllophora crispa* (Table). The contribution of *Ericaria crinita* and *Gongolaria barbata* to the total macrophyte reserves does not exceed 50 %.

In this area in 1964, the phytomass reserve of *Ericaria crinita* and *Gongolaria barbata* was 24.8 $t \cdot ha^{-1}$, and the phytomass reserve of *Phyllophora crispa* was 2.6 $t \cdot ha^{-1}$ in the depth range of 5–10 m [18]. These values are only slightly higher than comparable values in 2020 (Table), confirming the relatively unchanged state of benthic vegetation in the study area in this depth interval.

At a depth of more than 10 m, ***a slightly inclined plain, composed of gravel-sand deposits with broken shells and dominated with Phyllophora crispa (5)*** was recorded. For this underwater landscape, the maximum supply of *Phyllophora crispa* was noted (Table). The share of *Cystoseira* species is less than 33 % (of the total macrophyte reserves). More than half a century ago, at depths of 10–15 m, the stock of *Phyllophora crispa* phytomass reached 9.7 $t \cdot ha^{-1}$, which is three times higher than the value recorded in 2020 [19].

A sharp decline in the stock of *Phyllophora crispa* phytomass indicates the need to preserve this landscape. Since this species is protected at the international, state and regional levels [9], the underwater landscapes with phyllophora phytocenosis must be classified as **RWA**.

The obtained research results indicate that at present, underwater landscapes and their plant components are distinguished by a high degree of preservation in the coastal waters of the western coast of Sevastopol. This is confirmed in the article by I.K. Evstigneeva and I.N. Tankovskaya [21]. According to the work of these authors, the results of phytoindication along the western coast of Sevastopol show a widespread dominance of oligosaprobic macrophyte species, an abundance of mesosaprobic species and a small share of polysaprobic species, which corresponds to the ratio of saprobiological groups in clean areas of the sea. Taking into account high biological and landscape diversity of the studied region, it is advisable to develop an ecological framework of the coastal zone, which will make it possible to identify areas with different environmental management regimes.

Thus, when identifying the main structural elements of the ecological framework of the western coastal area of Sevastopol, the biocentric and landscape approaches were used for the first time. As studies have shown, both approaches to the formation of the ecological framework of the coastal zone are complementary and reflect different aspects of its organization. It is characteristic that with a biocentric approach, special attention is paid to the preservation of living organisms (species diversity of aquatic organisms, presence of rare and endangered species, etc.). Thus, in the paper by S.E. Sadogursky and colleagues [22], it was noted that the qualitative and quantitative indicators of coastal marine biota are highest in areas where thickets of macrophytes are noted. It should be noted that some indicators of macrophytobenthos presented by the authors in the article correspond to the criteria for a comprehensive assessment of the ecological state of marine natural complexes, which underlie the protection of the marine environment in the European Union [10]. The landscape approach enables us to identify the main framework-forming underwater landscapes, as well as to determine their relative positions, ensuring ecological balance in the coastal zone. At the same time, the use of two approaches for the formation of ecological networks of marine areas requires further development and additional field research.

Conclusions:

1. For the first time, an ecological framework has been developed for the western coast of Sevastopol and its functional elements have been identified. It is shown that for its formation it is advisable to use complementary approaches: landscape and biocentric.

---

[9] Rodwell, J.R, García Criado, M., Gubbay, S., Borg, J., Otero, M., Janssen, J.A.M., Haynes, T., Beal, S., Nieto, A. [et al.], 2016. *European Red List of Habitats. Part 1: Marine Habitats*. Luxembourg: Publications Office of the European Union, 52 p. https://doi.org/10.2779/032638

[10] EU, 2008. *Directive 2008/56/EC of the European Parliament and of the Council of 17 June 2008. Marine Strategy Framework Directive.* Available at: https://eur-lex.europa.eu/legal-content/en/ALL/?uri=CELEX%3A32008L0056 [Accessed: 12 September 2023].

2. The coastal zone of the studied region was mapped, six underwater landscapes were identified, and a map of the landscape structure was compiled. It is shown that the landscape map is a cartographic basis of the ecological framework.

3. Quantitative and qualitative indicators of macrophytobenthos were calculated and used as criteria to substantiate the ecological framework elements.

4. It has been established that for the coastal region under study, KEWA include underwater landscapes with *Cystoseira* phytocenosis, TWA – landscapes with *Cystoseira – Phyllophora* phytocenosis, and RWA – landscapes with *Phyllophora* phytocenosis. All elements of the eco-framework have different environmental management regimes.

5. The obtained results and the proposed approach can be used to form the ecological framework of the marine waters of the city of Sevastopol and the Republic of Crimea.

REFERENCES

1. Dyakonov, K.N. and Khoroshev, A.V., eds., 2019. [*Theory and Methods of Landscape Planning*]. Moscow: Tovarishchestvo Nauchnyh Izdaniy KMK, 444 p. (in Russian).
2. Mirzekhanova, Z.G. and Ostroukhov, A.V., 2006. Ecological Frame of a Territory (on Example of the Vaninsk District of Khabarovsk Kray). *Izvestiya Rossiiskoi Akademii Nauk. Seriya Geograficheskaya*, (5), pp. 73–81 (in Russian).
3. Mikhno, V.B. and Kuchin, A.V., 2005. [On Development of Landscape-Ecological Frame of the Zadonsk District of Lipetsk Region]. *Proceedings of Voronezh State University. Series: Geography. Geoecology*, (2), pp. 19–28 (in Russian).
4. Mokievsky, V.O., 2009. Marine Protected Areas: Theoretical Background for Design and Operation. *Russian Journal of Marine Biology*, 35(6), pp. 504–514. doi:10.1134/S1063074009060091
5. Ivanov, A.N., 2003. [Problems of Marine Reserve Organization in Russia]. *Vestnik Moskovskogo Universiteta. Seria 5, Geografia*, (4), pp. 22–27 (in Russian).
6. Prygunova, I.L., 2005. Ecological Network of the Crimea. *Vestnik Moskovskogo Universiteta. Seria 5, Geografia*, (5), pp. 29–33 (in Russian).
7. Bokov, A.V., 2002. [Prospects for Development of Unified Nature Protection Network of Crimea]. Simferopol: Krymuchpedgiz, 192 p. (in Russian).
8. Mironova, N.V. and Pankeeva, T.V., 2021. Spatiotemporal Changes in the Macrophyto-Benthos in the Coastal Zone of Karanskii Nature and Landscape Reserve (Sevastopol, Black Sea). *Biology Bulletin*, 48(10), pp. 1941–1949. doi:10.1134/S1062359021100320
9. Mitina, N.N. and Chuprina, E.V., 2012. *Subaquatic Landscapes of the Black and Azov Seas: Structure, Hydroecology, Protection.* Moscow: FGUP "Tipographya" Rosselhozakademii, 320 p. (in Russian).
10. Ivanov, A.N., 1998. [Landscape and Ecology Approach to Organization of Regional Systems of Protected Natural Areas]. *Vestnik Moskovskogo Universiteta. Seria 5, Geografia*, (3), pp. 16–21 (in Russian).
11. Gerasimov, A.P., 2006. [Application of Landscape Approach during Planning Regional Ecological Frames]. *Geographic Bulletin*, (1), pp. 14–17 (in Russian).
12. Malyutin, A.N., 2015. Biodiversity Conservation: On the Size of Marine and Coastal Protected Areas. *Vestnik of Far Eastern Branch of Russian Academy of Sciences*, (1), pp. 14–20 (in Russian).

13. Pankeeva, T.V., Mironova, N.V. and Kovardakov, S.A., 2017. Quantitative Parameters of Macrophytobenthos as Criteria for Validation of Water Areas Nature Conservation Value (the Sevastopol Region). *Regional Environmental Issues*, (1), pp. 28–33 (in Russian).
14. Goryachkin, Yu.N., Fedorov, A.P., Dolotov, V.V. and Udovik, V.F., 2020. Natural Conditions and Anthropogenic Change of the Coastal Zone in the Area of Kacha Village. *Ecological Safety of Coastal and Shelf Zones of Sea*, (4), pp. 5–21. doi:10.22449/2413-5577-2020-4-5-21 (in Russian).
15. Petrov, K.M., 1989. [*Subaquatic Landscapes: Theory, Research Methods*]. Leningrad: Nauka, 124 p. (in Russian).
16. Pankeeva, T.V. and Mironova, N.V., 2021. Landscape Structure of the Western Coast of Sevastopol. *Geopolitics and Ecogeodynamics of Regions*, 7(2), pp. 276–291. doi:10.37279/2309-7663-2021-7-2-272-287
17. Evstigneeva, I.K. and Tankovskaya, I.N., 2022. Diversity and Variability of Phytobenthos in the Western Coastal Area ofthe Crimean Peninsula. *Russian Journal of Applied Ecology*, (2), pp. 20–32. doi:10.24852/2411-7374.2022.2.20.32
18. Evstigneeva, I.K. and Tankovskaya, I.N., 2022. Benthic Algae of the Natural Monument "Coastal Aquatic Complex near Cape Lucullus" and their Spatial Distribution. *Proceedings of the T.I. Vyazemsky Karadag Scientific Station – Nature Reserve of the RAS*, 7(2), pp. 35–52. doi:10.21072/eco.2022.22.03
19. Kalugina-Gutnik, A.A. and Kulikova, N.M., 1974. [Bottom Vegetation near the Western Coast of Crimea]. In: IBSS, 1974. *Biology of Sea*. Kiev: Naukova Dumka. Iss. 32, pp. 111–132 (in Russian).
20. Pankeeva, T.V. and Mironova, N.V., 2022. Long-Term Dynamics of Underwater Landscapes of the Coastal Zone Cape Kosa Severnaya – Cape Tolsty (Sevastopol). *Ecological Safety of Coastal and Shelf Zones of Sea*, (2), pp. 70–85. doi:10.22449/2413-5577-2022-2-70-85
21. Evstigneeva, I.K. and Tankovskaya, I.N., 2023. The Ecological Structure of the Macroalgal Community in Western Crimea. *Ecosystem Transformation*, 6(1), pp. 108–120. doi:10.23859/estr-550529
22. Sagodursky, S.E., Belich, T.V. and Sagodurskaya, S.A., 2013. [Some Aspects of Formation of Aquatic Components of Regional and Local Ecological Networks in Crimea]. In: S. P. Ivanov, ed., 2013. [*Nature of Eastern Crimea. Assessment of Biodiversity and Development of Local Ecological Network Project*]. Kiev, pp. 79–85 (in Russian).

Submitted 28.04.2023; accepted after review 05.06.2023;
revised 28.06.2023; published 25.09.2023

About the authors:

Tatyana V. Pankeeva, Senior Research Associate, A.O. Kovalevsky Institute of Biology of the Southern Seas of RAS (2 Nakhimov Av., Sevastopol, 299011, Russian Federation), Ph.D. (Geogr.), **ORCID ID: 0000-0002-8933-6103, ResearcherID: AAC-8694-2022**, *tatyanapankeeva@yandex.ru*

Nataliya V. Mironova, Senior Research Associate, A.O. Kovalevsky Institute of Biology of the Southern Seas of RAS (2 Nakhimov Av., Sevastopol, 299011, Russian Federation), Ph.D. (Biol.), **ResearcherID: AAC-9421-2022, ORCID ID: 0000-0001-7110-7081**, *dr.nataliya.mironova@yandex.ru*

Anastasia V. Parkhomenko, Postgraduate Student, Marine Hydrophysical Institute of RAS (2 Kapitanskaya St., Sevastopol, 299011, Russian Federation), **ORCID ID: 0000-0002-2378-7067**, **ResearcherID: 5090-2023**, *avparkhomenko52@gmail.com*

Contribution of the authors:

Tatyana V. Pankeeva – problem statement, literature systematization and analysis, landscape study arrangement, analysis and description of the study results, preparation of the manuscript, cartographic materials and list of references

Nataliya V. Mironova – macrophytobenthos sample processing, analysis and description of the study results, preparation of the manuscript

Anastasia V. Parkhomenko – preparation of cartographic materials, preparation of the manuscript

All the authors have read and approved the final manuscript.

Original article

Effect of Intra-Annual Dynamics of Ecosystem Components on Ecological Risk: Model Assessments

N. V. Solovjova

P.P. Shirshov Institute of Oceanology, Russian Academy of Sciences, Moscow, Russia
e-mail: soloceanic@yandex.ru

Abstract

The article proposes a model for assessing ecological risk taking into account the intra-annual dynamics of the main components of the ecosystem. Based on model calculations, ecological risk assessments are given for variations in the intra-annual state of low-productive ecosystems of the Arctic shelf and the effect of technogenic stressors. The proposed approach combines ecological risk models and observational data. The calculations made it possible to obtain model estimates of the intra-annual dynamics of ecological risk and permissible impacts on ecosystems from stressors in the conditions of development of Arctic shelf resources. The obtained preliminary results of calculations allowed us to identify areas of increased risk and take into account the different degree of requirements for the exclusion of type 1 and 2 errors due to the specifics of ecological safety tasks. An important practical result of the development of the risk assessment methodology is the identification of time intervals of impacts at which a dangerous situation is hidden by external well-being (type 2 error). The conducted modelling studies allow reallocating safety expenditures throughout the year so as to reduce risks during hazardous periods of offshore resource development and exclude cost overruns during relatively safe times. In other words, it is possible to resolve environmental and economic contradictions in risk management.

Keywords: ecological risk model, probability of acceptable impacts, Arctic shelf, ecosystem, mathematical modelling, phytoplankton biomass, anthropogenic impact

Acknowledgements: This work was prepared under state assignment no. 0128-2021-0004. The author expresses gratitude to the heads of the laboratories of P. P. Shirshov Institute of Oceanology of the Russian Academy of Sciences, in particular to V. A. Silkin, Dr. Sci. (Biol.), for discussing the directions of modeling environmental risk, M. V. Flint, Academician of the Russian Academy of Sciences, for organizing expedition work in the Arctic seas, and E. E. Sovga, Dr. Sci. (Geogr.) (MHI RAS), for assistance and support with submission of the work to *Environmental Safety of Coastal and Shelf Zones of Sea* journal.

For citation: Solovjova, N.V., 2023. Effect of Intra-Annual Dynamics of Ecosystem Components on Ecological Risk: Model Assessments. *Ecological Safety of Coastal and Shelf Zones of Sea*, (3), pp. 86–97.

Влияние внутригодовой динамики компонентов экосистемы на экологический риск: модельные оценки

Н. В. Соловьева

Институт океанологии имени П. П. Ширшова РАН, Москва, Россия
e-mail: soloceanic@yandex.ru

Аннотация

Предложена модель оценки экологического риска с учетом внутригодовой динамики основных компонентов экосистемы. На основе модельных расчетов даны оценки экологического риска при вариациях внутригодового состояния низкопродуктивных экосистем арктического шельфа и действии техногенных стрессоров. Проведенные расчеты позволили получить модельные оценки внутригодовой динамики экологического риска и допустимого воздействия на экосистемы со стороны стрессоров в условиях освоения ресурсов арктического шельфа. Полученные предварительные результаты расчетов позволили выделить области повышенного риска и учесть различную степень требований к исключению ошибок 1-го и 2-го рода, обусловленных спецификой задач экологической безопасности. Важным практическим результатом разработки методики оценок риска является выявление временны́х интервалов воздействий, при которых опасная ситуация скрыта внешним благополучием (ошибка 2-го рода). Проведенные модельные исследования открывают возможность перераспределять экономические затраты на безопасность в течение года так, чтобы снизить риски в опасные периоды разработки морских ресурсов и исключить перерасход средств в относительно безопасное время. Другими словами, можно снизить эколого-экономические противоречия в управлении риском.

Ключевые слова: модель экологического риска, вероятность допустимых воздействий, арктический шельф, экосистема, математическое моделирование, биомасса фитопланктона, антропогенное воздействие

Благодарности: работа подготовлена в рамках государственного задания № 0128-2021-0004. Автор выражает благодарность руководителям лабораторий Института океанологии им. П. П. Ширшова РАН, в частности доктору биологических наук В. А. Силкину, за обсуждение направлений моделирования экологического риска, академику Российской академии наук М. В. Флинту за организацию экспедиционных работ в морях Арктики и доктору географических наук Е. Е. Совге (МГИ РАН) за помощь и поддержку работы при представлении в журнал «Экологическая безопасность прибрежной и шельфовой зон моря».

Для цитирования: *Соловьева Н. В.* Влияние внутригодовой динамики компонентов экосистемы на экологический риск: модельные оценки // Экологическая безопасность прибрежной и шельфовой зон моря. 2023. № 3. С. 86–97. EDN JKDPNP.

Introduction

The relevance of ecological risk assessments as integral characteristics of the state of marine ecosystems is determined not only by the wide range and rate of change in parameters, but also by the presence of processes of various genesis in oceanologically contrasting water areas. Intensive development of marine

resources causes the effect of technogenic stressors on natural processes of various origins: hydrophysical, hydrochemical, hydrobiological, geological. In this case, there is a need for an integral quantitative assessment of the state of marine ecosystems under such conditions. It is not possible to obtain a reliable risk assessment within a single discipline. The very concept of ecological risk requires interdisciplinary approaches as an integral characteristic of the state of the ecosystem. In this case, contradictions can arise in combining the requirements of each of the disciplines separately. Thus, in the practice of developing shelf resources, economic and ecological requirements are directed differently.

When making business decisions, as a rule, economic indicators come to the fore, which is reflected in the main accepted form of ecological risk assessment, which comes down to assessing the following product: *event probability* × *damage*. In this case, priority is given to the economic component [1] and leads to a decrease in the importance of assessing the ecological component in projects aimed at the development of shelf resources.

For the Arctic shelf, the task of calculating the dynamics of ecological risk is especially relevant in connection with increasing climate change and the prospective development of the mineral and biological resources of the region. In this sense, understanding the dynamics of marine ecosystems in the context of global changes [2] makes it possible to calculate risks [1–7]. Existing approaches to ecological risk assessments can take into account a combination of stressors of different nature and the diversity of responses of marine ecosystems to external effect [4]. For the Arctic marine ecosystems, risk assessment methods ERA [4] in combination with the dynamic object-oriented Bayesian network DOOBN [8] and DBN [9] are known. To assess the risk of oil spills in the Arctic, models have been developed taking into account the toxicity of biotransformation [10].

The analysis of current situation with risk assessments shows that to increase the efficiency and relevance of methods, the most preferable way is to combine different approaches. Ecological risk assessment using system models at various levels of ecosystem organization is an evolutionary step in maintaining ecological safety. However, it is not enough to take into account the cumulative effect of stressors under static conditions only. It is necessary to combine the dynamics of stressors with the dynamics of ecosystem functioning. In order to advance in this direction, this article proposes an approach based on the synthesis of probabilistic risk models and field observation data.

The purpose of the research was to obtain model assessments of the influence of the intra-annual dynamics of ecosystem components (in particular, phytoplankton) on the dynamics of ecological risk under the influence of technogenic stressors. Observational data on phytoplankton biomass in low-productive ecosystems of the Arctic shelf were used for the modelling.

Materials and methods

For model studies of intra-annual risk variations in low-productive ecosystems of the Arctic shelf, observational data on seasonal variations in phytoplankton biomass in the Kara, Laptev, East Siberian Seas and main waters of the Chukchi Sea were used [11–21]. The low productivity of ecosystems in these water areas is stipulated by strong density stratification due to the intense desalination of the surface 5–12-meter water layer effected by the river flow into the marginal Arctic seas [12, 13]. Seasonal convection on the Arctic shelf for the most part does not overcome the stability of density stratification [21], and the process of enrichment of the photic layer with nutrients does not occur [12, 13]. This natural barrier is not weakened by such modern climate changes as an increase in the ice-free period and warming of the surface layer of water [13, 21]. Such features determine the low level of productivity and effect the ecological risk under the influence of stressors in the conditions of shelf resource development.

The ecological risk is regarded as the probability of death of a biological system (in particular, a population) under conditions of anthropogenic impact during a fixed period of impacts from stressors. The impact of technogenic stressors and their multiple combinations is reflected in the natural intra-annual dynamics of ecosystems with periods of outbreaks and declines in the biomass of ecosystem components.

The risk-based ecological safety criterion has the following form [22] $K = \{y \le y_p\}$, where y – ecological risk; y_p – permissible risk.

At $y \le y_p$, a decision is made on ecological safety, at $y > y_p$ – on ecological danger [22]. It is impossible to obtain the exact value of ecological risk y in principle. It is possible to obtain only upper $\overline{y}$ and lower $\underline{y}$ risk assessments ($\underline{y} \le y \le \overline{y}$). The value of permissible ecological risk lies in the interval between upper $\overline{y}$ and lower $\underline{y}$ assessments. For the criterion of ecological safety, the upper estimates $\overline{K} = \{\overline{y} \leqq y_p\}$ will be used.

We will take into account L stressors ($i = \overline{1, L}$) that have a negative impact on the ecosystem functioning under natural conditions. Let us assume that the stressors can take k states ($k = \overline{1, K}$). Such states include, for example, normal operating conditions and emergency events in the operation of technical means effecting the ecosystem. In accordance with Boole's inequalities, $\max\limits_i y_i = y_l \le y \le y_h = \sum_{i=1}^{L} y_i$, where y_i – risk from the i-th stressor [23, 24]. Ecosystem components (biomass of populations of organisms) can experience rises and falls during the year: M – number of periods of rise and fall during the year ($m = \overline{1, M}$). Observational data give maximum values of population biomass on rises $N_{\max}$ and falls N_{cr}. We will take into account the imposition of the effects of technogenic stressors on the natural dynamics of the ecosystem, for example, by modelling the impact of a technical resource development system

in the *k*-th state on the aggregated component of the ecosystem (phytoplankton) with seasonal variations in its biomass.

In the general case, for intra-annual risk depending on time we have the following relations [5–7, 23, 24]

$$y_k(t) \le \sum_{k=1}^{K} q_k \sum_{m=1}^{M} p_{km} y_{km} = \sum_{k=1}^{K} q_k \sum_{m=1}^{M} \left(p_{am} y_{am} + p'_{am}\, y'_{am} \right)_k = \sum_{k=1}^{K} q_k y_a(t),$$

$$y_a(t) \le \frac{1 - \overline{Ev}(t)/N_{\max}}{\left(1 - N_{cr}/N_{\max}\right)^2}, \qquad (1)$$

$$p_{am} = \frac{t_m}{t},\ p'_{am} = \frac{t'_m}{t},\ \sum_{m=1}^{M} \left(t_m + t'_m\right) = t,$$

$$\sum_{m=1}^{M} \left(p_{am} + p'_{am}\right) = 1, \quad \sum_{k=1}^{K} q_k = 1,$$

where y_i – risk from a separate *i*-th impact from stressors (a technical object); q_k – probability of the *k*-th state of a technical object; p_{mk} – conditional probability of the *m*-th state of the ecosystem at the *k*-th state of the technical system; y_{imk} – conditional risk from a separate *i*-th impact factor for the *k*-th state of a technical object, and the *m*-th state of the ecosystem; $\overline{Ev}(t)$ – mathematical expectation of the population biomass value; $y_k(t)$ – intra-annual biosystem risk at the *k*-th state of a technical object; p_{am} – probability of a biosystem being in the *m*-th intra-annual state of biomass rise; y_{am} – risk at biomass rise; y'_{am} – risk at biomass fall; $\overline{y}_a$ – ecological risk throughout the year; y_{km} – biosystem risk probability at the *k*-th state of a technical object and the *m*-th state of the biosystem; t_m – duration of biomass rise; t'_m – duration of biomass fall. Formula (1) is used for the normal distribution of a random variable.

The model of intra-annual risk variations (1) makes it possible to move on to the assessment of the dynamics of the probability of acceptable impacts from stressors on the ecosystem. This hierarchy of actions reflects the priority of the environmental component in the development of marine resources [21]. For the case where the permissible probability of impacts depends on time *Q*(t), the ecoscreening equations [23, 24] were expanded to the following form [7]

$$Q(t) = \begin{cases} 1 \text{ for } y_k(t) \le y_d, \\ \dfrac{y_d}{y_k(t)} \text{ for } y_d < y_k(t) < 1, \\ y_d \text{ for } y_k(t) = 1, \end{cases} \qquad (2)$$

where $Q(t)$ – maximum permissible probability of anthropogenic impact on the ecosystem; $y_k(t)$ is determined by equations (1); y_d – maximum permissible risk for the ecosystem under various requirements for maintaining environmental quality.

The probability of the state of technical systems (accident, normal operating conditions, degree, and modes of impact) taken into account in the technical operation project, also represents the input data for the risk model. Approximate

acceptable risks of the impact of stressors on marine ecosystems were used for the calculations (Table).

According to data [25], the range of probability values of acceptable ecological risk for various types and stages of technological activity on the shelf ranges from 10^{-7} to 10^{-1}. To calculate $Q(t)$, values y_d were selected that correspond to increased ($y_d = 10^{-5}$), average ($y_d = 10^{-4}$), and insignificant ($y_d = 10^{-3}$) requirements for the ecosystem quality. Probability q_k of the technical system being at the k-th state (we assume $k = 3$) was chosen from the range from 10^{-3} to 10^{-1} (Table). Probability values of low $q_1 = 10^{-3}$, average $q_2 = 10^{-2}$, and high $q_3 = 10^{-1}$event frequency were chosen (Table).

The proposed method takes into account the ecosystem aggregated components. The efficiency of the method is confirmed by the results of calculating the risk for the aggregated component of the initial link of the food chain – phytoplankton.

Acceptable risks of stressors on marine ecosystems at the main stages of oil and gas resources development [25]

Type of anthropogenic impact on ecosystems	Impact scale		Estimated permissible risk
	Spatial	Temporal	
Seismic exploration	Local	Temporary	10^{-1}
Exploratory well drilling	Topical	Short-term	10^{-7}
Field operations from single platforms	Local	Temporary	10^{-5}
Regional field work	Regional	Long-term	10^{-2}
Construction of platforms, pipelines, etc.	Topical	Temporary	10^{-5}–10^{-7}
Operation of pipelines in accident-free mode	Regional	Long-term	10^{-5}
Tanker shipping in accident-free mode	Sub-regional	Temporary	10^{-7}

Generalization of the method to the case of all main components of the ecosystem will reveal the most vulnerable link in the food chain, which will determine the risk for the entire ecosystem. Model relations (1)–(2) generalized to the case of J populations make it possible to determine acceptable values of the probability of impacts from stressors in relation to the j-th population of the ecosystem. If the existence of all J populations is equally important to us, then the reliability of technical systems affecting the ecosystem should be subject to the requirement of an acceptable annual probability of accident $Q(t)$, satisfying the following condition $Q(t) = \min_j Q(t)_j$ [22, 23].

Observations of phytoplankton biomass are used as input data to the risk model. Summarizing observation data on the seasonal variation of phytoplankton biomass in the Kara, White, Laptev, East Siberian, and Chukchi Seas [11–20], we chose values $N_{\max}$, N_{cr}, p_{am}, p'_{am}, $\overline{Ev}(t)$ as input parameters of the risk model. The results of ecosystem modelling can also be used to obtain input data for the risk model [26, 27]. But with little knowledge of the seasonal dynamics of biomass of the main components of the Arctic shelf ecosystems, especially in connection with new climate changes, ecosystem modelling is still difficult.

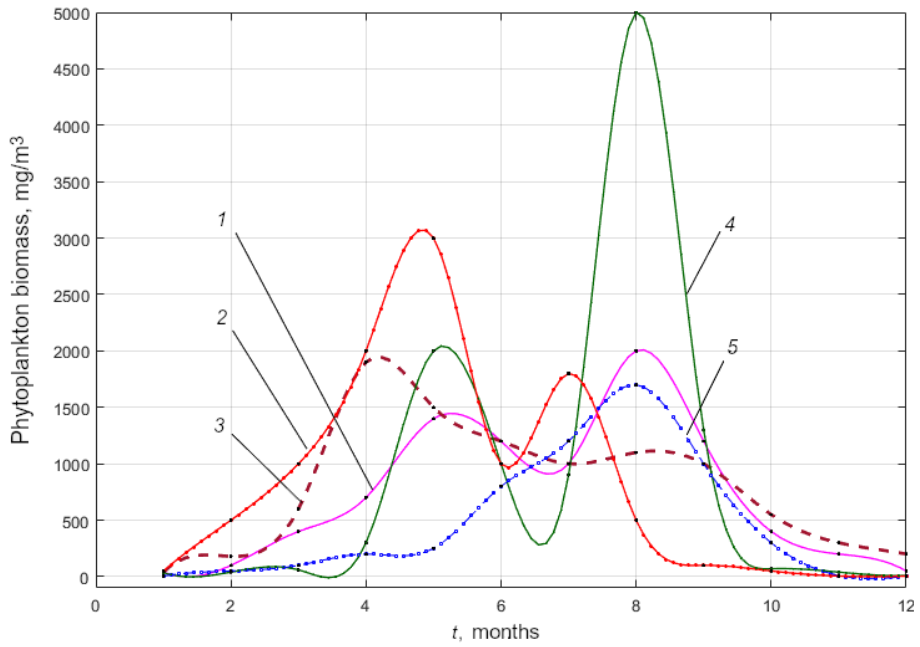

Fig. 1. The annual course of phytoplankton biomass according to gener-alized observations of freezing waters (*1*) [28]; the Barents, White and Chukchi Seas (*2*) [29]; non-freezing waters (*3*) [30]; the coastal part of the Kara Sea (*4*) [30]; the Kara, Laptev, East Siberian Seas (*5*) [11–20]

Dynamics of phytoplankton biomass in highly productive ecosystems with two maxima (the Barents, Bering, Chukchi (Barrow Canyon) [12, 13], White Seas, estuarine and slope frontal zones) and low-productive (the main water area of the Kara and Chukchi Seas, Laptev, East Siberian Seas [11–20]) vary greatly (Fig. 1). No spring phytoplankton blooms in a significant part of low-productive areas (the Kara Sea) confirmed by expeditionary observations [11–20], are stipulated by stable density stratification. Based on the above expeditionary observations, the following values were selected for a low-productive ecosystem: $N_{\max} = 1.7 \cdot 10^3$ mg/m^3, $N_{cr} = 10$ mg/m^3, $p_{am} = t_m/t = 1/6$, and $\overline{Ev}(t)$ (curve *5* in Fig. 1) as input values to risk model (1).

Calculation results

Calculation according to model (1)–(2) showed that intra-annual variations in ecological risk y_k (Fig. 2, *a*) ranged from 0 to 0.8. Calculated permissible impact probability values $Q(t)$ from 0 to 0.2 correspond to the specified probabilities of impacts from stressors (Fig. 2, *b*). This is typical throughout almost the entire year except for the phytoplankton biomass peak (Fig. 2). Only at the phytoplankton biomass peak (Fig. 2, *b*), an impact probability of 80 to 100 % can be assumed for a low-productive ecosystem.

The performed calculations confirm the initial assumption about the influence of the intra-annual dynamics of ecosystem components on the intra-annual dynamics of risk. Confirmation of such an influence results in adjustments to static matrix risk assessment methods.

The results obtained made it possible to calculate the dependence of the permissible probability of impact on the ecosystem on the ecological risk $Q(y_k)$ in the range of values $q_k = 10^{-5}$–10^{-1} and $y_d = 10^{-5}$–10^{-3} (Fig. 3). The calculation revealed areas of increased danger and relative safety (Fig. 3) under various combinations of impacts and the required environmental quality.

An important practical result of the conducted research can be considered the emerging opportunity to identify type 1 and 2 errors. The peculiarity of environmental problems in the presence of type 1 and 2 errors is associated with different severity of the consequences if they persist. The concepts of errors are taken from statistical theory, and type 1 error means mistaking a safe situation for a dangerous one, while type 2 error corresponds to the fact that a dangerous situation is hidden by external well-being [21–23]. In the case of type 1 error, excessive reinsurance associated with a false alarm is not as dangerous, although it involves unreasonable costs, as type 2 error. Model calculations (Fig. 3) revealed such areas. Analysis of all combinations of impacts and environmental quality requirements possible in practice will make it possible to determine the areas of such errors. In its turn, this will allow reallocating environmental safety expenditures throughout the year in order to minimize costs. In other words, harmonization of environmental and economic requirements for the safe development of shelf resources is achieved.

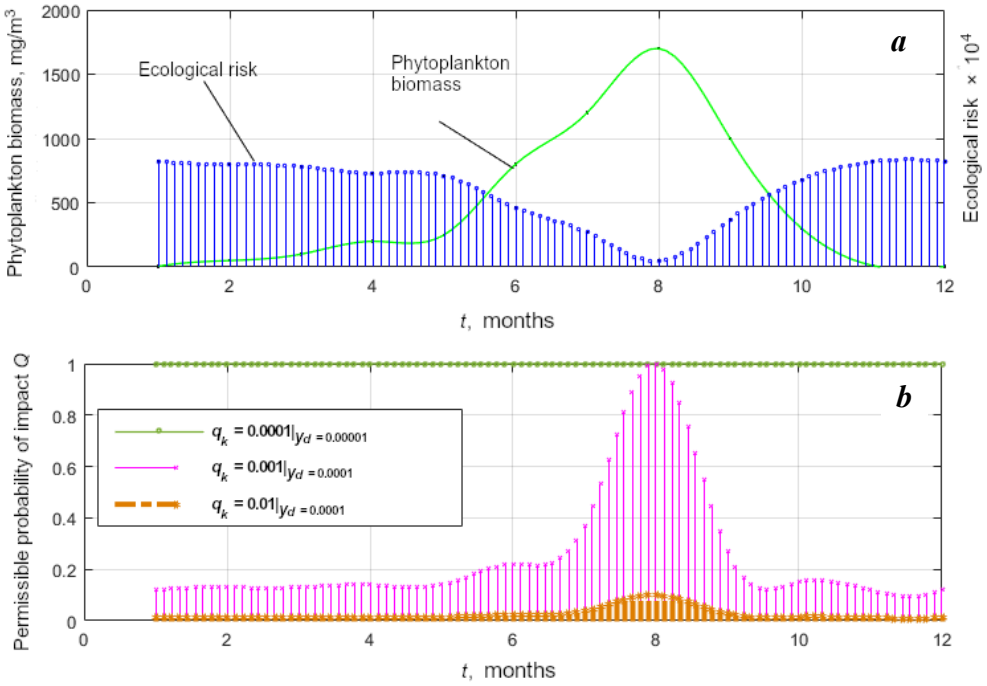

Fig. 2. Generalized annual course of phytoplankton biomass in low-productive ecosystems of the Arctic according to observations [11–20] and model intra-annual variations of ecological risk values (*a*) and the annual course of the permissible probability of impacts $Q(t)$ from stressors in the range of values $q_k = 10^{-5}$–10^{-2}; $y_d = 10^{-4}$–10^{-3} (*b*)

Increasing the accuracy of ecological risk assessments requires the use of large volumes of data on processes of different nature: physical, chemical, biological, geological, technogenic. In our case, part of the data used on the components of ecosystems, on stressors of technogenic and natural origin relates to parameters that undergo quick changes in the water layer. This part of the data satisfies the *3V* requirements characteristic of *BigData* [31], which will make it possible to link the proposed risk assessment approach with *BigData* technologies in the future. The synthesis of *BigData* modelling and technologies is stipulated by the need to analyze quickly all possible combinations of stressors of different nature with a large number of parameters and to impose impacts on the spatiotemporal natural dynamics of the ecosystem in real time [31]. In this sense, remote sensing data is of great importance, providing information on the oceanological parameters of the marine environment, including hydrobiological ones, in particular the concentration of chlorophyll a [25, 26].

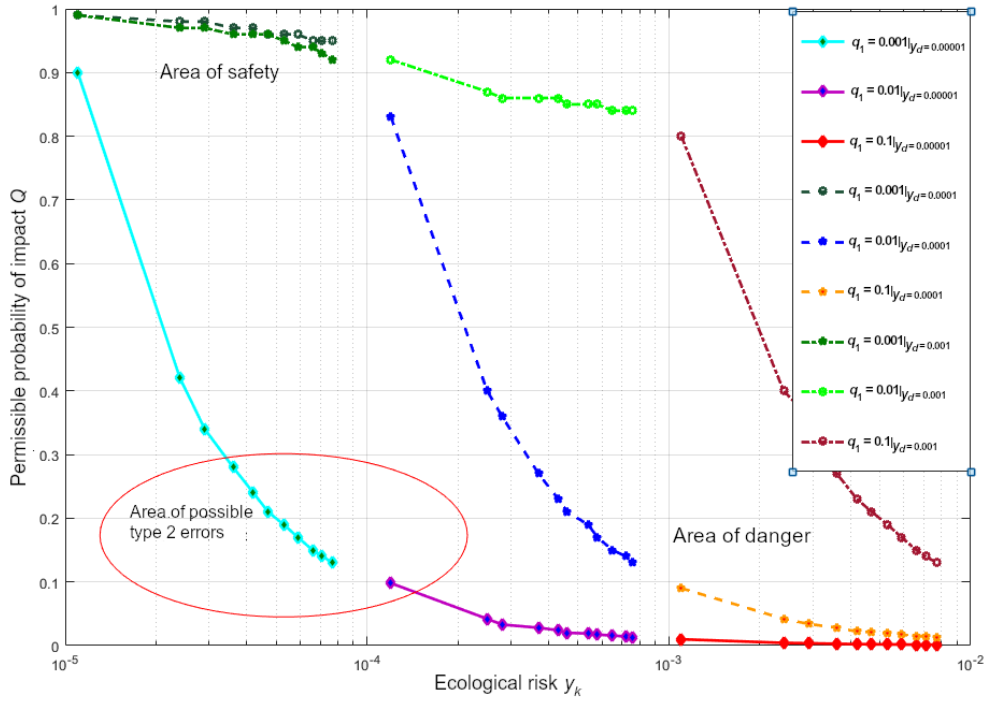

Fig. 3. Calculation of the dependence of the permissible probability of impact on the ecosystem on the environmental risk $Q(y_k)$ at values $q_k = 10^{-5}$–10^{-1} and $y_d = 10^{-5}$–10^{-3}

Conclusions

In this work, the influence of seasonal dynamics of ecosystem components on ecological risk intra-annual variations is confirmed by model calculations. The results obtained are one of the stages in creating a quantitative method for calculating risk, taking into account not only the parameters of stressors, but also intra-annual variations in the state of the ecosystem under natural operating conditions. An important result of the research was the calculation of the dependence of the permissible probability of impact on the ecosystem on ecological risk $Q(y_k)$, which made it possible to identify the areas of type 1 and 2 errors.

Improvement of the assessment of ecological risk requires expanding data on stressors of technogenic origin. The influence of various modes of technological processes, degree, frequency, and time of impacts of technical systems and human economic activities in the shelf waters must be taken into account in the dynamics of both technogenic processes and the ecosystem itself. Expanding the range and content of risk model input data will make it possible to bring the proposed method closer to *BigData* technologies.

Preliminary calculations of intra-annual risk variations presented in this paper, performed in accordance with the proposed methods in order to identify dangerous situations, showed the efficiency of the approach and the possibility of extending the calculations to marine ecosystems of various water areas.

REFERENCES

1. Fath, B.D., Asmus, H., Asmus, R., Baird, D., Borrett, S.R., de Jonge, V.N., Ludovisi, A., Niquil, N., Scharler, U.M. [et al.], 2019. Ecological Network Analysis Metrics: The Need for an Entire Ecosystem Approach in Management and Policy. *Ocean and Coastal Management,* 174, pp. 1–14. doi:10.1016/j.ocecoaman.2019.03.007
2. Elliott, M., Borja, A. and Cormier, R., 2020. Activity-Footprints, Pressures-Footprints and Effects-Footprints – Walking the Pathway to Determining and Managing Human Impacts in the Sea. *Marine Pollution Bulletin*, 155, 111201. doi:10.1016/j.marpolbul.2020.111201
3. Elliott, M., Cutts, N.D. and Trono, A., 2014. A Typology of Marine and Estuarine Hazards and Risks as Vectors of Change: A Review for Vulnerable Coasts and their Management. *Ocean and Coastal Management*, 93, pp. 88–99. doi:10.1016/j.ocecoaman.2014.03.014
4. Chen, S., Chen, B. and Fath, B.D., 2013. Ecological Risk Assessment on the System Scale: A Review of State-of-the-Art Models Future Perspectives. *Ecological Modelling*, 250, pp. 25–33. doi:10.1016/j.ecolmodel.2012.10.015
5. Solovjova, N.V., 2019. Ecological Risk Modelling in Developing Resources of Ecosystems Characterized by Varying Vulnerability Levels. *Ecological Modelling*, 406, pp. 60–72. doi:10.1016/j.ecolmodel.2019.05.015
6. Solovjova, N.V., 2020. Risk Assessment Simulation for Shelf Ecosystems Based on the Ecoscreening and Dynamic Methods Synthesis. *Estuarine, Coastal and Shelf Science,* 243, 106881. doi:10.1016/j.ecss.2020.106881
7. Solovjova, N.V., 2021. Ecological Risk Simulation Assessment in Marine Ecosystems of the Arctic shelf. *Marine Pollution Bulletin*, 169, 112577. doi:10.1016/j.marpolbul.2021.112577
8. Sajid, Z., Khan, F. and Veitch, B., 2020. Dynamic Ecological Risk Modeling of Hydrocarbon Release Scenarios in Arctic Waters. *Marine Pollution Bulletin*, 153, 111001. doi:10.1016/j.marpolbul.2020.111001
9. Arzaghi, E., Abbassi, R., Garaniya, V., Binns, J. and Khan, F., 2018. An Ecological Risk Assessment Model for Arctic Oil Spills from a Subsea Pipeline. *Marine Pollution Bulletin*, 135, pp. 1117–1127. doi:10.1016/j.marpolbul.2018.08.030
10. Fahd, F., Veitch, B. and Khan, F., 2019. Arctic Marine Fish 'Biotransformation Toxicity' Model for Ecological Risk Assessment. *Marine Pollution Bulletin*, 142, pp. 408–418. doi:10.1016/j.marpolbul.2019.03.039
11. Silkin, V., Pautova, L., Giordano, M., Kravchishina, M. and Artemiev, V., 2020. Interannual Variability of *Emiliania huxleyi* Blooms in the Barents Sea: *In Situ* Data 2014–2018. *Marine Pollution Bulletin*, 158, 111392. doi:10.1016/j.marpolbul.2020.111392
12. Flint, M.V., Poyarkov, S.G., Rimsky-Korsakov, N.A., 2016. Ecosystems of the Russian Arctic-2015 (63rd Cruise of the Research Vessel Akademik Mstislav Keldysh"). *Oceanology*, 56, pp. 459–461. doi:10.1134/S0001437016030061
13. Flint, M.V., Poyarkov, S.G. and Rymsky-Korsakov, N.A., 2018. Ecosystems of the Siberian Arctic Seas-2017 (Cruise 69 of the R/V *Akademik Mstislav Keldysh*). *Oceanology*, 58, pp. 315–318. doi:10.1134/S0001437018020042
14. Sukhanova, I.N., Flint, M.V., Druzhkova, E.I., Sazhin, A.F. and Sergeeva, V.M., 2015. Phytoplankton in the Northwestern Kara Sea. *Oceanology*, 55, pp. 547–560. https://doi.org/10.1134/S0001437015040141
15. Sukhanova, I.N., Flint, M.V., Pautova, L.A., Stockwell, D.A., Grebmeier, J.M. and Sergeeva, V.M., 2009. Phytoplankton of the Western Arctic in the Spring and Summer of 2002: Structure and Seasonal Changes. *Deep Sea Research Part II: Topical Studies in Oceanography*, 56(17), pp. 1223–1236. doi:10.1016/j.dsr2.2008.12.030
16. Matishov, G.G., Dzhenyuk, S.L. and Moiseev, D.V., 2017. Climate and Large Marine Ecosystems of the Arctic. *Herald of the Russian Academy of Sciences*, 87, pp. 30–39. doi:10.1134/S1019331617010087

17. Makarevich, P.R. and Oleinik, A.A., 2009. Structure of the Annual Cycle of Phytoplankton Community Evolution in the Ob-Yenisei shoal of the Kara Sea. *Doklady Earth Sciences*, 426, pp. 669–671. doi:10.1134/S1028334X09040357
18. Mosharov, S.A., Demidov, A.B. and Simakova, U.V., 2016. Peculiarities of the Primary Production Process in the Kara Sea at the End of the Vegetation Season. *Oceanology*, 56, pp. 84–94. https://doi.org/10.1134/S0001437016010100
19. Demidov, A.B., Kopelevich, O.V., Mosharov, S.A., Sheberstov, S.V. and Vazyulya, S.V., 2017. Modelling Kara Sea Phytoplankton Primary Production: Development and Skill Assessment of Regional Algorithms. *Journal of Sea Research*, 125, pp. 1–17. doi:10.1016/j.seares.2017.05.004
20. Demidov, A.B., Mosharov, S.A. and Makkaveev, P.N., 2014. Patterns of the Kara Sea Primary Production in Autumn: Biotic and Abiotic Forcing of Subsurface Layer. *Journal of Marine Systems*, 132, pp. 130–149. doi:10.1016/j.jmarsys.2014.01.014
21. Fleishman, B.S., 2008. *Fundamentals of Systemology*. New York: Lulu, 184 p.
22. Fleishman, B.S., 1984. Contribution to the Theory of Adaptation with Application to Ecology. *Ecological Modelling*, 26(1–2), pp. 21–31. doi:10.1016/0304-3800(84)90090-5
23. Fleishman, B.S., 1991. Hyperbolic Law of Reliability and its Logarithmic Effects in Ecology. *Ecological Modelling*, 55(1–2), pp. 75–88. doi:10.1016/0304-3800(91)90066-A
24. Patin, S.A., 2017. *Oil and Continental Shelf Ecology. Vol. 1: Offshore Oil and Gas Industry: Actual Situation, Prospects, Factors of Impact*. Moscow: VNIRO Publishing, 326 p. (in Russian).
25. Belyaev, V.I., 1987. [*Marine System Modelling*]. Kiev: Naukova Dumka, 201 p. (in Russian).
26. Belyaev, V.I. and Konduforova, N.V., 1990. [*Mathematical Modelling of Shelf Ecological Systems*]. Kiev: Naukova Dumka, 240 p. (in Russian).
27. Flint, M.V., 2015. [Bioresources of the Russian Arctic Seas: Changes Influenced by Climate and Anthropogenic Factors, Ecosystem Basis of Protection]. In: N. P. Laverov, V. I. Vasiliev and A. A. Makosko, eds., 2015. [*Scientific and Technical Issues of Arctic Exploration*]. Moscow: Nauka, pp. 55–71 (in Russian).
28. Druzhkova, E.I. and Makarevich, P.R., 2008. Annual Cycle of nanophytoplankton in Coastal Waters of the Barents Sea. *Biology Bulletin*, 35(4), pp. 428–435. doi:10.1134/S106235900804016X
29. Ilyash, L.V., Ratkova, T.N., Radchenko, I.G. and Zhitina, L.S., 2012. [Phytoplankton of the White Sea]. In: A. P. Lisitsin, ed., 2012. [*System of the White Sea. Vol. 2. Water Column and Atmosphere, Cryoshpere, River Runoff, and Biosphere Interacting with it*]. Moscow: Nauchny Mir, 605–639 (in Russian).
30. Makarevich, P.R. and Larionov, V.V., 2011. Annual Cycle of the Planktonic Phytocenosis in the Ob-Enisei Shallow Zone of the Kara Sea. *Russian Journal of Marine Biology*, 37(1), pp. 3–8. doi:10.1134/S1063074011010093
31. Gvishiani, A.D., Lobkovsky, L.I. and Solovjova, N.V., 2022. Prospects for Synthesizing Ecological Risk Models and Big Data Technologies for Marine Ecosystems. *Fizika Zemli*, (4), pp. 101–112. doi:10.31857/S0002333722040044 (in Russian).

Submitted 29.05.2023; accepted after review 07.06.2023;
revised 28.06.2023; published 25.09.2023

About the author:

Natalia V. Solovjova, Chief Research Associate, P.P. Shirshov Institute of Oceanology, RAS (36 Nakhimovskiy Ave., Moscow, Russia, 117997), Dr.Sci. (Phys.-Math.), **ORCID ID: 0000-0002-4268-7790, ResearcherID: AAZ-2398-2020, Scopus Author ID: 6507375823**, *soloceanic@yandex.ru*

The author has read and approved the final manuscript.

Original article

Experimental Study of Ultrasound Effect on Microperiphyton of Artificial Substrates for Fouling Protection of Technical Water Supply Circuit of Nuclear Power Plants

E. L. Nevrova [1] *, A. N. Petrov [1], N. A. Moroz [2], A. B. Kasyanov [2]

[1] *A.O. Kovalevsky Institute of Biology of the Southern Seas of RAS, Sevastopol, Russia*

[2] *All-Russian Research Institute for Nuclear Power Plants Operation JSC, Moscow, Russia*

* *e-mail: el_nevrova@mail.ru*

Abstract

During exploitation of nuclear power plants, biofouling forms in the elements of the technical water supply circuit, which results in equipment malfunction, underproduction of electricity, and economic losses. One of the methods to prevent biofouling on immersed surfaces is ultrasound exposure. To study the peculiarities of biofouling development in water pipelines of a nuclear power plant, the impact of an ultrasonic device on the formation of benthic diatom algae (Bacillariophyta) – the primary stage in the succession of the microfouling community – was assessed. Microperiphyton consisting of diatoms, bacteria, and protozoa, forms biofilm on surfaces and promotes active development of macrofouling community leading to further reduction of efficiency of nuclear power plants. Long-term experiments were carried out in the laboratory and nearshore marine area to study the influence of ultrasonic device at different power and duration of exposure on periphyton development on steel and concrete samples. It was found that increasing the intensity of the ultrasonic device has a pronounced effect on microfouling of substrates reducing the abundance and species richness of diatoms. Based on the results, it was recommended to extend the experiments using a full-function ultrasonic device of higher power during exploitation of a nuclear power plant.

Keywords: biofouling, ultrasonic protection methods, nuclear power plant process equipment, benthic diatom, Bacillariophyta

Acknowledgments: The work was carried out in the Benthic Ecology Department of the Federal Research Center of IBSS under state assignment no. 121030100028-0 (“Regularities of formation and anthropogenic transformation of biodiversity and bioresources of the Azov-Black Sea basin and other regions of the World Ocean”) and under initiative works of VNIIAES JSC. The authors are grateful to leading engineers of IBSS S. A. Trofimov and Yu. I. Litvin and to engineer of VNIIAES JSC S. L. Tarasyuk for carrying out the experiments, as well as to head of Laboratory of Microscopy of IBSS V. N. Lishaev for SEM microphotographing.

For citation: Nevrova, E.L., Petrov, A.N., Moroz, N.A. and Kasyanov, A.B., 2023. Experimental Study of Ultrasound Effect on Microperiphyton of Artificial Substrates for Fouling Protection of Technical Water Supply Circuit of Nuclear Power Plants. *Ecological Safety of Coastal and Shelf Zones of Sea*, (3), pp. 98–113.

Экспериментальное изучение воздействия ультразвука на микроперифитон искусственных субстратов с целью защиты от биопомех систем технического водоснабжения атомных электростанций

Е. Л. Неврова [1] *, **А. Н. Петров** [1], **Н. А. Мороз** [2], **А. Б. Касьянов** [2]

[1] *ФГБУН ФИЦ «Институт биологии южных морей им. А.О. Ковалевского РАН», Севастополь, Россия*

[2] *АО «Всероссийский научно-исследовательский институт по эксплуатации атомных электростанций», Москва, Россия*

* *e-mail: el_nevrova@mail.ru*

Аннотация

При эксплуатации атомных электростанций в элементах системы технического водоснабжения формируются биопомехи, приводящие к нарушению эксплуатации оборудования, недовыработке электроэнергии и экономическим потерям. Одним из методов предотвращения биообрастания на погружных поверхностях является воздействие ультразвука. С целью изучения особенностей развития биообрастания в водоводах атомной электростанции оценено воздействие ультразвукового устройства на формирование таксоцена бентосных диатомовых водорослей (Bacillariophyta) – первичного звена сукцессии сообщества микрообрастания. Микроперифитон, состоящий из диатомовых, бактерий и простейших, образует биопленку на поверхностях и способствует активному развитию сообщества макрообрастания, приводя к дальнейшему снижению эффективности атомных электростанций. В условиях лаборатории и морской акватории проведены длительные эксперименты по исследованию влияния работы ультразвукового устройства при разной мощности и продолжительности излучения на развитие перифитона на образцах субстрата из стали и бетона. Выявлено, что повышение интенсивности работы ультразвукового устройства оказывает выраженное влияние на микрообрастания субстратов, снижая плотность поселения и видовое богатство диатомовых. По итогам исследования рекомендовано расширение экспериментов с использованием полнофункционального ультразвукового устройства более высокой мощности при эксплуатации атомной электростанции.

Ключевые слова: биообрастание, ультразвуковые методы защиты, технологическое оборудование АЭС, бентосные диатомовые, Bacillariophyta

Благодарности: исследование проведено в отделе экологии бентоса ФИЦ ИнБЮМ РАН по госзаданию № 121030100028-0 (тема: «Закономерности формирования и антропогенная трансформация биоразнообразия и биоресурсов Азово-Черноморского бассейна и других районов Мирового океана»), а также в рамках инициативных работ АО «ВНИИАЭС». Авторы благодарны вед. инж. ИнБЮМ С. А. Трофимову, Ю. И. Литвину, инж. 1 кат. АО «ВНИИАЭС» С. Л. Тарасюку за помощь при проведении экспериментов, а также начальнику лаборатории микроскопии ИнБЮМ В. Н. Лишаеву – за помощь при фотографировании на СЭМ.

Для цитирования: Экспериментальное изучение воздействия ультразвука на микроперифитон искусственных субстратов с целью защиты от биопомех систем технического водоснабжения атомных электростанций / Е. Л. Неврова [и др.] // Экологическая безопасность прибрежной и шельфовой зон моря. 2023. № 3. С. 98–113. EDN JCUYKV.

Introduction

In recent decades, there has been a tendency to rearrange thermal and nuclear power plants (TPP, NPP) to sea coasts to take in large volumes of water required for technical water supply circuit (TWSC). This raises various problems related to the development of fouling organisms in water pipelines. Conventionally, these problems are divided into three types [1]: physical fouling of pipelines and operational biofouling caused by it; mechanical damage and death of hydrobionts (plankton and larvae of benthic species, fish eggs, and juveniles) after their passing through water supply circuits [2]; impact of waste water (including thermal water) on coastal aquatic ecosystems [2,3]. Thus, marine fouling is both an environmental and anthropogenic-technological phenomenon that must be taken into account when developing a concept for biofouling protection [1, 4].

The formation and growth of fouling communities (micro- and macrophytes, mollusks, barnacles, tubular polychaetes, ascidians, etc.) on the TWSC of an NPP is facilitated by a bacterial-algal biofilm, the initial stage of periphyton succession on the submerged equipment surfaces in water. Intensive development of fouling in the NPP heat sinks and replenishment supply reservoirs results in complex disruptions to the TWSC and corrosion intensification. Moreover, the working cross-section of pipelines and heat exchangers decreases, technological systems (including safety ones) fail, which leads to a decrease in the efficiency of NPP power units and economic losses [5–7]. In recent years, the total damage from biofouling at NPPs and TPPs has exceeded 11 billion rubles.

Anti-biofouling measures are divided into physical, chemical, and biological or complex [1, 5, 8]. Physical methods include cleaning the TWSC with compressed air, increasing the temperature of water in pipelines, cathodic protection, generating an electric field, ultraviolet (UV) or ultrasonic (US) exposure [1, 4, 8]. US anti-fouling methods include sounding of equipment, which causes a cavitation effect in the tissues of aquatic organisms, thus reducing their ability to settle on the substrate and grow subsequently [1, 6]. It is known that almost complete death of the larvae of a bivalve mollusk zebra mussel, is caused by continuous ultrasonic exposure with a power of 100–800 W, a voltage of 438 V, and a frequency of 17–22 kHz for several days, while the percentage of death increases sharply when increasing sound pressure frequency and strength [5, 6, 9, 10]. High energy consumption can be stated as the disadvantage of this method.

Some of the most pressing challenges for *RosEnergoAtom* JSC are to monitor the biofouling development, to take preventive measures, and to minimize its impact on the operation of the NPP TWSC [6]. Based on the implementation of the preliminary project results “Development of Technology for Combating Biofouling of Technological Equipment of Circulating Water Supply Circuits

at Nuclear Power Plants (AP-19/246)" by *All-Russian Research Institute for Nuclear Power Plants Operation* JSC, it was revealed that the ultrasonic device (USD) is an effective anti-fouling tool. Thus, its using promotes to perform comprehensive preventive protection of equipment from fouling and avoids shutting down the TWSC, taking it out for repairs and cleaning [1, 6]. Tests in the Laboratory of environmental protection in the Rostov NPP showed that a prototype of the USD destroyed the druses of the zebra mussel (*Dreissena polymorpha L.*) that were strongly adhered to the water-immersed elements of the TWSC [6].

In 2021–2022, together with the Benthos Ecology Department of the Federal Research Center of IBSS, the advanced USD exposure on the formation of fouling on artificial substrates was tested. The laboratory stage of the experiment was performed under conditions that simulating marine environment; the experiment in the water area was performed in the marine water areas near the building of Radiobiological Department (RBD) of the IBSS.

The choice of benthic diatoms (Bacillariophyta) as test objects is based on their importance in aquatic ecosystems as a primary trophic link, mass distribution and predominance in microphytobenthos in terms of numbers, high biomass, and huge species richness [11]. Due to their sensitivity to environmental factors, diatoms can be indicators for the water quality assessing, as well as in testing the effectiveness of anti-fouling devices and biocidal paints and varnishes [11–13]. Microfouling, consisting of bacteria, diatoms and protozoa, forms a primary biofilm on underwater surfaces, including the TWSC [7, 12], which provides to the active development of the macrofouling community and leads to a further decrease in the NPP operating efficiency [7, 14].

This work is aimed to evaluate the USD efficacy with different operation modes for protecting hydrotechnical facilities from microfouling based on studying of benthic diatoms taxocene structure during long-term laboratory and field experiments. The tasks are as follows: 1) to identify differences in the abundance and species richness of benthic diatoms during the formation of microphytoperiphyton on concrete and steel plates; 2) to assess the dynamics of diatom fouling intensity of various substrates in the control and under different operating modes of the USD.

Material and methods

During the first stage, in laboratory conditions simulating marine environment, the following samples of the substrate were used: metal plates 5.5 × 6.5 cm from A-3 stainless steel and M-500 concrete plates 10 × 18 cm. The samples were fixed on holders and placed in 40-liter containers – control (CC) and test (TC) ones, 13 pieces of steel and concrete plates in each (Fig. 1, *a, b*). The containers were filled with natural seawater taken from Sevastopol Bay. The water in the containers was changed every two days, and each series of experiments was run for four weeks. During the experiment, periphyton components were successively deposited on steel and concrete samples: bacteria → diatoms → zoobenthos larvae. The TC was treated with ultrasound generated by a cassette of five high-frequency emitters with their constant power of 500 W, frequency of 27.1–27.3 kHz and current strength of 3 A.

Fig. 1. Long-term laboratory experiment: *a* – control container (CC) with concrete and stainless steel plates; *b* – test container (TC) with the ultrasonic device (USD) and similar plates; *c* – devices for setting the time and power modes of USD operation (*top*) and HAILEA device for water cooling and temperature control (*bottom*)

The frequency of USD exposure was three times a week for 4 hours (Fig. 1, *c*). The distance from the USD to the water surface in the TC was 10 cm; the CC was isolated from the ultrasonic unit with sheets of foam plastic, plexiglass, and dense rubber 1.5 cm thick. To avoid heating of sea water in the TC during the USD operation, a HAILEA device was used, which thermostated the water temperature in both containers to 19.0 ± 0.5 °C (Fig. 1, *c*). The laboratory experiment included constant lighting conditions (8/16 hours) and ventilation necessary for the alive organisms. The experiment continued for four months (September to December 2021).

Every month, two samples of concrete and steel plates were removed from each container, microphytoperiphyton from their surface was scraped off from area of 5.5 × 6.5 cm and rinsed with filtered sea water. The total volume of each lavage was adjusted to 100 ml, the cells were counted with Carl Zeiss Axiostar+ light microscope × 400 (LM). Taxonomic identification of diatoms was carried out using permanent slides and micrographs obtained with Hitachi SU3500 scanning electron microscope (SEM).

To assess the microperiphyton abundance, diatom cells were counted in a Goryaev chamber (hemocytometer) in duplicate, then the results were recalculated per 1 m^2 of substrate surface [11]:

$$N = \frac{(aV)}{(S \cdot 10^{-4} \quad 7 \cdot 10^{-3})},$$

where a – number of cells in 0.007 mm^3; V – specified sample volume, 100 mm^3; S – sample surface area, in our experiment – 35.75 cm^2.

For the second stage of experiment (in the seawater area), control (CS) and test (TS) stands were made with steel and concrete plates attached to them. The stands had been exposed for five months (from April to September 2022) at a depth of 0.5–0.7 m at the water area bottom (Fig. 2). The USD was installed above the TS .

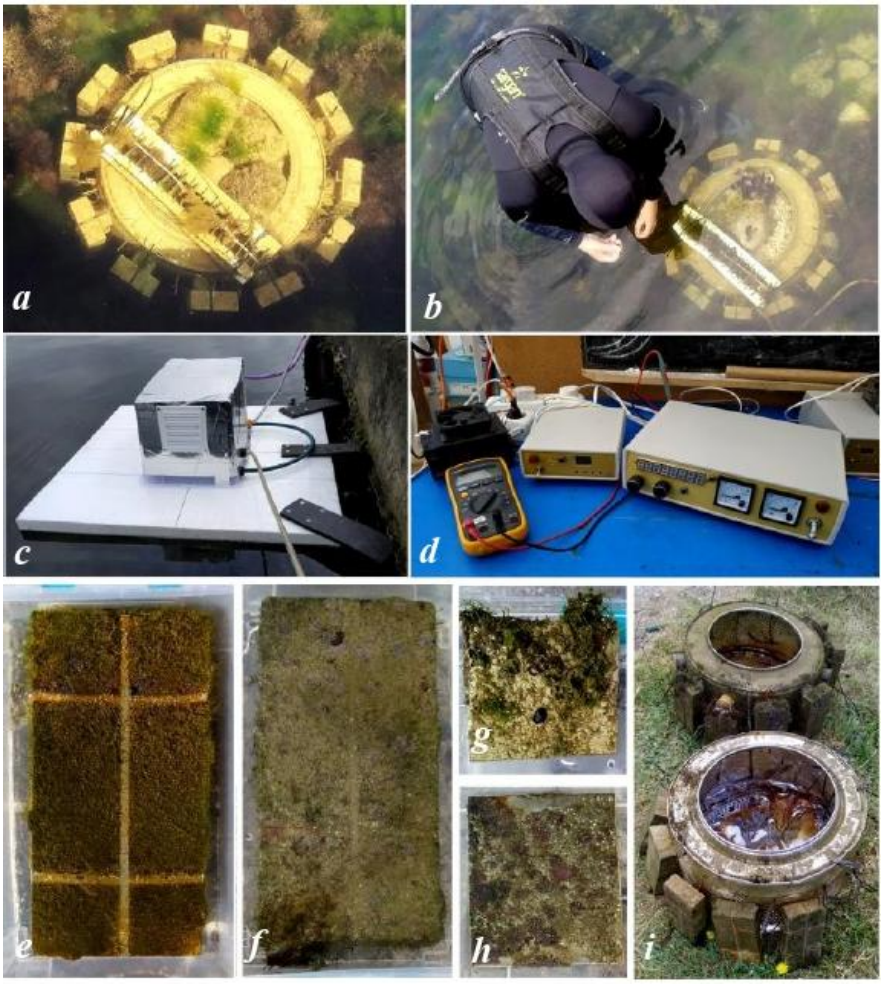

F i g . 2 . Long-term experiment in the water area: *a* – general view of the control stand (CS) with concrete and steel plates; *b* – sampling by a diver; *c*– USD installed above the test stand (TS); *d* – devices for setting and maintaining the time and power modes of USD operation; concrete plates after 5-month exposure: *e* – control; *f* – after exposure to USD; steel plates after 5-month exposure: *g* – control; *h* – after exposure to USD; *i* – control (*top*) and test (*bottom*) stands after 5-month exposure to sea water

on a floating platform and was protected by a special cover from the wave, precipitation, and solar irradiation impact (Fig. 2, *c*). The distance from the emitters to the water surface was 20 cm. The control stand (CS) was installed in the water area at a distance of 30 m from the TS behind a concrete block, which shielded the CS from the USD exposure. During the experiment, the water temperature in the water area increased seasonally from 10 to 25.0 ± 0.5 °C. Every month, two plates of each type of substrate were removed from both stands and the abundance and species richness of diatoms were determined in the laboratory using the aforementioned method [11].

During the first 3 months, the TS was exposed to USD with the following working parameters: power – 500 W, frequency – 27.5 ± 5 % kHz, current strength – 3 A, period of operation – three times a week, 4 hours a day. Since July 2022, duration of TS treatment with the USD was extended to 8 hours a day, five times a week (Fig. 2, *d*). The experiment was terminated on 21.09.2022, due to beginning of storm season.

Results and discussion

Laboratory experiment. After the first stage of experiment, different conditions of sea water in containers were observed. In the TC, the concrete and steel plates remained visually clean, and the water was clear throughout the whole observation period. The water in the CC became muddy after two weeks (despite the regular water replacement every two days), probably due to metabolites released by fouling organisms and diatom polysaccharides. During the experiment, the parameters of abundance and species richness of diatoms in the CC on both concrete and steel plates significantly exceeded the level in the TC (Fig. 3). After four months, the average abundance of diatoms on concrete in the CC was $90.327 \cdot 10^6$ ind./m^2, the number of species was 14 (Fig. 3, *a*), and in the TC – only $0.893 \cdot 10^6$ ind./m^2, with 3 species (Fig. 3, *b*), respectively. It should be noted that in the first month of US exposure, diatom cells were not observed on the steel plates in the CC and TC. This fact can be caused by the smoothness of the steel surface, which does not facilitate the settling and primary adhesion of diatoms and larvae of microzooperiphyton organisms. After four months, the average abundance of diatoms on steel plates in the CC was $124.28 \cdot 10^6$ ind./m^2, the number of species was 11 (Fig. 3, *c*), and in the TC the abundance was $7.14 \cdot 10^6$ ind./m^2 and 3 species only (Fig. 3, *d*).

Based on the laboratory experiment result, it was concluded that even with a relatively weak power of ultrasonic sounding, the USD exposure provided preventive protection of concrete and metal substrates from colonization by the main components of phytoperiphyton. In addition, the effect of US exposure resulted in the mechanical cleaning the plates' surface from contaminants and hydrobiont metabolites.

Field experiment. During the field experiment in the water area, which included the fouling formation, the following phyto- and zoocomponents of periphyton sequentially settled on metal and concrete substrate: bacteria, diatoms, macrophytes seedlings (Chlorophyta, Ochrophyta, Rhodophyta), larvae of mollusks,

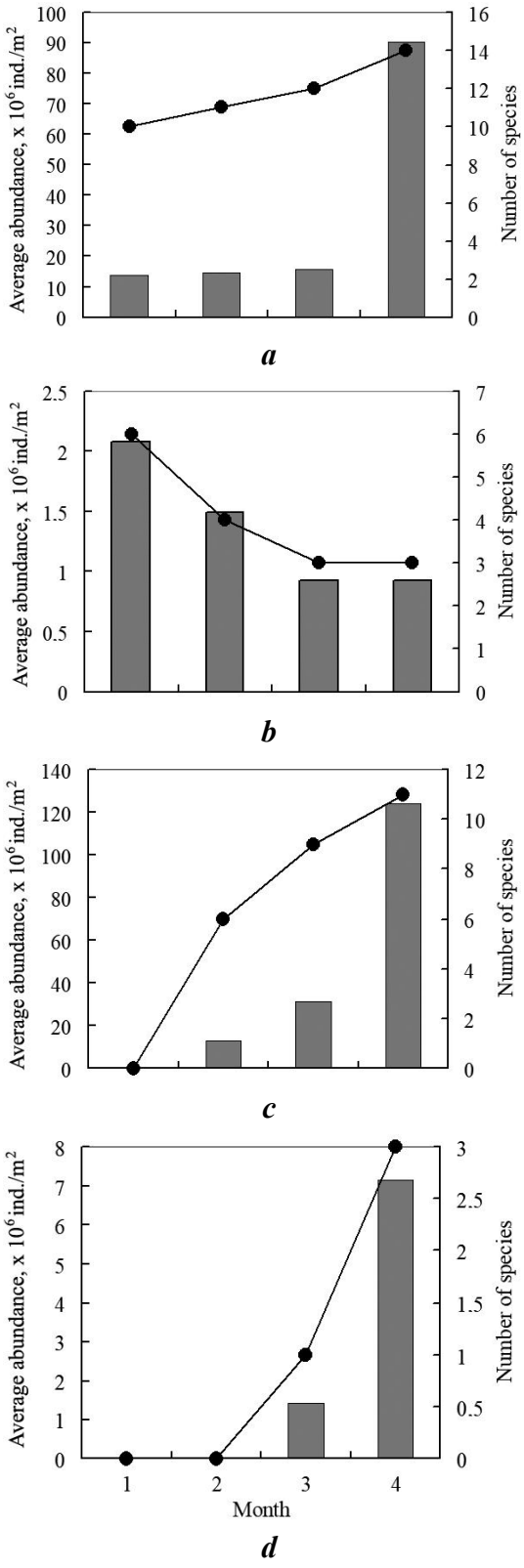

Fig. 3. Laboratory experiment: values of benthic diatoms in the control and exposed to the USD on concrete (*a* – CC; *b* – TC) and steel plates (*c* – CC; *d* – TC). The bars are abundance and the circles are species richness of diatoms

polychaetes, and barnacles. Variability in parameters of micro-phytoperiphyton on both types of substrates was revealed. It might be caused by a number of reasons, including changes in the hydrological regime and activation of diatoms reproduction as a stress response to the USD impact in the initial period of experiment.

The results of the first month of field experiment showed that USD action with its power of 500 W, sounding frequency of 27.5 ± 5% kHz, and current strength of 3 A with the exposure duration four hours a day, three times a week, significantly stimulated micro-phytoperiphyton development on concrete and steel samples at the experimental stand (TS) (Fig. 4).

At the first month of exposure, the lowest abundance of diatoms was observed on the CS concrete and steel plates ($45.5 \cdot 10^6$ and $14 \cdot 10^6$ ind./m^2, respectively). On the contrary, the abundance of diatoms at the TS were tens of times higher than at the CS: $1302 \cdot 10^6$ ind./m^2 on the concrete samples and $472 \cdot 10^6$ ind./m^2 on the steel ones.

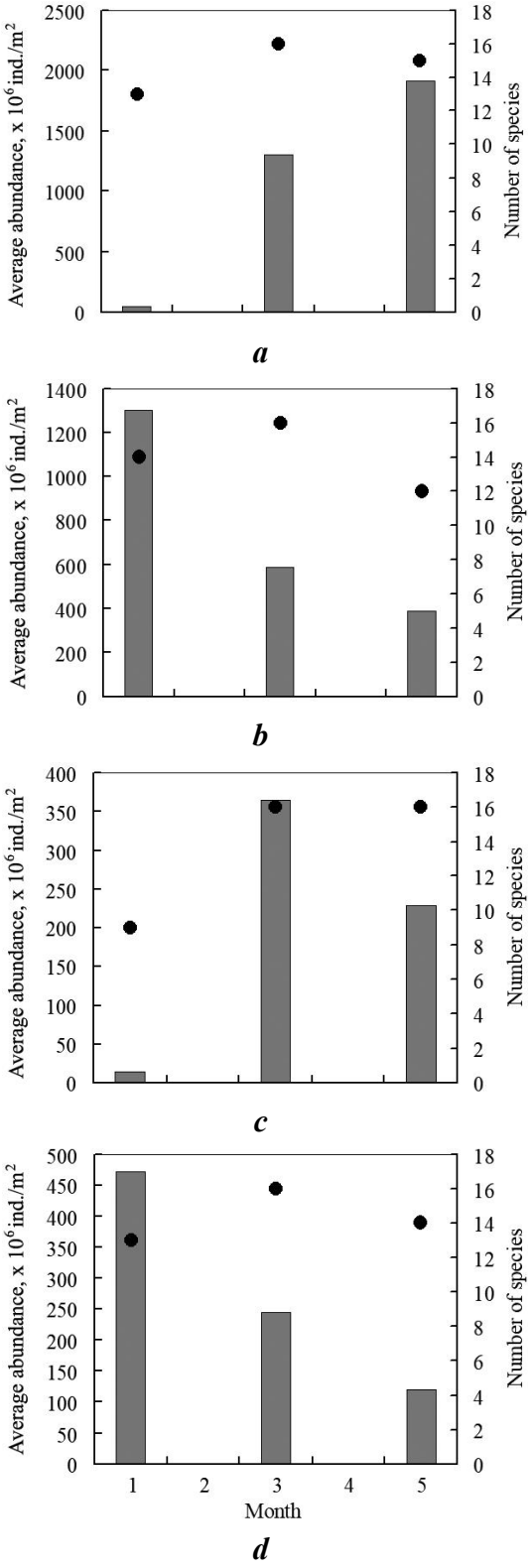

Fig. 4. Field experiment: values of benthic diatoms in the control and exposed to the USD on concrete (*a* – CS; *b* – TS) and steel (*c* – CS; *d* – TS). The bars are abundance and the circles are species richness of diatoms

At the TS, the highest species richness of Bacillariophyta was registered at the first month: 14 species on the concrete (Fig. 4, *b*) and 13 species – on the steel (Fig. 4, *d*). Apparently, during this period of the experiment, the USD effect with the specified operation parameters does not suppress the microperiphyton development and also causes stimulating effect, which was previously registered in similar studies by other authors [1, 10]. Taking into account the results of the first month, the USD intensity was increased: from July, the duration of sounding was 8 hours a day, 5 times a week. The parameters of sonic power, frequency and current strength did not change. After a three-month exposure at the CS, the abundance of diatoms on concrete was $1305 \cdot 10^6$ ind./m^2, while it decreased by more than half at the TS – to $585 \cdot 10^6$ ind./m^2 (Fig. 4, *a*, *b*). On steel at the CS, $365.5 \cdot 10^6$ ind./m^2 were counted, and at the TS – $244.5 \cdot 10^6$ ind./m^2 (Fig. 4, *c*, *d*). The species richness of diatoms at the CS and TS was the same: 16 species each on both types of substrates.

After five months of the TS exposure, the abundance of diatoms decreased significantly compared to

the CS (see Fig. 2, *i*). The same pattern was observed upon final examination: the phytoperiphyton density on concrete and steel plates at the CS differed significantly (see Fig. 2, *e*, *f*) from such samples at the TS (see Fig. 2, *g*, *h*). The lowest abundance of diatoms at the final stage of experiment was observed in the TS steel plates fouling ($121 \cdot 10^6$ ind./m^2). Twice as many cells were recorded on the steel CS samples – $228 \cdot 10^6$ ind./m^2 (Fig. 4, *c*, *d*). On the TS concrete substrate, the abundance of Bacillariophyta was four times lower ($385 \cdot 10^6$ ind./m^2) than at the CS ($1553.5 \cdot 10^6$ ind./m^2) (Fig. 4, *a*, *b*). Obviously, the intensity of diatom colonization of a smooth surface of steel plates is lower than that on concrete substrate with a rough surface providing better cell adhesion. Importantly, the abundance of diatoms on both types of plates at the TS after five months of exposure to the increased USD operation mode reduced significantly in compare to the initial stage of the experiment.

Within microphytoperiphyton 30 mass benthic species belonging to 21 genera, 17 families, 13 orders and 3 classes of Bacillariophyta were identified (Fig. 5). Representatives of class Bacillariophyceae predominated with 22 species against 5 species from class Fragilariophyceae and 3 species from class Coscinodiscophyceae. Regardless of the experimental conditions and type of substrate, small-celled species from genera *Navicula* Bory 1822 and *Nitzschia* Hassall 1845, characterized by the highest division rate and resistance to stress factors, sharply prevailed.

At the fifth month of experiment on concrete plates at the CS, the maximum abundance of *Nitzschia* sp.1 and *Navicula perminuta* Grunow (1178.5·106 ind./m^2 and $831 \cdot 10^6$ ind./m^2, respectively) was marked. The list of subdominants included *Thalassiosira excentrica* (Ehrenb.) Cleve ($203.5 \cdot 10^6$ ind./m^2), *Nitzschia longissima* (Bréb. ex Kütz.) Grunow ($87 \cdot 10^6$ ind./m^2), *Caloneis liber* (W. Sm.) Cleve ($31.5 \cdot 10^6$ ind./m^2), *Nitzschia* sp. 2 ($19 \cdot 10^6$ ind./m^2), *Amphora marina* (W. Sm.) Chase ($11 \cdot 10^6$ ind./m^2), *Licmophora gracilis* (Ehrenb.) Grunow($9 \cdot 10^6$ind./m^2), *Pleurosigma elongatum* W. Sm. ($4.5 \cdot 10^6$ind./m^2), *Cylindrotheca closterium* (Ehrenb.) Reimann et Lewin($4 \cdot 10^6$ ind./m^2), *Entomoneis paludosa* (W. Sm.) Reimer ($3 \cdot 10^6$ ind./m^2). The abundance of other species varied from 0.5 to 2.5·106 ind./m^2.

Thus, an increase in the duration and frequency of the USD action after five months of exposure in the marine water area had a pronounced inhibitory effect on the diatom taxocene formation (the main component of microperiphyton), contributing to reducing in its abundance and species richness on both types of substrate. In general, the results from our experiments are consistent with the previously obtained results of other researchers on assessing the ultrasound effect on the resistance and survival of different groups of fouling. In particular, it was shown [10] that even with a short-term (up to 1–2 min.) of USD exposure with a frequency about 17 kHz and sound pressure from 1700 to 5000 bar, loss of ability to settle and subsequent almost 100% elimination of zooperiphyton larvae (cyprises of barnacles, etc.) were registered. Combined application of USD (power 0.12 kW and frequency 25 kHz) and 30 W UV-lamp revealed that UV-US effect

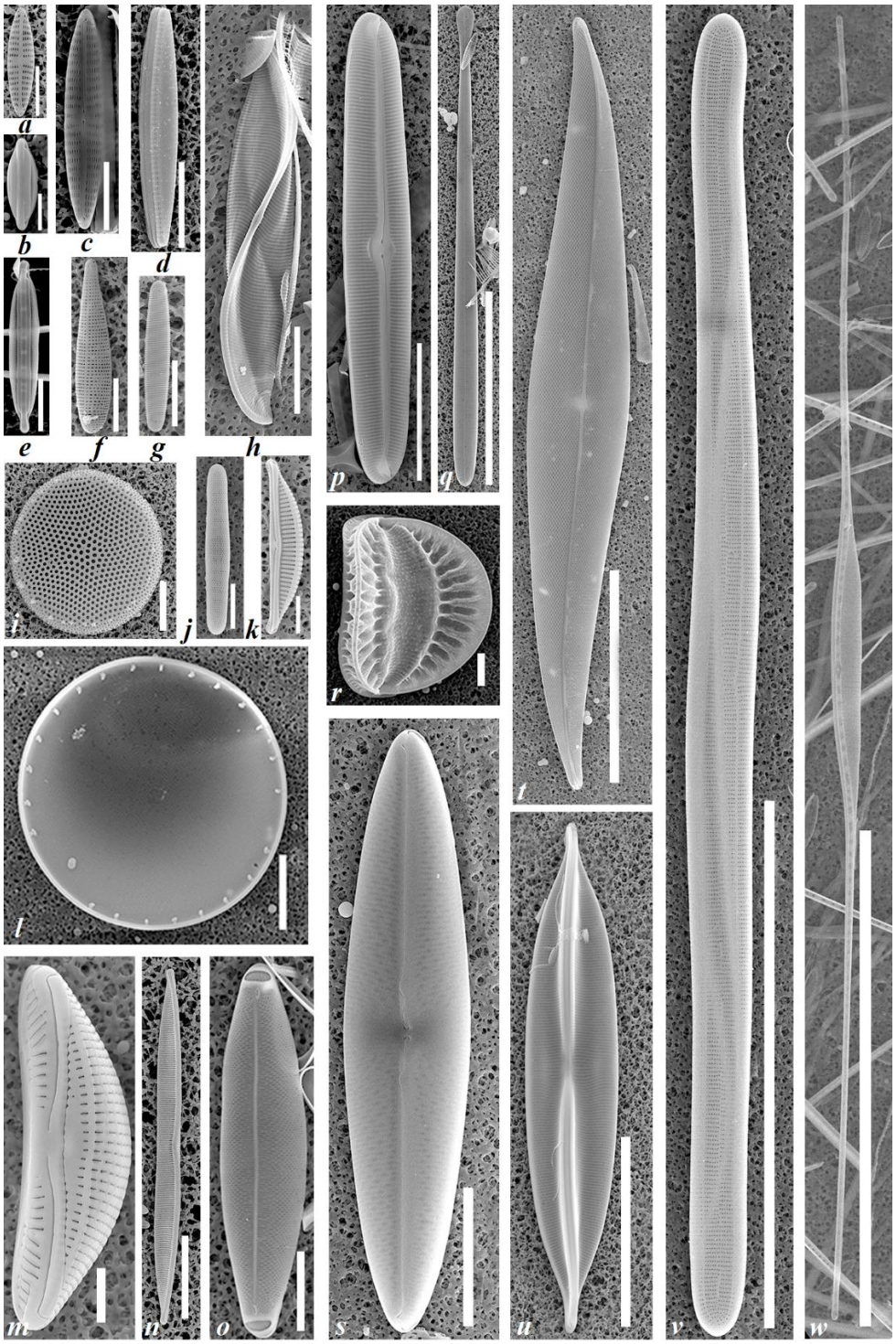
a
b
c
d
e
f
g
h
i
j
k
l
m
n
o
p
q
r
s
t
u
v
w

Fig. 5. Dominant species of benthic diatoms on concrete and steel substrates (SEM): *a – Navicula perminuta; b – Nitzschia* sp.1*; c – Navicula parapontica;d – Tabularia affinis; e – Nitzschia sp.2; f – Licmophora gracilis; g – Microtabella delicatula; h – Entomoneis paludosa; i – Thalassiosira excentrica; j – Grammatophora marina; k – Amphora sp.; l – Actinocyclus subtilis; m – Amphora marina; n – Nitzschia hybrida; o – Striatella unipunctata; p – Caloneis liber; q – Licmophora flabellata; r – Campylodiscus thuretii; s – Trachyneis aspera; t – Pleurosigma elongatum; u – Plagiotropis lepidoptera; v – Ardissonea crystallina; w – Nitzschia longissima. Scale bar: a, c,e, f, g, k, m* – 5 μm; *b* – 3 μm; *d, h, i, j, o, s, r* – 10 μm; *l, p, s* – 20 μm; *q, t* – 50 μm; *u* – 30 μm; *v, w* – 100 μm

on fouling of water supply device lead to significant decrease in the occurrence of *Ciliata* and *Oligochaeta* after 72 hours of exposure, but at the same time it had not noticeable effect on the number of amoebae, rotifers, and other forms of parasitic ciliates [9].

We have to point out that effect of microalgae development stimulation observed at the beginning of the *in situ* experiment was noted before [1)] as the first stage (activation) of a test object response when exposed to various toxicants, electromagnetic fields, and other stressors [13, 14]. Apparently, this phenomenon is stipulated by the short-term reaction of microalgae to the USD impact, which is expressed by mobilization of their adaptive capabilities and cell division intensification [15]. At the third month of the USD exposure with increased parameters, a reduction of abundance of diatoms was noted, that reflects a falling resilience at the second stage of stress (inhibition). It is known that the USD sounding to a biological object and their direct impact can destroy the membranes and organelles of unicellular organisms, as well as inactivate its enzymes [15–17].

And finally, at the fifth month of the experiment, the third stage of stress begins (depletion of adaptive capabilities and elimination of diatoms), which was expressed in the diatom cells number reduction by several times on both types of substrates at the TS. The ultrasound spreads well over a large area in water and can prevent the attachment of free-living forms of organisms, especially microperiphyton, destroy microplankton and bacteria even at a distance from the operating USD, thereby worsening the food resource of predators, and also suppress

---

[1)] Gelashvili, D.B., 2016. [*Principles and Methods of Ecological Toxicology*]. Nizhny Novgorod: Izd-vo NNGU, 704 p. (in Russian).

the viability of some groups of fouling. The effectiveness of ultraviolet and ultrasound combined treatment to increase water quality during its purification and disinfection from pathogenic organisms when used in aquaculture and in closed water supply circuits has been approved [17, 18].

It should be noted that US sounding, unlike hard radiation, do not have an accumulating effect, therefore long-term US action with low intensity does not cause any noticeable changes in periphyton organisms. In contrast, short-term high-power pulse US treatment can have a more pronounced efficacy on fouling than weak, but continuous US exposure. However, even with prolonged US exposure by a weak and obviously non-lethal doses, it is still impossible to establish the degree of periphyton inhibition only by the absence of a response from organisms. Thus, there can be no signs of suppressive effect to different groups of biota when the ultrasound action is below a threshold level, but the opposite effect can occur – referring to the aforementioned stimulation of the development and growth of fouling organisms, as was observed at the TS in the initial stage of the field experiment.

Based on the experimental results in the water area, we can conclude that since the sensitivity of different groups of periphyton to ultrasound treatment is different, we have to find universal threshold parameters to achieve the greatest USD effect (excluding hard doses dangerous for biota). For example, larvae of barnacles can die and fall off experimental plates even at low levels of the US action, while adhered juvenile barnacles or small mollusks can remain viable even at higher sounding levels. To improve the USD efficacy, the seasonal aspects of periphyton succession on various substrates should also be taken into account. Evidently that during the spring-summer's peak fouling development and the highest intensity of formation of the primary biofilm on the TWSC surfaces, the USD action should be higher than at the autumn-winter period.

In general, the results of laboratory and field studies revealed that the problem to provide the US protection of TWSC equipment against biofouling should be solved not only by increasing the USD power and intensity, which apparently causes the rapid and complete death of all ecological and taxonomic groups of periphyton on treated surfaces. Also, one should define such parameters of sounding that can preventively supress the fouling: settling and adhesion of microphytes, macrophytes, and zoobenthos, their subsequent growth and development. It seems important to expand laboratory and field experiments in order to study the US action of various durations and frequencies on the survival and development of different groups of periphyton to achieve the maximum effect in TPP and NPP TWSC protection. Minimisation the negative impact of ultrasound on the state of other components of aquatic ecosystems of water-cooling reservoirs should also be taken into consideration.

Conclusion

The stimulation of microperiphyton development on both concrete and steel substrates at the initial stage of the experiment studying the ultrasound effect was revealed.

Increasing the duration and frequency of the USD exposure had a pronounced effect on the diatoms – main component of the microperiphyton on concrete and steel substrates. After five months of the experiment with the increased USD intensity, a significant reducing of abundance and species richness of diatoms on steel and concrete was registered, compared to previous months. Small-celled species from genera *Navicula* and *Nitzschia* dominated on both types of substrate, regardless of the experimental conditions. A total of 30 species of benthic diatoms belonging to 21 genera, 17 families, 13 orders and 3 classes of Bacillariophyta were marked.

The results of laboratory and field tests make it possible to recommend to extend the experiments using a full-function USD of higher power directly during the exploitation of an NPP.

REFERENCES

1. Zvyagintsev, A.Y., Poltarukha, O.P. and Maslennikov, S.I., 2015. Fouling of Technical Water Supply Marine Systems and Protection Method Analysis of Fouling on Water Conduits (Analytical Review). *Water: Chemistry and Ecology*, (1), pp. 30–51 (in Russian).
2. Mileykovsky, S.A., 1981. [Impact of Passing through Cooling Water Systems of Coastal Power Stations and Industrial Plants on the Reproduction and Productivity of Marine and Estuarine Plankton, Benthos and Nekton]. In: O. G. Reznichenko and I. V. Starostin, eds., 1981. [*Fouling and Biocorrosion in Water Environment*]. Moscow: Nauka, pp. 131–137 (in Russian).
3. Kartasheva, N.V., Fomin, D.V., Popov, A.V., Kuchkina, M.A. and Minin, D.V., 2008. An Estimation of Influence Reservoir-Cooler Nuclear and Thermal Power Stations on Zooplankton. *Vestnik Moskovskogo Universiteta. Seriya 16: Biologiya*, (3), pp. 30–35 (in Russian).
4. Dürr, S. and Thomason, J.R., eds., 2010. *Biofouling*. Chichester: Blackwell Publishing Ltd, 456 p.
5. Kalaida, M., Novikova, G., Sinyutina, T. and Shmakova, A., 2008. [Struggle against Biofouling – an Important Problem of Energy and Sources Saving]. *Energetika Tatarstana*, (2), pp. 51–55 (in Russian).
6. Moroz, N.A., Nevrova, E.L., Zamyslova, T.N., Kasyanov, A.B., Petrov, A.N. and Revkov, N.K., 2021. [Methods of Fouling Control at Nuclear Power Plants]. In: M. I. Orlova and V. A. Rodionov, eds., 2021. [*Problems of Development of New Generation Protective Coatings against Corrosion, Biofouling and Icing for Marine, Coastal and Terrestrial Objects*]. Saint Petersburg: Izd-vo SPbGEU, pp. 94–103 (in Russian).
7. Protasov, A.A., ed., 2011. *Techno-Ecosystem of the Nuclear Power Plant. Hydrobiology, Abiotic Factors, Ecological Estimations*. Kyiv: Institute of Hydrobiology NAS of Ukraine, 234 p. (in Russian).
8. Farberov, V.G., Chionov, V.G., Leonov, S.V., Zelenina, E.S. and Popov, A.V., 2004. Methods for Protecting Cooling Ponds of Thermal and Nuclear Power Stations against Biofouling. *Thermal Engineering*, 51(6), pp. 471–474 (in Russian).

9. Klimov, V.A., Nikiforov-Nikishin, A.L., Kochetkov, N.I. and Gorbunov, A.V., 2022. Change in Composition of Periphyton of Filtration Elements in Recirculation Aquaculture Systems under Combined Impact of UV Radition and Ultrasound. *Vestnik of Astrakhan State Technical University. Series: Fishing Industry*, (4), pp. 113–122. doi:10.24143/2073-5529-2022-4-113-122 (in Russian).
10. Dolgopolskaya, M.A. and Akselband, A.M., 1964. [The Effect of Ultrasonic on Marine Fouling Organisms and the Fouling Process]. *Trudy Sevastopolskoy Biologicheskoy Stantsii,* (17), pp. 309–324 (in Russian).
11. Nevrova, E.L., 2022. *Diversity and Structure of Benthic Diatom Taxocenes (Bacillariophyta) of the Black Sea*. Sevastopol: IBSS, 329 p. (in Russian).
12. Kovalchuk, Y.L., Nevrova, E.L. and Shalaeva, E.A., 2008. *Diatom Fouling of Solid Substrates*. Moscow: KMK, 174 p. (in Russian).
13. Petrov, A.N. and Nevrova, E.L., 2023. Experimental Evaluation of Toxic Resistance of Benthic Microalgae Thalassiosira excentrica Cleve 1903 (Bacillariophyta) under the Copper Ions Impact. *Vestnik of MSTU*, 26(1), pp. 78–87. doi:10.21443/1560-9278-2023-26-1-78-87
14. Railkin, A.I., 2008. [*Colonization of Solid Bodies with Benthic Organisms*]. Saint Petersburg: Izd-vo Sanktpeterburgskogo universiteta, 427 p. (in Russian).
15. Gerde, J.A., Montalbo-Lomboy, M., Yao, L., Grewell, D. and Wang, T., 2012. Evaluation of Microalgae Cell Disruption by Ultrasonic Treatment. *Bioresource Technology*, 125, pp. 175–181. https://doi.org/10.1016/j.biortech.2012.08.110
16. Zhang, G., Zhang, P., Wang, B. and Liu, H., 2006. Ultrasonic Frequency Effects on the Removal of *Microcystis aeruginosa*. *Ultrasonics Sonochemistry*,13(5), pp. 446–450. doi:10.1016/j.ultsonch.2005.09.012
17. Blume, T., Martinez, I. and Neis, U., 2002. Wastewater Disinfection Using Ultrasound and UV Light. In: U. Neis, ed., 2002. *2nd International Conference: Ultrasound in Environmental Engineering, Hamburg, Germany, 21–22 March 2002*. Hamburg, Vol. 35, pp. 117–138.
18. Annisha, O.D.R., Li, Z., Zhou, X., Stenay Jr., N.M.D. and Donde, O.O., 2019. Efficacy of Integrated Ultraviolet Ultrasonic Technologies in the Removal of Erythromycin- and Quinolone-Resistant *Escherichia coli* from Domestic Wastewater through a Laboratory-Based Experiment. *Journal of Water, Sanitation and Hygiene for Development*, 9(3), pp. 571–580. doi:10.2166/washdev.2019.021

Submitted 27.04.2023; accepted after review 15.06.2023;
revised 28.06.2023; published 25.09.2023

About the authors:

Elena L. Nevrova, Chief Research Associate, A. O. Kovalevsky Institute of Biology of the Southern Seas of RAS (2 Nakhimova Ave, Sevastopol, 299011, Russian Federation), Dr.Sci. (Biol.), **ORCID ID: 0000-0001-9963-4967, Scopus Author ID: 35277386100, ResearcherID: D-8434-2016,** *el_nevrova@mail.ru*

Aleksey N. Petrov, Head of the Benthic Ecology Department, A. O. Kovalevsky Institute of Biology of the Southern Seas of RAS (2 Nakhimova Ave, Sevastopol, 299011, Russian Federation), Ph.D. (Biol.), **ORCID ID**: **0000-0002-0137-486X, Scopus Author ID: 8973404400, ResearcherID: F-7084-2016**, *alexpet-14@mail.ru*

Natalia A. Moroz, Head of the Department of Biochemical Technologies and Engineering Support, VNIIAES JSC (25 Ferganskaya St, Moscow, 109507, Russian Federation), Ph.D. (Tech.), *sv_nata@mail.ru*

Anatoly B. Kasyanov, Leading Engineer, VNIIAES JSC (25 Ferganskaya St, Moscow, 109507, Russian Federation), *papa_triod@mail.ru*

Contribution of the authors:

Elena L. Nevrova – study task statement, analysis and interpenetration of the results, taxonomic identification of diatoms, preparation of graphical materials, article forming

Aleksey N. Petrov – analysis and discussion of the results, review of literature on the study topic, manuscript editing

Natalia A. Moroz – task statement, experiment maintenance, analysis and discussion of the results

Anatoly B. Kasyanov – experiment planning, development and technical maintenance of the experiment instrumental basis, conduction of the experiment, analysis and discussion of the results

All the authors have read and approved the final manuscript.

Original article

Are Polymer-Based Single-Use Face Masks Subject to Biofouling in Seawater?

A. V. Bondarenko *, L. I. Ryabushko, A. A. Blaginina

A. O. Kovalevsky Institute of Biology of the Southern Seas of RAS, Sevastopol, Russia
* *e-mail*: *gonzurassa@mail.ru*

Abstract

The paper presents for the first time the results of an experimental study of the species composition and quantitative characteristics: species richness (S), abundance (N) and biomass (B) of the microalgae and cyanobacteria in the fouling of synthetic single-use face masks as a technogenic substrate. Fouling experiments were conducted for two months and for one year in 2021–2022 in Karantinnaya Bay (the Black Sea). The surface of masks and microfouling suspensions were studied using light and electron microscopy. In total, 48 taxa from 5 phyla were noted: Cyanoprocaryota – 3 species, Bacillariophyta – 36, Dinophyta – 6, Haptophyta – 2, Ochrophyta – 1. After a two-month exposure of masks, 30 species were found, and 40 species were found after a one-year exposure, 22 species were shared. For the first time for the bay, we have identified benthic species of diatoms *Cocconeis guttata* and *Karayevia amoena*. Out of 14 benthic typical colonial fouling species of diatoms, *Tabularia fasciculata* was on all masks with 100 % occurrence. Solitary-living species were also recorded among the frequently encountered ones: potentially toxic *Halamphora coffeiformis* and bentoplanktonic *Cylindrotheca closterium*. The features of the mask fouling at different exposure periods in the sea are the absence of the formation of diatoms colonies, unlike fouling on other anthropogenic and natural substrates, and low quantitative characteristics at different periods: after a two-month exposure, the corresponding values were: S – 10–15 species, N – 9200–13100 cells/cm^2, and B – 0.001–0.02 mg/cm^2; after a one-year exposure, the same were: S – 8–14 species, N – 4900–8400 cells/cm^2, B – 0.01–0.03 mg/cm^2.

Keywords: diatoms, cyanobacteria, microalgae, fouling, single-use face masks, Crimea, coastal waters, Black Sea

Acknowledgements: The work was performed under state assignment of IBSS of RAS "Research of control mechanisms for production processes in biotechnological complexes with the aim of developing scientific foundations for obtaining biologically active substances and technical products of marine genesis", state registration no. 121030300149-0. We would like to express our gratitude to Chief Research Associate, Dr.Sci. (Biol.), V. I. Ryabushko for the idea of studying and support, to S. V. Shchurov for sampling and hydrological indicators, and to V. N. Lishaev for processing the material in the SEM.

For citation: Bondarenko, A.V., Ryabushko, L.I. and Blaginina, A.A., 2023. Are Polymer-Based Single-Use Face Masks Subject to Biofouling in Seawater? *Ecological Safety of Coastal and Shelf Zones of Sea*, (3), pp. 114–128.

Подвержены ли биообрастанию синтетические медицинские маски в морской воде?

А. В. Бондаренко *, Л. И. Рябушко, А. А. Благинина

Институт биологии южных морей им. А. О. Ковалевского РАН, Севастополь, Россия
** e-mail: gonzurassa@mail.ru*

Аннотация

Впервые представлены результаты экспериментального изучения видового состава и количественных характеристик (обилие видов, численность и биомасса) микроводорослей и цианобактерий в обрастании синтетических медицинских масок в качестве техногенного субстрата. В 2021–2022 гг. в б. Карантинной (Черное море) были проведены эксперименты по обрастанию в течение двух месяцев и одного года. Поверхность масок и суспензии микрообрастаний изучали с использованием световой и электронной микроскопии. Всего обнаружено 48 таксонов из 5 отделов: Cyanoprocaryota – 3 вида, Bacillariophyta – 36 видов, Dinophyta – 6 видов, Haptophyta – 2 вида, Ochrophyta – 1 вид. При двухмесячной экспозиции масок найдено 30 видов, при годичной – 40, при этом 22 вида были общими. Впервые для бухты нами указаны бентосные виды диатомовых водорослей *Cocconeis guttata* и *Karayevia amoena*. Из 14 пеннатных типичных колониальных видов-обрастателей диатомовых водорослей на всех масках со 100 %-ной встречаемостью отмечен вид *Tabularia fasciculata*, среди одиночноживущих видов часто отмечались потенциально токсичный *Halamphora coffeiformis* и бентопланктонный *Cylindrotheca closterium*. Особенностью обрастания является отсутствие образования колоний диатомовых водорослей, в отличие от обрастания на других антропогенных и природных субстратах, и низкие количественные показатели при разных сроках экспозиции – при двухмесячной соответствующие значения составляли: обилие видов – 10–15 видов, численность – 9200–13 100 кл./см^2 и биомасса – 0.001–0.02 мг/см^2; при годичной – обилие видов – 8–14 видов, численность – 4900–8400 кл./см^2, биомасса – 0.01–0.03 мг/см^2.

Ключевые слова: диатомовые водоросли, цианобактерии, микроводоросли, обрастание, синтетические медицинские маски, крымское прибрежье, Черное море

Благодарности: работа выполнена по теме государственного задания ФИЦ ИнБЮМ РАН «Исследование механизмов управления продукционными процессами в биотехнологических комплексах с целью разработки научных основ получения биологически активных веществ и технических продуктов морского генезиса» (номер гос. регистрации 121030300149-0). Выражаем благодарность гл. н. с., д. б. н. В. И. Рябушко за идею изучения и поддержку, С. В. Щурову – за отбор проб и гидрологические измерения, В. Н. Лишаеву – за обработку материла в СЭМ.

Для цитирования: Бондаренко А. В., Рябушко Л. И., Благинина А. А. Подвержены ли биообрастанию синтетические медицинские маски в морской воде? // Экологическая безопасность прибрежной и шельфовой зон моря. 2023. № 3. С. 114–128. EDN MYZVXK.

Introduction

The plastisphere of the World Ocean contains 8–12 million tons of waste, and in recent years, due to the COVID-19 pandemic that has covered the entire world, single-use three-layer face masks have been added to the variety of anthropogenic debris entering marine ecosystems and accumulating there. Based on the annual estimate of global production of 52 billion masks, researchers estimate that 1.56 billion masks entered the World Ocean in 2020 (Fig. 1), representing between 4680 and 6240 tons of plastic pollution [1].

Like any other type of solid human-made waste entering marine ecosystems, face masks are an additional anthropogenic substrate for colonization by various organisms, mainly micro- and meiobenthic forms. The most studied substrates atypical for the natural habitat of hydrobionts in the sea include substrates of anthropogenic origin (glass, wood, plastic, synthetic polymer-based materials, etc.), which are populated mainly by bacteria, diatoms and cyanobacteria [1)] and participate in the transformation of the substrate and its partial utilization in the sea in different ways [2–12].

It has also been noted that bacteria, fungi, cyanobacteria and mainly diatoms create persistent biofilms on plastic and glass materials, subsequently competing for the substrate [1)] with invertebrates and macrophytes [5, 13].

As a substrate, a three-layer face mask represents a set of polymer-based fibers that form a textile fabric. Such masks are made from various non-woven materials, most often spunbond, mainly spunbond polypropylene. Spunbond is a microporous material that is resistant to aggressive environments and water, as well as to high and low temperatures. It has high strength, does not rot or mold. It is indicated that in the environment this material does not have any ability to form toxic compounds, and this determines its environmental safety [14].

Fig. 1. Used polymer-based single-use face masks washed up on the coast (URL: https://oceansasia.org)

However, the polymer-based material of single-use face masks determines the process of their long-term degradation under natural conditions in the sea.

[1)] Balycheva, D.S., 2014. [*Species Composition and Structural and Functional Characteristics of Periphyton Microalgae of Anthropogenic Substrates in the Crimean Coastal Part of the Black Sea.* Extended Abstract of Doctoral Dissertation]. Sevastopol, 24 p. (in Russian).

In this case, the destruction of synthetic fabric occurs almost immediately after entering the aquatic environment and is accompanied by the gradual release of microscopic polypropylene fibers that are capable of absorbing organic and inorganic pollutants, which leads to the toxicity of microplastics [12]. Consequently, masks have become a potential source of microplastic pollution of marine ecosystems with a known negative impact on various communities of aquatic organisms – from microforms of animals and plants to the largest representatives of the living world [12, 15–18].

It should also be taken into account that the polypropylene density (0.91 g/cm^3) is less than the water density (0.99 g/cm^3), and the outer layer of face masks is waterproof, so such personal protective equipment can move for a long time by currents in the water column of seas and oceans. Species that have colonized the surface of this substrate in one area can be transported over significant distances and become invasive in new water areas. In addition, biofilms formed in the water column on artificial polymer substrates can lead to the loss of buoyancy of these materials and their subsequent burial in bottom sediments, i. e., transition from one biotope to another. All this indicates the global scale of the problem of marine plastic pollution and the relevance of studying physico-chemical and biological processes in the plastisphere. The Black Sea is an inland body of water, which makes it very difficult to protect its biota from pollution, especially from plastic waste.

In connection with the above stated and also due to the lack of data in the literature concerning the biodegradation of face masks that run into the sea, the question comes up whether these synthetic materials are colonized at all and whether the processes of their biodestruction occur under the influence of microalgae and cyanobacteria at different exposure periods in the sea.

The purpose of this article is an experimental study of the species composition and quantitative characteristics of microalgae and cyanobacteria in the fouling of polymer-based single-use face masks at different exposure periods in Karantinnaya Bay (the Black Sea).

Materials and methods

To study the species composition, number, and biomass of the microalgae and cyanobacteria fouling single-use face masks in the sea, as well as to visually assess the integrity of the synthetic material after different periods of stay in sea water, the following experiment was carried out. A vertical collector, which consists of perforated plastic containers fixed on a rope with a buoy and an anchor with masks attached to them, was mounted in the area of a mussel and oyster farm in Karantinnaya Bay (44°61′83″ N, 33°50′34″ E) (Crimean coastal waters of the Black Sea). Holes in the walls of the containers provided constant access of sea water with micro- and meioorganisms living in it. The location depth of the containers was 3 m. At the same depth, a hermetically sealed cylinder with masks was fixed in sterile sea water. Accordingly, such masks were not exposed to the biotic factor while maintaining the influence of a number of abiotic factors, such as temperature, salinity, illumination, hydrodynamics, etc.

Some of the experimental masks were taken out two months (from 05.10.2021 to 10.12.2021) and a year (from 05.10.2021 to 09.11.2022) after their immersion in the sea. The masks remaining on the collector are the subject of subsequent study of fouling processes and observation of the polymer-based material degradation with longer exposure.

During the two-month exposure of the material, the water temperature varied within the range of 12.8–19.6 °C, and the salinity made 17.84–18.07 PSU. During the one-year exposure, the water temperature had positive values with its minimum in February 2022 (8 °C) and maximum in August (26.1 °C), and water salinity varied within the range of 17.84–18.52 PSU.

In the laboratory, the masks were cleaned of fouling. The study of the qualitative and quantitative characteristics of microalgae and cyanobacteria on the surfaces of the masks and in the resulting suspensions was carried out in light microscopes (LM) such as *Olympus CX*31 and *Axioskop* 40 (*C. Zeiss*) at a magnification of 10 × 20, 10 × 40, and 10 × 100. For a detailed study of cell morphology and identification of the species of diatoms, sample preparation was carried out for examination in a scanning electron microscope (SEM) *Hitachi SU*3500. Samples were prepared in two ways. In the first case, fibers and pores on the surface of single-use face masks were studied without treating the material with acids. At five points on the mask fabric, squares measuring 0.5 × 0.5 cm were randomly selected and cut out, left to dry completely in air, and then a thin layer of gold – palladium was sprayed on. The second case was to treat the resulting suspensions with acids according to the methods [19, 20] to clean the shells of diatoms and obtain their photographs, which was necessary for species identification.

Determination of the species composition of microalgae and cyanobacteria was carried out using monograph [21] and a number of papers [2), 3), 4), 5), 6)]. Names are given according to the algae database [7)]. The species richness (*S*), abundance (*N*), and biomass (*B*) of living microalgae cells were taken into account in a Goryaev chamber (hemocytometer) with a volume of 0.9 mm^3 according to the formulas of V.I. Ryabushko [22]. The species richness was determined as the number of species found in the counting chamber when viewing samples from each specific sample of experimental material.

---

2) Guslyakov, N.E., Zakordonets, O.A. and Gerasimyuk, V.P., 1992. [*Atlas of Benthic Diatoms of the Nortwestern Black Sea and Adjecent Waterbodies*]. Kiev: Naukova Dumka, 112 p. (in Russian).

3) Konovalova, G.V., 1998. [*Dinoflagellates of Far East Seas of Russia and Adjacent Water Areas of the Pacific Ocean*]. Vladivostok: Dalnauka, 298 p. (in Russian).

4) Komárek, J. and Anagnostidis, K., 1999. *Cyanoprokaryota. 1 Teil: Chroococcales. Süßwasserflora von Mitteleuropa.* Bd 19/1. Heidelberg, Berlin: Spektrum Akademischer Verlag, 523 p.

5) Witkowski, A., Lange-Bertalot, H. and Metzeltin, D., 2000. *Diatom Flora of Marine Coast. Part I. Iconographia Diatomologica*. A.R.G. Gantner. Vol. 7, 925 p.

6) Ryabushko, L.I. and Begun, A.A., 2016. [D*iatoms of Microphytobenthos of the Sea of Japan (Synopsis and Atlas)*]. In two volumes. Sevastopol: PK "KIA".Vol. 2, 324 p. (in Russian).

7) Guiry, M.D. and Guiry, G.M. 2023. *AlgaeBase*. National University of Ireland, Galway. [online] Available at: https://www.algaebase.org [Accessed: 31 August 2023].

Results and discussion

LM and SEM-based visual analysis of surface samples of face masks over the exposure period of two months and one year in Karantinnaya Bay near the mussel and oyster farm showed that all layers of three-layer masks were saturated with detritus, silt and sand fractions, juvenile barnacles, fragments of mollusk shells, etc. (Fig. 2). Particularly pronounced sediment was observed on masks after a one-year exposure, on which a larger amount of detritus was noted (Fig. 2, *b*).

A study of the outer and inner layers of single-use face masks after a two-month exposure showed that there were no attached microalgae cells or their colonies on the fibers and in the pores of the polymer-based material (Fig. 3, *a*, *b*). The species observed in our experiment were found separately; they lay freely on the canvas (Fig. 3, *c*) or among the fibers.

Meanwhile, many authors note that during the formation of biofilms on the surface of various artificial substrates, some species of diatoms *Cocconeis*, *Amphora*, *Achnanthes*, *Mastogloia*, *Karayevia*, etc. are capable of attaching directly to the polymer-based material [6, 11, 23]. The ability of individual diatoms to modify the structure of the substrate due to dense attachment to its surface or even penetration into it is also indicated [23, 24].

In total, 48 species of microorganisms belonging to 5 phyla: Cyanoprocaryota – 3, Dinophyta – 6, Haptophyta – 2, Ochrophyta – 1, Bacillariophyta (the most diverse) – 36 species and IST belonging to 28 genera (see Table) were noted in the fouling of masks at different exposure periods.

Analysis of the species structure of diatoms shows that Bacillariohyceae (9 orders, 16 families, and 21 genera) is the basic class of their diversity, which is typical for the microphytobenthos of the Black Sea.

Fouling of masks after a two-month exposure is represented by 30 species, including 3 species of cyanobacteria and 27 species of microalgae, of which 20 belong to phylum Bacillariophyta, 4 – to Dinophyta, 2 – to Haptophyta, 1 – to Ochrophyta (Table).

Fig. 2. Light microscope (LM): meiobenthic fouling of the surface of face masks after a two-month (*a*) and one-year (*b*) exposure to the sea

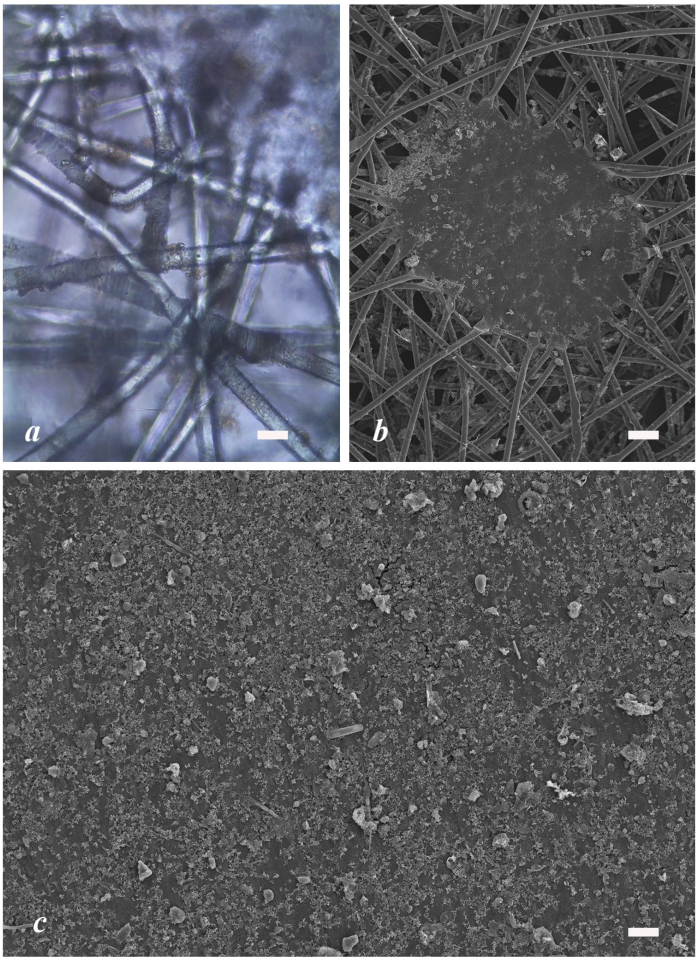

Fig. 3. The inner layer of a face mask of a two-month exposure: LM – polypropylene fibers (*a*), scanning electron microscope (SEM) – fiber pores (*b*); surface of the inner layer (*c*). Scale bar: 1000 μm (*a*), 100 μm (*b*), 10 μm (*c*)

The fouling of masks after a one-year underwater exposure amounted to 40 species and IST, of which 1 species each belongs to phyla Cyanoprocaryota and Ochrophyta, 32 – to Bacillariophyta, 4 – to Dinophyta, 2 – to Haptophyta (see Table). At different exposure times, 22 species were shared on the surface of the masks. For the first time for Karantinnaya Bay, we have identified benthic species of diatoms *Cocconeis guttata* and *Karayevia amoena*.

Most of the stated fouling microalgae are typical inhabitants of sea benthos, whose life activity is closely related to different types of substrates. The share of benthic species accounts for 67 %, planktonic species – 20 %, benthic-planktonic

The occurrence of microalgae and cyanobacteria species in the fouling of single-use face masks for 2021–2022 at different exposure periods in Karantinnaya Bay (Crimea, the Black Sea)

Taxon	Exposure period	
	Two months	One year
Bacillariophyta phylum		
Achnanthes brevipes C. Agardh 1824 *	+	+
Amphora ovalis (Kützing) Kützing 1844 *	+	+
A. pediculus (Kützing) Grunow 1875 *	+	+
Ardissonea crystallina (C. Agardh) Grunow 1880 *	+	+
Caloneis liber (W. Smith) Cleve 1894 *	–	+
Cerataulina pelagica (Cleve) Hendey 1937 **	+	–
Cocconeis guttata Hustedt et Aleem 1951 *	–	+
C. placentula Ehrenberg 1838 *	–	+
C. scutellum Ehrenberg 1838 *	–	+
Coscinodiscus sp. **	+	+
Cylindrotheca closterium (Ehrenberg) Reimann et Lewin 1964 ***	+	+
Grammatophora marina (Lyngbye) Kützing 1844 *	+	+
Diploneis bombus (Ehrenberg) Ehrenberg 1853 *	–	+
D. smithii (Brébisson) Cleve 1894 *	+	+
Halamphora coffeiformis (C. Agardh) Levkov 2009 *	+	+
Haslea subagnita (Proschkina-Lavrenko) Makarova et Karayeva 1985 *	+	–
Karayevia amoena (Hustedt) Bukhtiyarova 1999 *	–	+
Licmophora abbreviata C. Agardh 1831 *	–	+
Lyrella abrupta (W. Gregory) D.G. Mann 1990 *	–	+
Navicula ammophila var. *intermedia* Grunow 1882 *	+	+
Neosynedra provincialis (Grunow) D.M. Williams et Round 1986 *	–	+
Nitzschia lanceolata var. *minor* (Grunow) H. Peragallo et M. Peragallo 1900 *	–	+
N. sigma (Kützing) W. Smith 1853 *	–	+
Odontella aurita (Lyngbye) C. Agardh 1832 ***	–	+
Paralia sulcata (Ehrenberg) Cleve 1873 ***	+	–
Parlibellus delognei (Van Heurck) E.J. Cox 1988 *	+	+
Rhabdonema arcuatum (Lyngbye) Kützing 1844 *	–	+
Tabularia fasciculata (C. Agardh) Williams et Round 1986 *	+	+

Continued

Taxon	Exposure period	
	Two months	One year
T. parva (Kützing) D.M. Williams et Round 1986 *	+	+
Toxarium undulatum Bailey 1854 *	–	+
Trachyneis aspera (Ehrenberg) Cleve 1894 *	–	+
Tryblionella coarctata (Grunow) D.G. Mann 1990 *	–	+
T. hungarica (Grunow) Frenguelli 1942 *	+	–
T. punctata W. Smith 1853 *	+	+
Thalassionema nitzschioides (Grunow) Mereschkowsky 1902 ***	+	+
Thalassiosira sp. **	+	+
Dinophyta phylum		
Amphidinium sp. **	+	+
Prorocentrum compressum (Bailey) Abé ex Dodge 1975 ***	+	–
P. cordatum (Ostenfeld) J.D. Dodge 1976 ***	–	+
P. lima (Ehrenberg) F. Stein 1878 *	–	+
P. scutellum Schröder 1900 **	+	+
Protoperidinium brevipes (Paulsen) Balech 1974 **	+	–
Haptophyta phylum		
Anacanthoica acanthos (Schiller) Deflandre 1952 **	+	+
Emiliania huxleyi (Lohmann) W.W. Hay et H. Mohler 1967 **	+	+
Ochrophyta phylum		
Octactis speculum (Ehrenberg) F.H. Chang, J.M. Grieve et J.E. Sutherland 2017 **	+	+
Cyanoprocaryota/Cyanobacteria phylum		
Microcystis wesenbergii (Komárek) Komárek ex Komárek 2006 *	+	+
Pseudanabaena minima (G.S. An) Anagnostidis 2001 **	+	–
Spirulina tenuissima Kützing 1836 **	+	–
Total taxa:	30	40

* benthic species; ** planktonic species; *** benthic-planktonic species.

species – 13 % (Table). This ratio is close to the ratio on other artificial and natural substrates, which is described in the research work [1)] and in [4, 8, 9]. Diatom genera *Cocconeis* and *Tryblionella*, which include three species each, are characterized by the greatest diversity. The other ones are represented by one or two species (Table). Dinoflagellates of genus *Prorocentrum* (4 species) during two-month and one-year exposures were presented by two and three species, respectively. These algae, like diatom *Halamphora coffeiformis*, are potentially toxic species for biota and human [25].

Typical colonial benthic fouling species were found on the surface of the masks. They are *Tabularia fasciculata, T. parva, Grammatophora marina, Achnanthes brevipes, Ardissonea crystallina, Parlibellus delognei*, with benthic-planktonic species *Thalassionema nitzschioides*. Colonial species *Toxarium undulatum, Odontella aurita*, *Licmophora abbreviata, Rhabdonema arcuatum* were found only after a one-year exposure, while planktonic *Cerataulina pelagica* and bentic-planktonic *Paralia sulcata* were found only after a two-month exposure. Some species of diatoms are shown in SEM images: *Cocconeis placentula* (*a*), *C. guttata* (*b*), *Th. nitzschioides* (*c*), *C. closterium* (*d*), *A. brevipes* (*e*), *A. pediculus* (*f*), *Karayevia amoena* (*g*), *Halamphora coffeiformis* (*h*) (Fig. 4).

Cosmopolitan species *T. fasciculata* showed the maximum occurrence (100 %). Other species *A. pediculus*, *C. closterium*, *Gr. marina*, *H. coffeiformis*, *Tabularia parva*, *Thalassiosira* sp., dinophyte *Prorocentrum scutellum*, and haptophyte *Emiliania huxleyi* made 67 %, other species – from 17 % to 50 %.

It should be noted that, in comparison with other artificial substrates that we studied earlier, single-use face masks with two-month and one-year exposures turned out to be the least susceptible to fouling. Thus, in an experiment on the colonization of various polymer-based materials by organisms in Karantinnaya Bay in the summer and autumn period of 2018, it was shown that the surfaces of the plates were densely populated by various meiobenthos fouling species: bryozoans, hydroids, tunicates, etc., and 94 species were registered as part of microphytofouling, including diatoms (67) and cyanobacteria (27) [8]. In addition, 20 species of diatoms, which form the basis of the floristic diversity of fouling, are common to masks and various polymer-based substrates.

On all experimental samples of the studied polymer-based materials, massive colonial species *Gr. marina* and *Licmophora abbreviata* were constantly observed, somewhat less commonly – *Tabularia tabulata* and *T. fasciculata*, which are characterized by adhesion to various natural and artificial substrates and formation of colonies that can also attach to polymer-based material.

As for face masks, we noted a similar picture, however, of 14 colonial fouling species detected, microalgae were mainly represented individually, without the formation of colonies.

In addition to the floristic study of fouling on masks, despite the low quantitative indicators, we presented the corresponding values of the detected species concerning the species richness (*S*), abundance (*N*), and biomass (*B*), using a counting chamber. After a two-month exposure, *S* varied within 10–15 species,

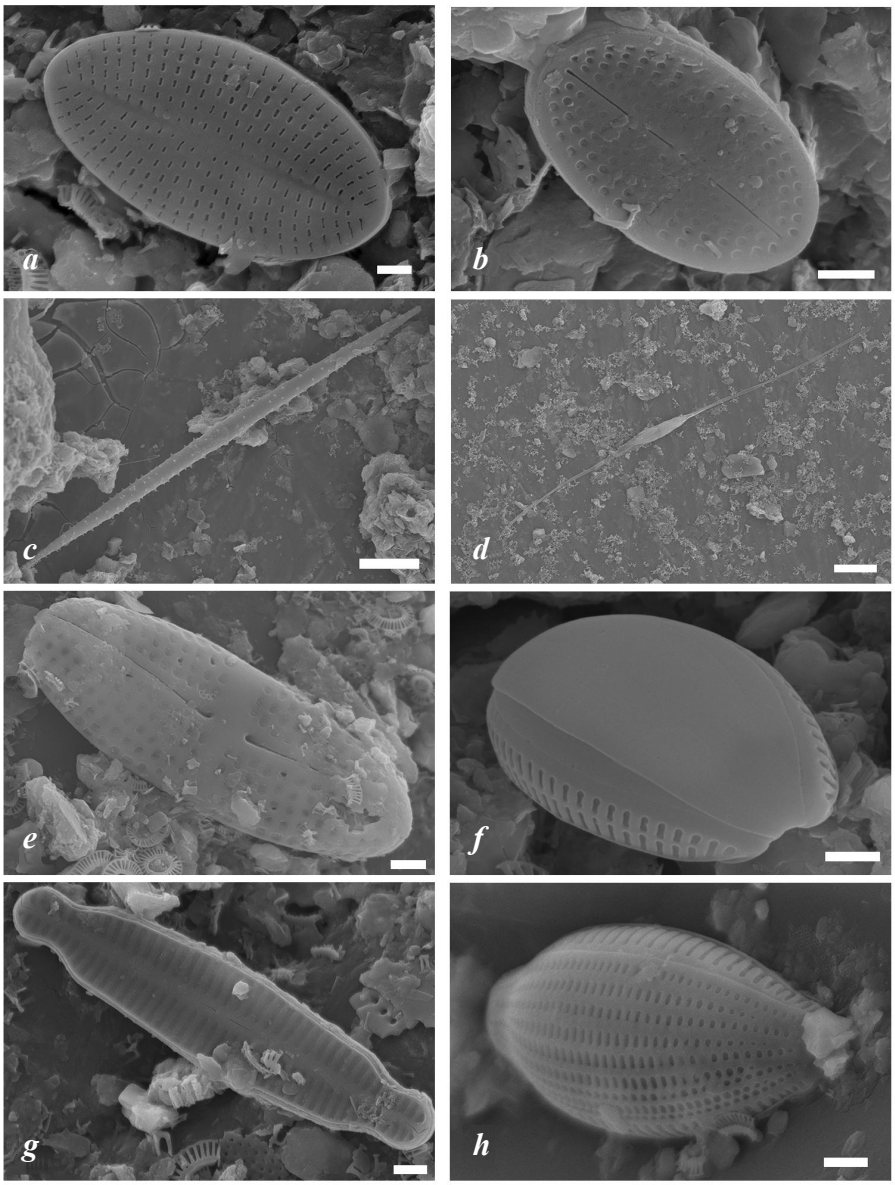

F i g. 4. Some diatoms in the fouling of single-use face masks surface, SEM: *Cocconeis placentula* (*a*), *C. guttata* (*b*), *Thalassionema nitzschioides* (*c*), *Cylindrotheca closterium* (*d*), *Achnanthes brevipes* (*e*), *Amphora pediculus* (*f*), *Karayevia amoena* (*g*), *Halamphora coffeiformis* (*h*). Scale bar: 1 μm (*a, f, g*), 2 μm (*e*, *h*), 10 μm (*b*, *c, d*)

N – 9200–13100 cells/cm^2, B – 0.001–0.02 mg/cm^2. After a one-year exposure, the corresponding values were as follows: S – 8–14 species, N – 4900–8400 cells/cm^2, and B – 0.01–0.03 mg/cm^2.

It is interesting to compare our information with data obtained from studying periphyton microalgae on experimental glass plates exposed in another part of the same bay from January 2007 to February 2008 for different periods (short-term – from 4 to 20 days; long-term – from 1 to 13 months) [4]. Right on the 20th day, a weak fouling of diatoms and then macroalgae seedlings was noticed on the plates, with its maximum in the spring at the end of a one-year exposure in water. A total of 99 taxa of microalgae are indicated from the following phyla: Bacillariophyta – 85, Dinophyta – 5, Chlorophyta – 4, Haptophyta – 2, and cyanobacteria – 3. 17 species of diatoms, 2 species of dinophytes, and one species each of haptophyte algae and cyanobacteria were shared by the glass plates and masks. During the cumulative exposure, the abundance of microalgae fouling of glass plates varied during the year from 26900 to 2180800 cells/cm^2, and the biomass varied within the range of 0.002–0.543 mg/cm^2.

It is shown in [12] that microplastics formed as a result of the degradation of masks are released into the environment almost from the first hours of its occurrence in it and contribute to an increase in the number and species diversity of the marine bacterial community. It is likely that masks become an attractive substrate for a variety of auto- and heterotrophic bacteria, which we have not studied.

Analysis of our own and literary sources showed that any substrates in the sea became colonized by microorganisms of plant and animal origin. As for microalgae, benthic diatoms have the greatest species diversity. Their richness and quantitative characteristics often depend on the type of substrate, season of the year, and environmental factors of the habitat.

The masks in Karantinnaya Bay were colonized by microalgae and cyanobacteria not so intensively as other anthropogenic substrates. This is especially true for the masks with a one-year exposure, which were subjected to the longest turbulent disturbances.

Conclusion

During the study period, 48 species from 5 phyla were noted: Cyanoprocaryota – 3 species, Bacillariophyta – 36, Dinophyta – 6, Haptophyta – 2, Ochrophyta – 1. After a two-month exposure, 30 species were found, and 40 species were found after a one-year exposure, 22 species were shared. For the first time for the bay, we have identified benthic species of diatoms *Cocconeis guttata* and *Karayevia amoena*. Out of 14 benthic typical colonial fouling species of diatoms on the surface of masks, cosmopolitan species *Tabularia fasciculata* showed the maximum occurrence (100 %). Solitary-living species were also recorded among the frequently encountered ones: potentially toxic *Halamphora coffeiformis* and bentoplanktonic *Cylindrotheca closterium*.

The features of the fouling of polymer-based single-use face masks at different exposure periods in the sea are the absence of formation of typical fouling species colonies and the lowest quantitative characteristics of microalgae compared

to other anthropogenic and natural substrates: after a two-month exposure, the following species richness (*S*) was identified – 10–15 species, abundance (*N*) – 9200–13100 cells/cm^2, and biomass (*B*) – 0.001–0.02 mg/cm^2; after a one-year exposure: *S* – 8–14 species, *N* – 4900–8400 cells/cm^2, *B* – 0.01–0.03 mg/cm^2.

Biodegradation of single-use face masks exposed to seawater for a year under the influence of microalgae and cyanobacteria manifests itself to a weak degree. Therefore, it is necessary to study this process with a longer exposure, taking into account the physicochemical factors affecting the polymer-based substrate.

References

1. Haddad, M.B., De-la-Torre, G.E., Abelouah, M.R., Hajii, S. and Alla, A.A., 2021. Personal Protective Equipment (PPE) Pollution Associated with the COVID-19 Pandemic along the Coastline of Agadir, Morocco. *Science of the Total Environment*, 798, 149282. doi:10.1016/j.scitotenv.2021.149282
2. Ryabushko, L.I. and Zavalko, S.E., 1992. Microphytofouling of Artificial and Natural Substrates in the Black Sea. *Botanicheskii Zhurnal,* 77(5), pp. 33–39 (in Russian).
3. Begun, A.A., Ryabushko, L.I. and Zvyagintsev, A.Yu., 2010. Quantitative Effect of Substratum Material and Time of its Exposition in the Sea on Development of Periphyton Diatoms. *Izvestiya TINRO = Transactions of the Pacific Research Institute of Fisheries and Oceanography*, 163, pp. 240–263 (in Russian).
4. Ryabushko, L.I., 2013. *Microphytobenthos of the Black Sea*. Sevastopol: ECOSI-Gidrofizika, 416 p. (in Russian).
5. Ryabushko, L.I. and Begun, A.A., 2015. *Diatoms of Microphytobenthos of the Sea of Japan*. In 2 volumes. Simferopol: N.Orianda, 288 p. (in Russian).
6. Ryabushko, L.I., Sapozhnikova, P.V., Bondarenko, A.V. and Kalinina, O.Yu., 2019. Diatom Foulings of Synthetic Polymer Materials in Karantinnay Bay (Crimea, the Black Sea). *Issues of Modern Algology*, (2), pp. 87–91. doi:10.33624/2311-0147-2019-2(20)-87-91 (in Russian).
7. Jacquin, J., Cheng, J., Odobel, C., Pandin, C., Conan, P., Pujo-Pay, M., Barbe, V., Meistertzheim, A.-L. and Ghiglione, J.-F., 2019. Microbial Ecotoxicology of Marine Plastic Debris: A Review on Colonization and Biodegradation by the "Plastisphere". *Frontiers in Microbiology*, 10, pp. 1–16. doi:10.3389/fmicb.2019.00865
8. Ryabushko, L.I., Bondarenko, A.V., Miroshnichenko, E.S., Lishaev, D.N. and Shiroyan, A.G., 2020. Diatoms and Cyanobacteria of Periphyton of Experimental Synthetic Polymer Materials in Karantinnaya Bay in the Black Sea. *Inland Water Biology*, 13, pp. 399−407. doi:10.1134/S1995082920020285
9. Ryabushko, L., Miroshnichenko, E., Blaginina, A., Shiroyan, A. and Lishaev, D., 2021. Diatom and Cyanobacteria Communities on Artificial Polymer Substrates in the Crimean Coastal Waters of the Black Sea. *Marine Pollution Bulletin*, 169, 112521. doi:10.1016/j.marpolbul.2021.112521
10. *Başak E., Şentürk Y., Aytan Ü.* Microbial Biofilm on Plastics in the Southeastern Black Sea. In: Ü. Aytan, M. Pogojeva and A. Simeonova, eds., 2020. *Marine Litter in the Black Sea*. Istanbul: Turkish Marine Research Foundation. Iss. 56, pp. 268−286. Available at: https://tudav.org/wp-content/uploads/2020/10/MarineLitterintheBlackSea_tudav.pdf [Accessed: 27 July 2023].
11. *Sapozhnikov Ph., Snigirova A., Kalinina O.* Microphytes Assemblages on the Neusto-plastics from the Northern Black Sea. In: Ü. Aytan, M. Pogojeva and A. Simeonova, eds., 2020. *Marine Litter in the Black Sea*. Istanbul: Turkish Marine Research Foundation. Iss. 56, pp. 287−302. Available at: https://tudav.org/wp-content/uploads/2020/10/MarineLitterintheBlackSea_tudav.pdf [Accessed: 27 July 2023].

12. Liao, J., Ji, S. and Chi, Y., 2022. Effects of Discarded Masks on the Offshore Microorganisms during the COVID-19 Pandemic. *Toxics*, 10(8), 426. doi:10.3390/toxics10080426
13. Salta, M., Wharton, J.A., Blache, Y., Stokes, K.R. and Briand, J.-F., 2013. Marine Biofilms on Artificial Surfaces: Structure and Dynamics. *Environmental Microbiology*, 15(11), pp. 2879–2893. doi:10.1111/1462-2920.12186
14. Timoshin, N.M. and Timoshina, Yu. A., 2014. [Non-Woven Fabric for Medical Use]. *Vestnik Kazanskogo Tehnologicheskogo Universiteta*, 17(13), pp. 123−125 (in Russian).
15. Aragaw, T.A., 2020. Surgical Face Masks as a Potential Source for Microplastic Pollution in the COVID-19 Scenario. *Marine Pollution Bulletin*, 159, 111517. doi:10.1016/j.marpolbul.2020.111517
16. Garcés-Ordóñez, O., Mejía-Esquivia, K.A., Sierra-Labastidas, T., Patiño, A., Blandón, L.M. and Díaz, L.F.E., 2020. Prevalence of Microplastic Contamination in the Digestive Tract of Fishes from Mangrove Ecosystem in Cispata, Colombian Caribbean. *Marine Pollution Bulletin,* 154, 111085. doi:10.1016/j.marpolbul.2020.111085
17. Zaikov, K.S. and Sonolev, N.A., 2021. Marine Plastic Debris Pollution in the Western Sector of the Russian Arctic. *Arctic and North*, (43), pp. 246–252. doi:10.37482/issn2221-2698.2021.43.246 (in Russian).
18. De-la-Torre, G.E. and Aragaw, T.A., 2021. What we Need to Know about PPE Associated with the COVID-19 Pandemic in the Marine Environment. *Marine Pollution Bulletin*, 163, 111879. doi:10.1016/j.marpolbul.2020.111879
19. Simonsen, R., 1962. Untersuchungen zur Systematik und Oekologie der Bodendiatomeen der Westlichen Ostsee. *Internationale Revue der Gesamten. Hydrobiologie Beihefte*, 1, pp. 9−144.
20. Blaginina, A. and Ryabushko, L., 2021. Finding of a Rare Species of Diatom *nanofrustulum shiloi* (Lee, Reimer et Mcenery) Round, Hallsteinsen & Paasche, 1999 in the Periphyton of the Coastal Waters of the Black Sea. *International Journal on Algae*, 23(3), pp. 247−256. doi:10.1615/InterJAlgae.v23.i3.40
21. Proshkina-Lavrenko, A.I., 1963. [*Diatoms of the Black Sea Benthos*]. Moscow, Leningrad: Nauka, 243 p. (in Russian).
22. Ryabushko, V.I., Aleev, M.Yu., Radchenko, V.N., Ryabushko, L.I. and Chubchikova, I.N., 2003. Application of Some Bio-indicators for Assessment of State of Impact Marine Ecosystem. In: MHI, 2003. *Ekologicheskaya Bezopasnost' Pribrezhnoy i Shel'fovoy Zon i Kompleksnoe Ispol'zovanie Resursov Shel'fa* [Ecological Safety of Coastal and Shelf Zones and Comprehensive Use of Shelf Resources]. Sevastopol: ECOSI-Gidrofizika. Iss. 2, pp. 144–154 (in Russian).
23. Sapozhnikov, Ph.V., Salimon, A.I., Korsunsky, A.M., Kalinina, O.Yu., Senatov, F.S., Statnik, E.S. and Cvjetinovic, Ju., 2020. Features of Formation of Colonial Settlements of Marine Benthic Diatoms on the Surface of Synthetic Polymer. *Marine Biological Journal*, 5(2), pp. 88–104. doi:10.21072/mbj.2020.05.2.08
24. Korsunsky, A.M., Sapozhnikov, P.V., Everaerts, J. and Salimon, A.I., 2019. Nature's Neat Nanostructuration: The Fascinating Frustules of Diatom Algae. *Materials Today*, 22, pp. 159–160. doi:10.1016/j.mattod.2019.01.002
25. Ryabushko, L.I., 2003. *Potentially Harmful Microalgae of the Azov and Black Sea Basin*. Sevastopol: ECOSI-Gidrofizika, 288 p. (in Russian).

Submitted 04.05.2023.; accepted after review 25.05.2023;
revised 28.06.2023; published 25.09.2023

About the authors:

Anna V. Bondarenko, Senior Research Associate, A. O. Kovalevsky Institute of Biology of the Southern Seas of RAS (2 Nakhimova Ave, Sevastopol, 299011, Russian Federation), Ph.D. (Biol.), **ORCID ID: 0000-0003-2202-4014**, *gonzurassa@mail.ru*

Larisa I. Ryabushko, Chief Research Associate, A. O. Kovalevsky Institute of Biology of the Southern Seas of RAS (2 Nakhimova Ave, Sevastopol, 299011, Russian Federation), Dr.Sci. (Biol.), **ORCID ID: 0000-0003-0443-9929**, *larisa.rybushko@yandex.ru*

Anastasiia A. Blaginina, A. O. Kovalevsky Institute of Biology of the Southern Seas of RAS (2 Nakhimova Ave, Sevastopol, 299011, Russian Federation), Ph.D. (Biol.), **ORCID ID: 0000-0001-7115-4427**, *aablagini@ibss-ras.ru*

Contribution of the authors:

Anna V. Bondarenko – material processing and manuscript writing

Larisa I. Ryabushko – statement of the task and objectives of the comprehensive study, manuscript editing

Anastasiia A. Blaginina – preparation of samples to obtain illustrations in the SEM

All the authors have read and approved the final manuscript.

Original article

Hydrocarbons Composition of Water and Suspended Matter of the Ham Luong River (Southeast Asia)

O. V. Soloveva [1], E. A. Tikhonova [1] *,
Yu. S. Tkachenko [1], Nguyen Trong Hiep [2]

[1] *A.O. Kovalevsky Institute of Biology of the Southern Seas of RAS, Sevastopol, Russia*
[2] *Southern Branch of Joint Vietnam-Russia Tropical Science and Technology Research Center, HoChiMinh, Vietnam*
* *e-mail: tihonoval@mail.ru*

Abstract

The qualitative and quantitative composition of water and suspended matter hydrocarbons was assessed. The transformation of these compounds during their migration in the «water-suspension» system of the river delta in a tropical climate was studied on the example of one of the deepest branches of the Mekong River (Ham Luong River) in Vietnam. The material for the study was samples of surface and bottom water taken along the riverbed in November–December 2022. The physicochemical parameters of the environment were measured using a multimeter *in situ*. The qualitative and quantitative composition of hydrocarbons in the water and suspended matter was determined by gas chromatography on the basis of the Scientific and Practical Center for Spectrometry and Chromatography of the FRC IBSS. Biogeochemical markers of the origin of hydrocarbons were used to identify probable sources of organic matter. Individual physicochemical indicators of the aquatic environment (pH, O_2, salinity, temperature, concentration of suspended matter) were characteristic for the rivers of the lower Mekong River and were within the limits characterizing the favorable state of the reservoir during the wet season. The content of hydrocarbons in the water of the Ham Luong River averaged 0.061±0.019 mg·L^{-1}. These indicators were quite high, exceeding the sanitary standards (0.05 mg·L^{-1}) for fishery reservoirs, or approaching this value. The concentration of hydrocarbons in suspended matter averaged 0.019±0.009 mg·L^{-1}. An increase in the content of hydrocarbons in the suspended phase was noted in the area where the river flows into the sea, in comparison with the sections of the river located upstream. Hydrocarbons in the water were of mixed origin, and contained both biogenic components of autochthonous and allochthonous origin, and traces of oil pollution. In suspended matter, along with biogenic compounds, there are also biodegraded petroleum compounds. Organic compounds, both of allochthonous and petroleum origin, coming from the catchment areas of the Ham Luong River, which is especially pronounced during the wet season, as well as from the surface of the river, further undergone biotransformation during the transition to a suspended state. As a result, the composition of n-alkanes in suspended matter differed significantly from that in water samples.

Keywords: hydrocarbons, n-alkanes, water, suspended matter, biogeochemical markers, tropical river, Mekong River, Ham Luong River, Vietnam

Acknowledgments: The study was carried out by researchers of the Joint Vietnam-Russia Tropical Science and Technology Research Center and the A.O. Kovalevsky Institute of Biology of Southern Seas of RAS according to their research projects: 1) Ekolan E3.4. Ecosystem of the Mekong River in the context of global climate change and anthropogenic impact; and 2) Molismological and biogeochemical foundations of homeostasis of marine ecosystems (state registration no. 121031500515-8).

For citation: Soloveva, O.V., Tikhonova, E.A., Tkachenko, Yu.S. and Nguyen Trong Hiep, 2023. Hydrocarbons Composition of Water and Suspended Matter of the Ham Luong River (Southeast Asia). *Ecological Safety of Coastal and Shelf Zones of Sea*, (3), pp. 129–142.

Углеводородный состав воды и взвеси реки Хамлуонг (Юго-Восточная Азия)

О. В. Соловьёва [1], Е. А. Тихонова [1] *, Ю. С. Ткаченко [1], Нгуен Чонг Хиеп [2]

[1] *ФГБУН ФИЦ Институт биологии южных морей имени А. О. Ковалевского РАН, Севастополь, Россия*

[2] *Южное отделение Совместного Российско-Вьетнамского Тропического научно-исследовательского и технологического центра, Хошимин, Вьетнам*

** e-mail: tihonoval@mail.ru*

Аннотация

Проведена оценка качественного и количественного состава углеводородов воды и взвешенного вещества с учетом их трансформации при миграции в системе вода – взвесь дельты реки на примере одного из самых полноводных рукавов Меконга (р. Хамлуонг) на территории Вьетнама в условиях тропического климата. Материалом для исследования послужили пробы поверхностной и придонной воды, отобранные вдоль русла реки в ноябре – декабре 2022 г. Физико-химические параметры среды измеряли *in situ* с помощью мультиметра. Качественный и количественный состав углеводородов в воде и взвеси определяли методом газовой хроматографии. Для идентификации вероятных источников поступления органических веществ использовали биогеохимические маркеры происхождения углеводородов. Значения отдельных физико-химических показателей водной среды (pH, O_2, соленость, температура, концентрация взвешенного вещества) являются характерными для исследуемой р. Хамлуонг. Эти значения находились в пределах, характеризующих благополучное состояние водоема во влажный сезон. Содержание углеводородов в воде р. Хамлуонг в среднем составляло 0.061 ± 0.019 мг·л$^{-1}$. Данное значение является достаточно высоким и превышает санитарные нормы (0.05 мг·л$^{-1}$) для рыбохозяйственных водоемов или приближаются к ним. Концентрация углеводородов во взвешенном веществе составляла в среднем 0.019 ± 0.009 мг·л$^{-1}$. В районе впадения реки в море содержание углеводородов во взвешенной фазе было выше, чем на участках реки, находящихся выше по течению. Углеводороды в воде были смешанного происхождения. Во взвешенном веществе наряду с биогенными соединениями отмечаются также биодеградированные соединения нефтяной природы. В результате биотрансформации состав н-алканов в пробах взвешенного вещества и в пробах воды существенно различается.

Ключевые слова: углеводороды, н-алканы, вода, взвесь, биогеохимические маркеры, тропическая река, река Меконг, река Хамлуонг, Вьетнам

Благодарности: работа выполнена в рамках НИР Совместного Российско-Вьетнамского Тропического научно-исследовательского и технологического центра (СРВТНИиТЦ) «Эколан Э-3.4. Экосистема реки Меконг в условиях глобальных климатических изменений и антропогенного воздействия», темы госзадания ФГБУН ФИЦ «Институт биологии южных морей имени А. О. Ковалевского РАН (ФИЦ ИнБЮМ) «Молисмологические и биогеохимические основы гомеостаза морских экосистем» (№ гос. регистрации: 121031500515-8).

Для цитирования: Углеводородный состав воды и взвеси реки Хамлуонг (Юго-Восточная Азия) / О. В. Соловьёва [и др.] // Экологическая безопасность прибрежной и шельфовой зон моря. 2023. № 3. С. 129–142. EDN DHTIBX.

Introduction

The total area of Vietnam's inland water bodies is about 6 % of the country's territory, so water resources are essential to the region's economy [1]. The Mekong River is one of the most important river systems in Vietnam and the twelfth longest river in the world [2]. One of the Mekong's branches with the highest water content is the Ham Luong River, which is 70 km long and 2800 m wide, it has an average depth of 11.3 m and an average water discharge [1)] of 10.2 $m \cdot s^{-1}$.

There are more than three thousand rivers and streams in Vietnam (over a hundred of them flow into the sea), many of them are characterized with a high degree of water pollution. The most polluted (due to various causes) are the Cau, Dai, Thi Vai, Dong Nai and Mekong Rivers. A 2018 report by the Ministry of Natural Resources and Environment of Vietnam notes that in the river catchment area, water pollution occurs due to mining activities. In the middle and lower reaches of the rivers (in these areas, cities, industrial areas, and rural settlements are usually located), their ecological state is deteriorating due to all kinds of waste entering the water. The pollution degree depends on hydrological factors (their influence increases in the dry season), as well as on the degree of control over pollution sources. In almost all ecologically unfavourable areas, organic substances are the cause of pollution [3].

Natural waters are a complex mixture of solutions of mineral salts and gases, as well as organic compounds in suspended and dissolved forms. At the same time, the content and qualitative composition of organic matter in a water body are determined not only by the natural features of the latter, but also by the nature and degree of influence of human activity on the water body [4]. Among important factors affecting the redistribution of organic matter in water, including hydrocarbons (HC), there are also physical and chemical parameters such as pH, salinity, temperature, etc. The pH level determines the development and activity of many organisms, the aggressiveness of water impact on metals and concrete. The water pH level also influences the processes of transformation of various forms of nutrients

[1)] Phung Thai Duong, 2015. [*Ecological and Geochemical State of the Mekong River Mouth (Republic of Vietnam) Based on Studies of Bottom Sediments*]. Extended Abstract of Doctoral Dissertation. Tomsk: NITPU, 26 p. (in Russian).

and changes the toxicity of pollutants [2]. Oxygen dissolved in water is one of the most important biohydrochemical indicators of the environment. It ensures the existence of aquatic organisms and characterizes the quality of water [5] used for various economic purposes. Oxygen deficiency is more often observed in water bodies with high concentrations of organic pollutants and in water bodies containing a large amount of nutrients and humic substances. In addition, oxygen concentration determines the direction and rate of processes of chemical and biochemical oxidation of organic and inorganic compounds [2].

HC genesis can be identified using various markers. In order to differentiate allochthonous and autochthonous origin, the ratio of terrigenous and autochthonous compounds C_{31}/C_{19}, C_{31}/C_{17}, the ratio of low-molecular-weight and high-molecular-weight homologues (LWH/HWH) is often used [6, 7]. Some biomarkers allow specifying the biogenic nature of compounds, in particular to assess the contribution of herbaceous and woody vegetation to the formation of the allochthonous component of HCs entering the bottom sediments. These are, e. g., C_{31}/C_{29} and ACL ratios [7]. To differentiate the petroleum and biogenic origin of detected HCs, such ratios are used as the carbon preference index (CPI), in particular CPI_2 (calculated for the high-molecular-weight part of the spectrum), ACL, LWH/HWH, and the ratio of isoprenoid alkanes (pristane and phytane), both one to the other and to individual normal homologues (Pr/Ph, C_{17}/Pr, C_{18}/Ph) [6, 7].

The work aims at assessment of the qualitative and quantitative composition of HCs in water and suspended matter of the Ham Luong River given the transformation of these compounds during their migration in the water–suspension system.

Material and methods

The material was water samples taken in November – December 2022 along the Ham Luong River riverbed (Stations *9–13*) taking into account the location of large industrial and urban facilities along its banks (Fig. 1). Sampling at each station was conducted in the cross section of the riverbed at three points (the right and left banks, the centre). Bottom and surface water was sampled in the central part of the riverbed, while near the banks, only surface water was sampled. The numbering of stations was retained in accordance with the schedule programme of Vietnamese rivers studies jointly with the Southern Branch of Joint Vietnam-Russia Tropical Science and Technology Research Center (JVRTSTRC). Chemical and physical characteristics of surface water (pH, Eh, salinity, temperature) of the Ham Luong River were determined *in situ* by the staff of the Environmental Analysis Laboratory of the Southern Branch of the JVRTSTRC using a YSI Professional Digital Sampling System (ProDSS) multi-parameter probe. Sample preparation was carried out in laboratory conditions by extraction of water samples with hexane [3]. The resulting extract was purified on a glass column filled

[2] State Standard, 1978. [*Nature Protection. Hydrospere, Use and Protection of Waters. Main Terms and Definitions*] (in Russian).

[3] Barabashin, T.O., ed., 2018. [*Guidance Manual on Chemical Analysis of Aquatic Ecosystem Elements. Primary Toxicants in Water, Bottom Sediments, Hydrobionts*]. Rostov-on-Don: MiniTaip, 436 p. (in Russian).

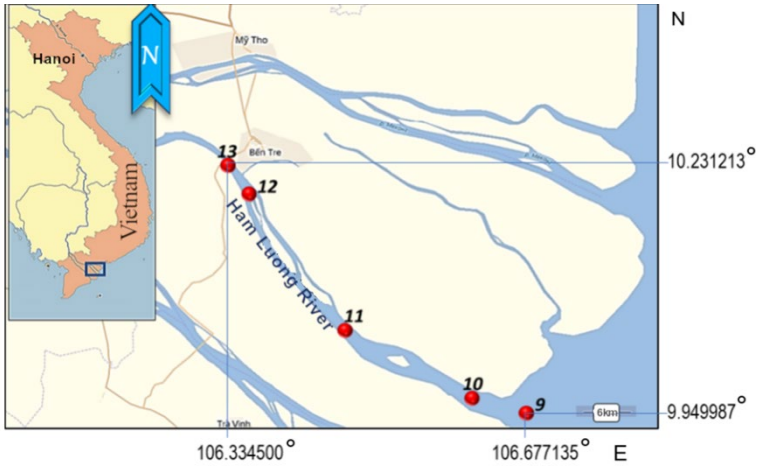

Fig. 1. Map of water sampling stations in the Ham Luong river (Vietnam) during the wet season, 2022

with aluminium oxide to remove polar compounds, concentrated to 1 mL and transported to the FRC IBSS laboratory.

Suspended matter was collected by vacuum filtration using a vacuum pump, Bunsen flask, filter unit and nitrocellulose filters with a pore diameter of 0.45 μm. The volume of filtered river water varied according to the rate of suspended matter deposition on the filters and was taken into account when calculating the hydrocarbon content of the suspension. The filters were dried under natural conditions, stored in a desiccator, and transported in airtight ziploc bags.

An aliquot of the extract (1 μL) was injected with a microsyringe into the heated to 250 °C evaporator of a gas chromatograph *Kristall 5000.2* with a flame ionisation detector (FID). HC separation was performed on a TR-1MS capillary column 30 m long, 0.32 mm in diameter, and with the stationary phase film thickness of 0.32 μm (TermoScientific). The column temperature was programmed from 70 to 280 °C (rate of temperature rise: 8 °C·min^{-1}). The carrier gas (nitrogen) flow in the column was 2.5 mL·min^{-1} without flow splitting. The detector temperature was 320 °C.

Quantitative determination of HC content was carried out by absolute calibration of FID by HC mixture (ASTMD2887 Reference Gas Oil standard sample (SUPELCO, USA)), that of n-alkanes – by a paraffinic HC standard sample in hexane with mass concentration of each component 200 μg·mL^{-1} and of pristane + phytane – 100 μg·mL^{-1} in hexane (SUPELCO, USA).

Determination of HCs and n-alkanes was carried out at the Scientific and Educational Center for Collective Use "Spectrometry and Chromatography" of FRC IBSS. To process the results for the determination of HC concentrations, *Chromatek Analytic 3.0* software was used (absolute calibration and percentage normalization method).

US-EPA indices [4] applicable to water bodies of different climatic zones were used to assess the well-being of waters of the study area by individual indicators, which allows using them for tropical water bodies as well [8, 9]. Correlation analysis was performed using Microsoft Excel 2010 analysis package. The strength of the correlation relationship was estimated based on the correlation coefficient (R). The approximation coefficient (R^2) was used to estimate the reliability of approximation of dependencies by a linear function.

The markers of HC genesis were determined according to the following ratios:

– *CPI*$_2$ (*Carbon Preference Index*) = (1/2){(C_{25} + C_{27} + C_{29} + C_{31} + C_{33} + C_{35}) / (C_{24} + C_{26} + C_{28} + C_{30} + C_{32} + C_{34}) + (C_{25} + C_{27} + C_{29} + C_{31} + C_{33} + C_{35}) / (C_{26} + C_{28} + + C_{30} + C_{32} + C_{34} + C_{36})};

– *Pr/Ph* – pristane to phytane ratio;

– *LWH/HWH* – low-molecular-weight homologue to high-molecular-weight homologue ratio;

– C_{31}/C_{19} – n-alkane C_{31} to n-alkane C_{19} ratio;

– C_{31}/C_{17} – n-alkane C_{31} to n-alkane C_{17} ratio;

– C_{31}/C_{29} – n-alkane C_{31} to n-alkane C_{29} ratio;

– C_{17}/Pr – n-alkane C_{17} to pristane ratio;

– C_{18}/Ph – n-alkane C_{18} to phytane ratio.

Results and discussion

The water temperature in the study area was around 29 °C (28.83–29.33 °C). Salinity ranged from 0.08 to 0.23 PSU and corresponded to fresh water. A regular increase of this parameter was observed while moving downstream (Fig. 2). At Stations *11–13* the salinity was the same (0.08–0.09 PSU), at Station *10* it was 0.15 PSU, and at the most seaward Station *9* it increased up to 0.23 PSU. Together with salinity, the suspended matter content of water was increasing (R = 0.97, R^2 = 0.93), growing approximately twofold in the mixing zone (Station *9*) (Fig. 2, *a*). The suspended matter content at the sampling stations varied from 23 to 110 mg·L^{-1} (Fig. 2, *b*) with a tendency to increase as we moved towards the river mouth. It should be noted that in most parts of the riverbed the suspended matter content in the bottom layer was on average 1.9 times higher than that in the surface layer. The exception was Station *9* located at the river mouth, where the suspended matter content at the surface was 1.4 times higher than that in the bottom layer.

Thus, a joint increase in salinity and suspended matter content was observed while moving downstream of the river. The marginal filter phenomenon formed in the river – sea mixing zone is described in the literature [10], where an increase in suspended matter content is observed as salinity increases up to 5 PSU while one moves towards the salt-water areas. This fact is associated with active processes of coagulation and flocculation, when dissolved organics, iron, aluminium,

[4] US-EPA, 1986. *Quality Criteria for Water 1986*. Washington, DC, USA: Office of Water Regulations and Standards, United States Environmental Protection Agency, 394 p. Available at: https://www.epa.gov/sites/default/files/2018-10/documents/quality-criteria-water-1986.pdf [Accessed: 27 September 2023].

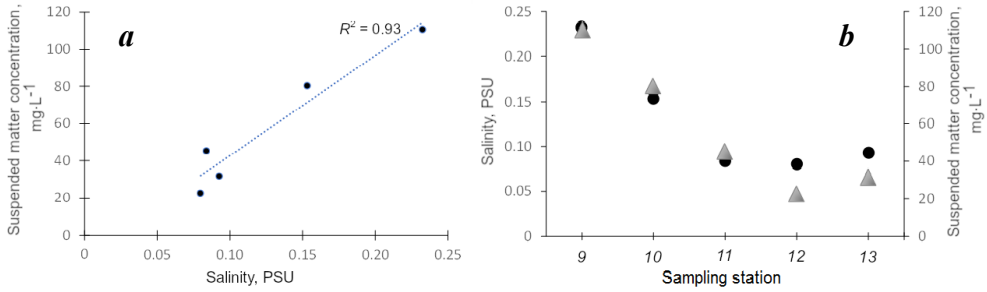

Fig. 2. Salinity (PSU) and concentration of suspended solids (mg·L^{-1}) in the water of the Ham Luong River (Vietnam) during the wet season, 2022: *a* – the ratio of salinity and suspended matter concentration; *b* – salinity (dots) and suspended matter concentration (triangles) at sampling stations

and a number of other elements pass from solution into suspension under the influence of electrolyte. Probably, we observed the increasing intensity of this very process in the study area even at an insignificant increase of water salinity.

According to monitoring studies [5], suspended sediment concentrations in the Mekong River branches, particularly the Ham Luong River, vary considerably ranging from 2.3 to 593 mg·L^{-1} with an average value of 80.6 mg·L^{-1}. Suspended matter concentrations depend on the season greatly: they decrease significantly from April to November and increase as the monsoon season begins. Thus, the average value [5] for the dry season is 36.9 mg·L^{-1}, and for the wet season it is 124 mg·L^{-1}. In the material we sampled in December 2022, the average suspended matter concentration was 58 mg·L^{-1}.

The water pH at all stations ranged 7.4–7.6, which corresponds to drinking water. According to the monitoring survey data [5], pH values in the lower reaches of the Ham Luong River are in the range of 6.3–8.7 (average 7.7). The values we obtained fall within this range and correspond to the target values (6–9) [4] of WQIhh (Water Quality Index for the Protection of Human Health) [11].

The dissolved oxygen content also varied insignificantly within the range of 5.14–5.57 mg·L^{-1}. The oxygen content in the water complies with the health standard values [6] for fishery water bodies (> 4 mg·L^{-1}), though it was slightly below the steady-state concentrations for this temperature range (7.62–7.52 mg·L^{-1}) [11], which is suggestive of active biological processes in the river waters.

---

[5] Mekong River Commission, 2018. *Lower Mekong Regional Water Quality Monitoring Report*. Vientiane, Lao: Mekong River Commission.

[6] *On the Approval of Water Quality Standards for Water Bodies of Commercial Fishing Importance, Including Standards for Maximum Permissible Concentrations of Harmful Substances in the Waters of Water Bodies of Commercial Fishing Importance*: Order of the Ministry of Agriculture of Russia dated December 13, 2016, No. 552 (in Russian).

The oxygen concentration in the lower reach of the studied river ranges from 4.12 to 9.27 mg·L^{-1} (average 6.45 mg·L^{-1}) [5]. The obtained values are typical for the water body and correspond to the target indicator (not less than 5 mg·L^{-1}).

Thus, the studied indicators were typical for the Ham Luong River and were within the limits indicating the favourable condition of the water body during the study season.

The HC content in the water of the Mekong River brunch under the study (Ham Luong River) ranged from 0.042 to 0.076 mg·L^{-1} (average 0.061 ± 0.019 mg·L^{-1}) (Fig. 3). These values are quite high and exceed the health standard limits (0.05 mg·L^{-1}) for fishery water bodies [6] or are near this value. Since the river under study is used both for fishing and aquaculture, these indicators characterize its unsatisfactory condition. The content of n-alkanes in the water was 0.015–0.043 mg·L^{-1} (average 0.028 ± 0.012 mg·L^{-1}). The proportion of n-alkanes to total HC content ranged from 31 to 57 % (average 44 ± 8 %). The reduced proportion of n-alkanes from HCs was at Station *9* located in the area, where the river flows into the sea. In general, HC and n-alkane concentrations changed synchronously (R = 0.91).

The HC content in suspended matter was in the range of 0.011–0.37 mg·L^{-1} (average 0.019 ± 0.009 mg·L^{-1}) (Fig. 3). It is noteworthy that the HC content in the suspended phase increased near Station *9* compared to upstream river sections. This fact, as noted above, can be associated with the transition of substances from the dissolved to suspended state with increasing water salinity in the river – sea mixing zone [12]. The HC content in the suspended matter correlated with its total amount (R = 0.78), which indicates a substantial contribution of biological processes to the suspended matter formation.

The concentration of n-alkanes varied from 0.004 to 0.10 mg·L^{-1} (average 0.006 ± 0.002 mg·L^{-1}) representing 28–41 % (average 36 ± 4 %) of the hydrocarbon mixture. Based on the small standard deviation, this fraction was quite constant, which

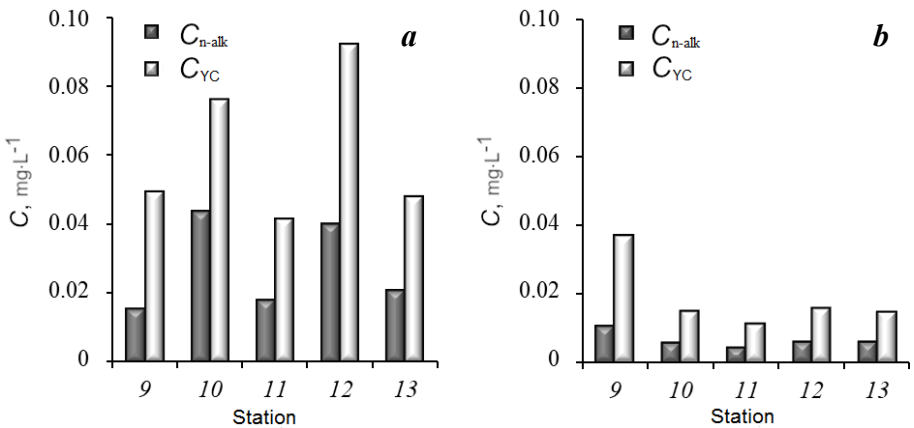

F i g . 3 . Hydrocarbon concentrations (mg·L^{-1}) in water (*A*) and suspended matter (*B*) of the Ham Luong River (Vietnam) during the wet season, 2022

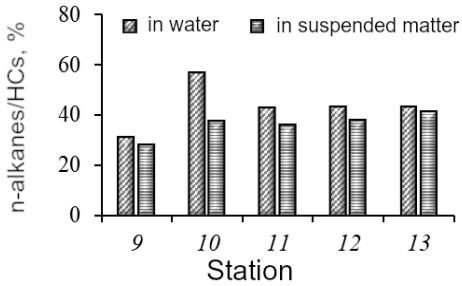

Fig. 4. Hydrocarbon and n-alkane ratio (%) in water and suspended matter of the Ham Luong River (Vietnam) during the wet season, 2022

may be a consequence of the uniformity of HC input sources and conversion mechanisms at the different sampling stations. The contents of HC and n-alkanes in the mixture varied synchronously (R = 0.98). For both water and suspended matter, the proportion of n-alkanes from HCs decreased in the area, where the river flows into the sea (Fig. 4).

The share of HCs in suspended matter accounted for 20 to 75 % (average 34 ± 21 %) of HCs in water as a whole. That is, the range of values was rather wide. This indicator for n-alkanes ranged within 13–68 % (average 29 ± 20 %), which also characterizes the instability of this indicator.

At all stations, n-alkanes from C_{17} to C_{32} were identified in the unfiltered water sample. At Stations *11–13*, the compound C_{33} was also identified. In general, the distribution of n-alkanes was uniform, which may indicate the presence of compounds of petroleum origin (Fig. 5). A C_{17} peak was noted, which is associated with planktonic production [6]. Another group of C_{26}–C_{29} maxima stands out. The odd-numbered compounds in this range are genetically associated with terrestrial vegetation (C_{27}, C_{29}) [6]. The even-numbered compounds (C_{26}, C_{28}) are probably related to bacterial synthesis [7] [13] and also correspond to the presence of humus admixture in organic matter and macrophyte production [14]. Given that sampling was carried out during monsoon rains, the washout of humus compounds from the adjacent territories is not improbable.

In the suspended matter, n-alkanes were present in the C_{17}–C_{32} range. Compounds with a higher molecular weight were not recorded. At Station *13*, the heaviest homologue was C_{30}, and at Station *10* it was C_{31}. The main peak in the composition of n-alkanes in the suspended matter corresponded to C_{17} (19–27 %). It is due to active primary production [15, 16], which intensifies in the wet season because of the active input of biogenic compounds and high oxygenation of water [16]. The analyzed suspended matter probably had a significant number of phytoplanktonic organisms in its composition. At Stations *9* and *10*, the second peak corresponded to C_{21} (13 and 16 %), also of phytoplanktonic genesis. In general, the graph of n-alkane distribution in the suspended matter was smoother than that in water, which may indicate a deeper transformation of organic matter in the suspended matter. Thus, n-alkanes present in the suspended phase are predominantly autochthonous in nature and are associated with phytoplankton and bacterial production.

---

[7] Poshibaeva, A.R., 2015. [*Bacterial Biomass as Petroleum Hydrocarbon Source*]. Extended Abstract of Doctoral Dissertation. Moscow: 24 p. (in Russian).

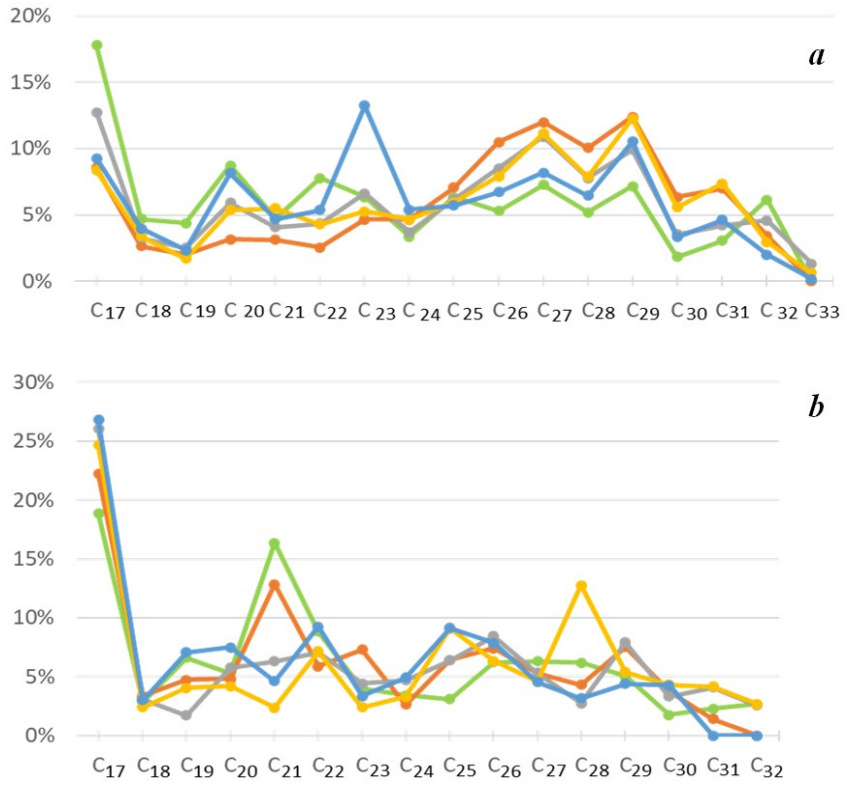

Fig. 5. Distribution of *n*-alkanes in water (*a*) and suspended matter (*b*) of the Ham Luong River (Vietnam) during the wet season, 2022: St. *9* (), St. *10* (), St. *11* (), St. *12* (), St. *13* ()

To identify potential sources of HC inputs, individual markers of organic matter genesis were calculated (Table). For water, the carbon preference indices for the high-molecular-weight region were almost the same and slightly exceeded a figure of one, which may be a consequence of the presence of oil contamination. The pristane to phytane ratio was also characterized by low values, which is typical of the presence of oil. The ratio of n-alkane C_{17} to pristan, C_{17}/Pr (Table) characterizes the presence of fresh oil. At the same time marker C_{18}/Ph ≈ 1 (Table), which indicates the presence of both fresh and degraded petroleum products.

It is known that the suspended matter is characterized by CPI values ≥ 1 [6]. In this study, this ratio was below a figure of one for the high-molecular-weight region, which indicates the predominance of biogenic and transformed petroleum HCs in the suspended matter phase. The pristane to phytane ratio Pr/Ph (Table) is indicative of the presence of oil, and C_{18}/Ph shows the predominance of its biodegraded components.

Calculated biogeochemical marker values for water and suspended matter of the Ham Luong River (Vietnam), 2022

Marker	Water					Suspended matter				
	Station number									
	9	*10*	*11*	*12*	*13*	*9*	*10*	*11*	*12*	*13*
CPI_2	1.2	1.2	1.3	1.4	1.4	0.5	0.7	0.7	0.4	0.6
Pr/Ph	0.2	0.1	0.0	0.0	0.2	0.3	0.2	0.1	0.1	0.1
LWH/ HWH	0.9	0.3	0.5	0.5	0.4	1.4	1.2	1.0	0.8	1.4
C_{31}/C_{19}	0.7	3.5	1.7	4.3	2.0	0.3	0.3	2.3	1.0	0.0
C_{31}/C_{17}	0.2	0.8	0.3	0.9	0.5	0.1	0.1	0.2	0.2	0.0
C_{31}/C_{29}	0.4	0.6	0.4	0.6	0.4	0.5	0.2	0.5	0.8	0.0
C_{17}/Pr	21.0	49.2	103.4	43.8	19.5	5.7	25.1	64.0	24.3	30.2
C_{18}/Ph	0.9	0.9	1.0	0.7	1.0	0.3	0.6	0.4	0.3	0.5

Thus, there is a situation when water contains both fresh and degraded oil, while biodegraded compounds of oil origin prevail in the suspended matter. It is known that during sedimentation oil components actively degrade [17], which is the reason for the presence of transformed compounds in the suspended phase. It is natural to expect active biodegradation processes of introduced organic compounds in the warm waters of the Ham Luong River. In some cases, even in Arctic ocean areas, in spite of low temperatures, the transformation of anthropogenic hydrocarbons goes so quickly that natural compounds dominate in the water and bottom sediments [18].

The markers allowing differentiating between autochthonous and allochthonous compounds (C_{31}/C_{17}, C_{31}/C_{19}) indicate the predominance of compounds coming from land into water. In the suspended matter, based on the marker values, allochthonous compounds are of subordinate value, which links the suspended matter to the productive and destructive processes in the riverbed. The LWH/HWH ratio (Table) for water corresponds to the predominance of terrigenous HCs [18]. In the case of suspended matter, this marker has high values, which can sometimes be a sign of fresh oil input. The main contribution to the sum of low-molecular-weight homologues in this case is made by C_{17} and C_{21}, the share of which is by times higher than the specific weight of other n-alkanes. Therefore, we can speak about the predominance of autochthonous compounds, which indicates active production processes in the water body.

The HCs in water are of mixed origin and contain both biogenic components of autochthonous and allochthonous nature and traces of oil pollution. In the suspended matter along with biogenic compounds, biodegraded compounds of oil nature

are also observed. Organic compounds of both allochthonous and petroleum origin come from the Ham Luong River catchment areas (which is especially pronounced during the wet season) as well as from the river surface. Further, these compounds undergo biotransformation after becoming suspended. As a result, the composition of n-alkanes in the suspended matter samples and integrated water samples differs significantly. This process is active, in part due to the high water temperature typical of the tropical region. Active biological processes in the river waters are also indicated by a slightly reduced oxygen content relative to steady-state concentrations, which is probably intensively consumed for oxidation of organic compounds.

Conclusion

Values of some physical and chemical parameters of the aquatic environment (pH, O_2, salinity, temperature, suspended matter concentration) were typical for the Ham Luong River and were within the limits indicating the favourable condition of the water body during the study season.

The HC content in the water of the studied branch of the Mekong (Ham Luong River) ranged from 0.042 to 0.076 $mg \cdot L^{-1}$, averaging 0.061 ± 0.019 $mg \cdot L^{-1}$. These values are quite high and exceed or are close to the health standard values (0.05 $mg \cdot L^{-1}$) for fishery water bodies.

The HC content in the suspended matter ranged from 0.011 to 0.37 $mg \cdot L^{-1}$, averaging 0.019 ± 0.009 $mg \cdot L^{-1}$. An increase in HC content in the suspended phase was observed in the area where the river flows into the sea compared to the upstream sections of the river.

The HCs in water are of mixed origin and contain both biogenic components of autochthonous and allochthonous nature as well as traces of oil pollution. In the suspended matter along with biogenic compounds, biodegraded compounds of oil nature are also observed. Due to active washout from the catchment area of the Ham Luong River (which is especially pronounced in the wet season) and from the surface of the river, organic compounds of various origins undergo significant biotransformation during transition into the suspended phase. As a result, the composition of n-alkanes in suspended matter samples and in integrated water samples differs significantly.

REFERENCES

1. Pavlov, D.S. and Zvorykin, D.D., 2014. *Ecology of Inland Waters of Vietnam*. Moscow: Tovarishchestvo nauchnykh izdaniy KMK, 435 p. doi:10.13140/2.1.5079.6325 (in Russian).
2. Dinh Nguyen An, 2021. Marine Environment Protection in Vietnam: Contemporary Issues and Challenges. In: V. M. Mazyrin and Vu Thuy Trang, eds., 2021. *Independent Vietnam: National Interests and Values*. Moscow: IFES RAS. Iss. 1, pp. 149–162. doi:10.24412/cl-36362-2021-1-149-162 (in Russian).

3. Tereshchenko, T.N., Proskurnin, V.Yu., Chuzhikova-Proskurnina, O.D. and Trong Hiep Nguyen, 2023. [Chemoecological Monitoring of Water State in the Ham Luong River Related to Heavy Metals and Metalloids (Mekong River Mouth, Vietnam)]. In: Maykop State Technological University, 2023. *Fundamental and Applied Aspects of Geology, Geophysics and Geoecology Using Modern Information Technologies. VII International Scientific and Practical Conference, Republic of Adygeya, Maykop, May 15–19, 2023*. *Part 2*. Maykop: Izd-vo "IP Kucherenko V.O.", pp. 214–220 (in Russian).
4. Rizhinashvili, A.L., 2008. The Parameters of Organic Matter and Carbonate System Components in Waterbodies under Intensive Anthropogenic Influence. *Vestnik of Saint Petersburg University. Physics and Chemistry*, (4), pp. 90–101 (in Russian).
5. Ponomarev, A.Ya., 2015. Dissolved Oxygen as an Important Biogeochemical Indicator of Water Quality. *Science Almanac*, (12-2), pp. 146–148. doi:10.17117/na.2015.12.02.146
6. Nemirovskaya, I.A., 2013. *Oil in the Ocean (Pollution and Natural Flow)*. Moscow: Nauchny Mir, 432 p. (in Russian).
7. Wang,X.-C., Sun, S., Ma, H.-Q. and Liu, Y., 2006. Sources and Distribution of Aliphatic and Polyaromatic Hydrocarbons in Sediments of Jiaozhou Bay, Qingdao, China. *Marine Pollution Bulletin*, 52(2), pp. 129–138. doi:10.1016/j.marpolbul.2005.08.010
8. Prati, L., Pavanello, R. and Pesarin, F., 1971. Assessment of Surface Water Quality by a Single Index of Pollution. *Water Research*, 5(9), pp. 741–751. doi:10.1016/0043-1354(71)90097-2
9. De Troyer, N., Mereta, S.T., Goethals, P.L.M. and Boets, P., 2016. Water Quality Assessment of Streams and Wetlands in a Fast Growing East African City. *Water*, 8(4), 123. doi:10.3390/w8040123
10. Lisitsyn, A.P., 1994. A Marginal Filter of the Oceans. *Okeanologiya*, 34(5), pp. 735–747 (in Russian).
11. Sor, R., Ngor, P.B., Soum, S., Chandra, S., Hogan, Z.S. and Null, S.E., 2021. Water Quality Degradation in the Lower Mekong Basin. *Water*, 13(11), 1555. doi:10.3390/w13111555
12. Nemirovskaya, I.A., 2004. [*Hydrocarbons in the Ocean (Snow-Ice-Water-Suspension-Bottom Sediments)*]. Moscow: Nauchnyi Mir, 328 p. (in Russian).
13. Nikolaev, Yu.A., Mulyukin, A.L., Stepanenko, I.Yu. and El'-Registan, G.I., 2006. Autoregulation of Stress Response in Microorganisms. *Microbiology*, 75(4), pp. 420–426. doi:10.1134/S0026261706040096
14. Lisitsyn, A.P., ed., 2021. *The Barents Sea System*. Moscow: GEOS, 672 p. (in Russian).
15. Tashlikova, N.A., Kuklin, A.P. and Bazarova, B.B., 2009. Primary Production of Phytoplankton, Epiphitic Seaweed and the Higher Water Plants in the Channels of the Selenga River Delta. *Bulletin of KrasGAU*, (9), pp. 106–111 (in Russian).
16. Yáñez-Arancibia, A. and Day, J., 1982. Ecological Characterization of Terminos Lagoon, a Tropical Lagoon-Estuarine System in the Southern Gulf of Mexico. *Oceanologica Acta*, 5(4), pp. 431–440.
17. Nemirovskaya, I.A., Kochenkova, A.I. and Khramtsova, A.V., 2020. Hydrocarbons at the Geochemical Barrier the Northern Dvina – the White Sea. *Water Resources*, 47(3), pp. 438–447. doi:10.1134/S0097807820030148
18. Nemirovskaja, I.A., 2017. Hydrocarbons in Waters and Sediments of Coastal Marine Regions of Arctic. *Environmental Monitoring and Ecosystem Modelling*, 28(1), pp. 41–55. doi:10.21513/0207-2564-2017-1-41-32 (in Russian).

Submitted 01.06.2023; accepted after review 04.06.2023;
revised 28.06.2023; published 25.09.2023

About the authors:

Olga V. Soloveva, Leading Research Associate, A. O. Kovalevsky Institute of Biology of the Southern Seas of RAS (2 Nakhimova Ave, Sevastopol, 299011, Russian Federation), Ph.D. (Biol.), **ORCID ID: 0000-0002-1283-4593, Scopus Author ID: 57208499211, ResearcherID: X-4793-2019,** *kozl_ya_oly@mail.ru*

Elena A. Tikhonova, Leading Research Associate, A. O. Kovalevsky Institute of Biology of the Southern Seas of RAS (2 Nakhimova Ave, Sevastopol, 299011, Russian Federation), Ph.D. (Biol.), **ORCID ID: 0000-0002-9137-087X, Scopus Author ID: 57208495804, ResearcherID: X-8524-2019**, *tihonoval@mail.ru*

Yulia S. Tkachenko, Junior Research Associate, A. O. Kovalevsky Institute of Biology of the Southern Seas of RAS (2 Nakhimova Ave, Sevastopol, 299011, Russian Federation), **ORCID ID: 0009-0001-1752-1043,** *yulechkatkachenko.90@mail.ru*

Nguyen Trong Hiep, Head of Laboratory, Southern Branch of Joint Vietnam-Russia Tropical Science and Technology Research Center, (No. 3, 3/2 St., Dist. 10, Ho Chi Minh, 740500, Vietnam), Ph.D. (Chem.), *hiepnguyen@vrtc.org.vn*

Contribution of the authors:

Olga V. Soloveva – problem statement, analysis of the obtained results, discussion of the results, writing of the article

Elena A. Tikhonova – literature review, calculation of biogeochemical indices, discussion of the results

Yulia S. Tkachenko – preparation of samples for the determination of hydrocarbons, formatting of the article

Nguyen Trong Hiep – participation in sampling, measurement of physical and chemical parameters of water

All the authors have read and approved the final manuscript.